Institute of Energy Technology-Pontoppidanstræde 101
Aalborg University, Denmark

# Reactive power control for Wind Power Plant with STATCOM

Conducted by group: WPS4-1051
Spring Semester, 2010

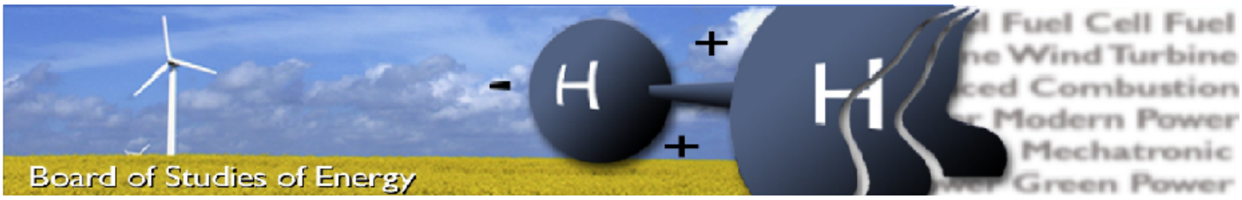


| | |
|---|---|
| **Title:** | Reactive power control for Wind Power Plant with STATCOM |
| **Semester:** | 10 |
| **Semester theme:** | Master Thesis |
| **Project period:** | 08.02.10 to 02.06.10 |
| **ECTS:** | 30 |
| **Supervisor 1:** | Remus Teodorescu |
| **Supervisor 2:** | Pedro Rodriguez |
| **Supervisor 3:** | Andrzej Adamczyk |
| **Project group:** | WPS 1051 |

**SYNOPSIS:**

Large Wind Power Plants (WPPs), comparable to the conventional power stations are the viable solution for delivering clean energy in near future. However a series of technical challenges appear when grid penetration levels of wind power become high. Especially the older WPPs are experiencing difficulties in ensuring higher quality power into the grid, as demanded by the more and more stringent grid codes.
Thus a proven solution to these problems is to install FACTS devices in the system. From this family, STATCOM is gaining popularity, therefore a system with WPP and STATCOM is proposed. First, a small scale system is modeled in Plecs environment. Two Voltage Source Converters are included, one is emulating the WPP and the other represents the STATCOM.
The WPP and STATCOM reactive power injection/absorption performance is analyzed. To validate the simulation results, laboratory experiments are further performed on a similar setup with two VSC connected to same PCC. Finally a large scale system involving an aggregated model of WPP, with PMSG and full scale converter was modeled in Matlab/Simulink. In conclusion, along with WPPs power capability curve STATCOM proves to offer comprehensive and fast reactive power compensation.

Piotr Lipnicki

Tiberiu Mihai Stanciu

| | |
|---|---|
| Copies: | 4 |
| Pages, total: | 92 |
| Appendix: | 19 |
| Supplements: | 4 CD |

**By signing this document, each member of the group confirms that all participated in the project work and thereby all members are collectively liable for the content of the report.**

# Preface

This present Master Thesis, entitled "Reactive Power Control for Wind Power Plant with STATCOM", is written by group WPS4-1051 formed by two students in the 4th Master semester at the Institute of Energy Technology, Aalborg University, Denmark. The project period is from $8^{th}$ February 2010 to $2^{nd}$ June 2010. The report consists of two parts, a main part and an appendix part. The project has been carried out within the areas of Electric Power Engineering and Grid Connection of Wind Power, and it is a proposed project from Vestas company.

The references to studied literature are shown in form of a number, placed into square brackets. The format of equation is (X,Y), where X is number of chapter and Y is the number of equation in that chapter. The figures are numbered Figure X.Y, in which X,Y are having the same significance as for the equations.

The appendices are labeled with capital letters, put in alphabetical order. The enclosed CD contains the report in Adobe PDF format, documentations used throughout the report and Simulink Models with their dSPACE implementation.

The authors would like to give special thanks to their supervisors Remus Teodorescu, Andrzej Adamczyk and Pedro Rodriguez for their support and valuable information provided throughout the project development period. Also the authors are grateful for the feedback offered by Florin Iov, who was their Vestas contact.

# Contents

# List of Abbreviations

| | |
|---|---|
| DSO | Distribution System Operator |
| FACTS | Flexible AC Transmission Systems |
| FOC | Field Oriented Control |
| FSPC | Full Scale Power Converter |
| FSWT | Fixed Speed WIND Turbine |
| GTO | Gate Turn-Off |
| IEC | International Electrotechnical Commission |
| IGBT | Insulated Gate Bipolar Transistor |
| IGCT | Integrated Gate Commutated Thyristor |
| PCC | Point of Common Coupling |
| PLL | Phase Locked Loop |
| PM | Permanent Magnet |
| PMSG | Permanent Magnet Synchronous Generator |
| PSPC | Partial Scale Power Converter |
| PVS-WT | Partial Variable Speed Wind Turbine |
| RMS | Root-Mean-Square |
| SCIG | Squirrel Cage Induction Generator |
| SOGI | Second Order Generalized Integrators |
| STATCOM | Static Synchronous Compensator |
| SVC | Static Var Compensation |
| SVC | Static Var Compensation |
| SVM | Space Vector Modulation |
| TSC | Thyristor Switched Capacitor |
| TSO | Transmission System Operator |
| TSR | Thyristor Switched Reactor |
| VSC | Voltage Source Converter |
| VSWT | Variable Speed Wind Turbine |
| WF | Wind Farm |
| WP | Wind Power |
| WPP | Wind Power Plant |
| WRIG | Wound Rotor Induction Generator |
| WTG | Wind Turbine Generator |

# List of Figures

Chapter 1

# Introduction

*This chapter presents an introduction to the report. The project background is described in first section, then there is definition of problem statement along with project description, goals and limitations. In the end there is presented a short overview of chapters.*

## 1.1 Background in Wind Power

Today, modern energy industry faces a growing awareness regarding the impact of conventional power generation on the environment. Issues such as limited fossil fuel reserves, climate change due to $CO_2$ emissions, brings to attention alternative technologies to generate electricity in a more sustainable manner [4].

As global energy demand is constantly rising, there is a great responsibility for society to develop the green technologies for reducing its impact on the environment. In the trend of diversifying the energy market, wind power is the most rapidly growing sector. After the oil crisis from three decades ago, wind power industry started to flourish. Since then wind turbine technology improved rapidly and it soon took the title of champion from all renewable sources of energy.

According to Global Wind Energy Council more than 160 GW of installed capacity has been achieved by the end of 2009 around the world. Also a total power increase of 35% is accomplished in the year 2009 in the world.Thus a new record per annum of installed wind power capacity has been reached, summing up in 38 GW around the world. Europe accounts for 50% of the total amount of installed Wind Power around the world [5]. Figure 1.1 shows the continuously growing trend of wind power installations inside European Union. This reference scenario shows that with installations of up to 300 GW by the year 2030, EU will have a 21% to 28% wind market penetration [2].

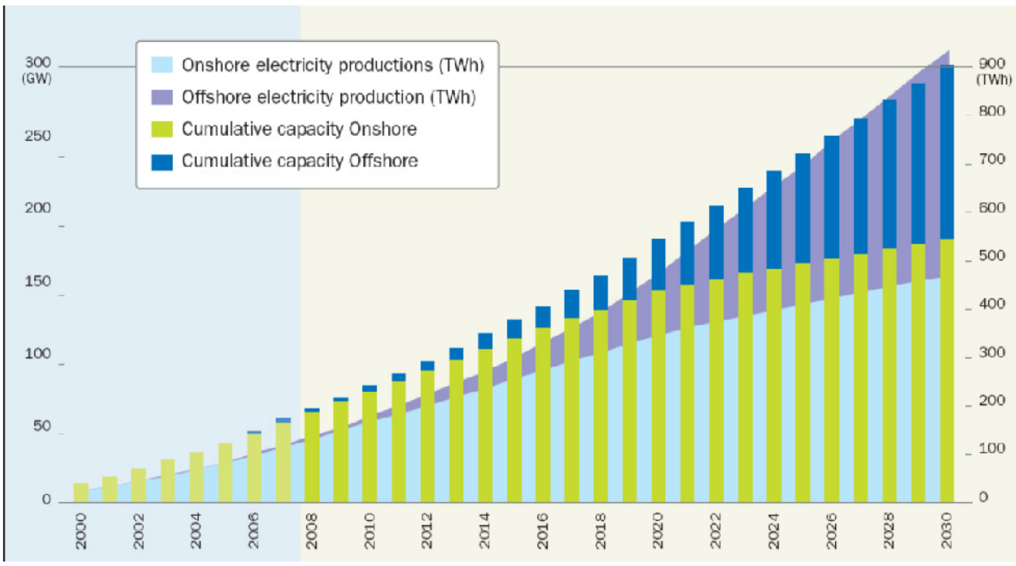


Figure 1.1: EU Wind Power Forecast for 2030 [1].

Along with the increasing demands for wind power, the turbine technologies are improving and thus equipment costs are reducing. Because the wind industry is a well established powerhouse on the renewable market, its prices per kWh are comparable with prices of the conventional energy generations. Unlike gas, coal and oil resources which in future will become scarce, and for which the technologies became mature decades ago, the wind energy is abundant and new improvements on aerodynamics and power electronic devices are still to come. Therefore by 2030 electricity production from wind will inevitably become cheaper than any other source of energy, currently having a high market share [2].

There is a good correlation between wind turbines costs and their sizes. Unlike solar panels, which remain at the same price regardless of array size, wind turbines become cheaper with increased system size. The practical explanation is that the power delivered by the wind turbine depends on the square of the rotor diameter. Figure 1.2 shows the evolution of wind turbine size with respect to year of production. It is seen that in the last 20 years the rotor diameter has increased by a factor of 10. Today state-of-the-art wind turbines, with 126 m for rotor diameter, produce 5 to 6 MW of power (from REPower and Enercon manufacturers [6]).

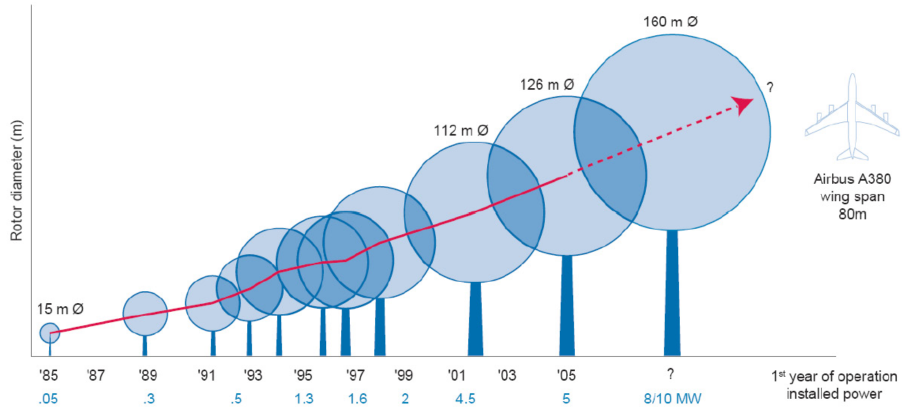


Figure 1.2: Increase of wind turbine size over the years [3].

In order to better control more and more wind power fed into the network, these MW range wind turbines are usually connected together either onshore or offshore to form a wind farm. However, including larger (hundreds of MW) wind farms into the grid, will rise the wind power penetration to a point at which it will have a significant impact on power system operation. Already some regulatory tasks needed for system stability, are being performed by wind power plants. With the ever increasing of wind power in the energy mix, Transmission System Operators (TSO) are forced to impose new requirements on the wind farms for the well-functioning of the power system network.

## 1.2 Problem statement

To ensure the stability of the system, regarding power quality and voltage level, all the grid codes demand that the Wind Power Plant (WPP) must be able to produce reactive power at the point of the common coupling (PCC). When dealing with WPP, adding the reactive power capability of each individual WT may not be sufficient to comply with the grid codes. This is due to the losses in connection cables and line losses between WPP and PCC. One solution is to use an external reactive power compensation, for example installing static synchronous compensator (STATCOM) at the PCC. The main objective of this project is to develop a reliable control strategy for WPP and STATCOM and investigation of the impact of the connection cable length on reactive power losses during steady state.

## 1.3 Project description

To fulfill the main goal of the project some basic considerations have to be stated. Modeling of the system will be done in MATLAB Simulink software. The following models are taken into account: wind model, rotor model, drive train model, permanent magnet synchronous generator (PMSG) model, converter models, STATCOM model, connection line model. Development control strategy for STATCOM and one control method for machine and grid side converter will be performed. The WPP will be simulated as an aggregated model. Figure 1.3 presents discussed concept. To verify obtained simulation results, experiments will be carried out using the dSPACE platform.

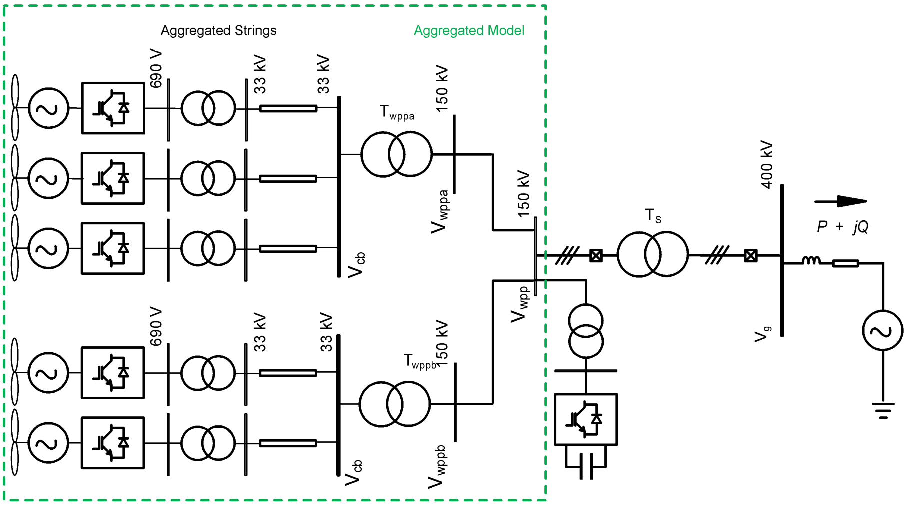


Figure 1.3: Simulated system.

The system will be emulated by two controlled voltage source converters. One of the VSC will represent the WPP and the other one will reproduce static synchronous compensator. Implemented laboratory setup is presented on Figure 1.4.

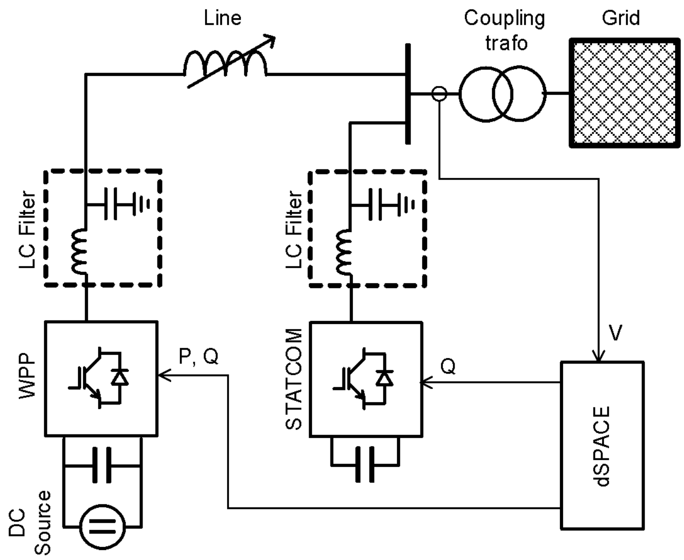


Figure 1.4: Laboratory system diagram.

## 1.4 Goals and Limitations

The goals of this thesis are:

- understanding the role of FACTs in WP application
- review of state-of-the-art in regards to the grid codes for WPP applications
- building a model with two VSC , first emulating the WPP and second the STATCOM
- verification of the built model and successful implementation in the laboratory
- extending research for large scale WPP analysis - investigation in terms of simulations
- study of the impact of the connection line of WPP on reactive power capability
- verification if obtained performances comply with the grid codes

This project is limited by several different factors:

- no literature describing VSC based STATCOM support for WPP with PMSG
- setup limitation - only two inverters are available instead of having a generator with full scale converter and STATCOM
- having a strong, stiff grid results in small range of impact on the grid voltage magnitude
- small power ratings of the converter - inability to use the entire power due to the supply safety protection
- the simulated VSC models, by means of mathematical equations, are ideal and thus switching losses or harmonic generation are not taken into consideration
- the $C_p$ curve for the 2MW WT was not available, therefore an approximation of the curve is made as stated in [11]
- the exact parameters for 2MW PMSG and 2MVAr VSC based STATCOM were not available, thus an approximation is made
- the connection cables between specific WT in WPP are not taken into consideration
- The WPP is modeled as an aggregated model. This means that WPP is actually modeled as a one wind turbine. As stated in the literature [11] this approach is reasonable if one is interested in power flow studies

## 1.5 Project outline

The project studies the control of STATCOM for WPP applications and the presented report is structured in six chapters.

- The first chapter may be seen as an introduction to the wind energy and discussions about the recent problems facing grid connection of large state-of-the-art WPP's. The chapter is followed up by the problem formulation and the objectives of the current project. The project limitations are also presented.
- The second chapter presents an overview of grid codes in Denmark (Energinet.dk) and Germany (EON.Net). The focus is made on reactive power / voltage control for WPP's connection to the grid. Furthermore, a presentation of the four main WT topologies in the market, highlighting their specific problems in regards to grid connection.

- The third chapter focuses on the Flexible AC Transmission System (FACTS) devices used in WPP applications. It describes the Static Var Compensator (SVC) as one of the most widely used in power systems, and the recent Static Synchronous Compensator (STATCOM) as one of the more advanced shunt devices used in power systems for var compensation.
- In Chapter 4 a presentation of the modeled system is given. First, a small scale system was modeled for purpose of laboratory implementation and validation. Next, a large scale model is built for the purpose of expanding the results to a real system with large WPP and STATCOM. Each of the components for modeling both the small scale system and the large scale system are described. Afterwards, the control methods used for the inverter emulating the WPP and for the inverter, representing STATCOM, are presented.
- Chapter 5 describes the study cases obtained from the simulations performed for all three modeled systems.
- In the last chapter the conclusions of the project are presented and also ideas for future work are proposed.

Chapter 2

# Grid codes requirements for Wind Power

*This chapter presents the grid codes requirements regarding the Wind Power along with the WPP capabilities to fulfill those demands.*

In earlier years of the wind power industry most individual wind turbines or first small wind farms were connected to distribution networks. Because the levels of integration were very small at that time, TSO's regarded connected wind turbines as negative loads. But as larger wind turbines were merging into wind farms with sizes starting to reach comparable levels with conventional power plants, TSO's concern grew due to power quality and network stability problems. As a result, based on a number of parameters, such as grid stiffness, transmission voltage levels, wind turbine topology, TSO's issued a number of requirements for wind turbines to fulfill in order to get grid connection agreement. These requirements were called grid codes, and they became more demanding as wind penetration levels grew and regional specific as well.

## 2.1 Grid codes

The grid codes regarding Wind Power are country specific. However each of the TSO's issue a number of different requirements. Some of them are described below in the following manner. First the active power regulations are issued, then the next section presents reactive power requirements. The third section explains the various control parameters for voltage quality assessments. Next the operation during grid disturbances is pointed out. The section regarding the reactive power is emphasized and demonstrated in a deeper manner due to its biggest relevancy to the project topic.

### 2.1.1 Active power regulation

The active power/frequency control demands that the active power deviation around actual output should stay in accordance with a voltage/frequency diagram stated in grid codes [22]. Several regulation techniques are defined in the grid codes. A power/frequency characteristic, or droop characteristic controls the slope of active power production. This control shall be adjusted according to TSO demands. Due to the fact that the active power regulation is not the topic of discussion of this report it will not be further investigated.

### 2.1.2 Reactive power regulation

Nowadays the WPP are required to be able to fulfill the reactive power and voltage control demands. Due to the current penetration level of Wind Power in the grid WPP must provide the reactive power exchange with the grid. The exchange rate and level is specified by the TSO. The given range defines for each operation set point the minimal amount of reactive power (lagging or leading) in respect to produced active power. Danish grid code states that wind farms need to control reactive power at PCC inside the narrow band along the rated value.The reactive power averaged over 10 seconds should be kept in the control band as in figure.In the Figure 2.1 it is stated that a WPP should be capable of producing reactive power of up to 10% from its rated active power generation. Also in case no active power is generated the WPP may consume no more 0.1 pu. reactive power. Figure 2.1 shows the Danish WPP requirement concerning reactive power flow at point of connection.

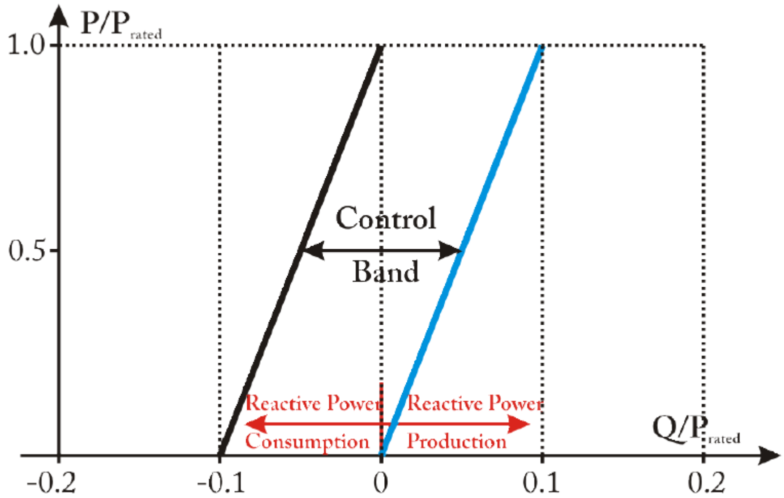


Figure 2.1: Reactive power control.

In Germany each new power generating unit connected to the grid must be able to meet the requirements presented in Figure 2.2. This figure shows one of the three possible variants of TSO demands. TSO selects one of the versions on the basis of relevant network characteristics.

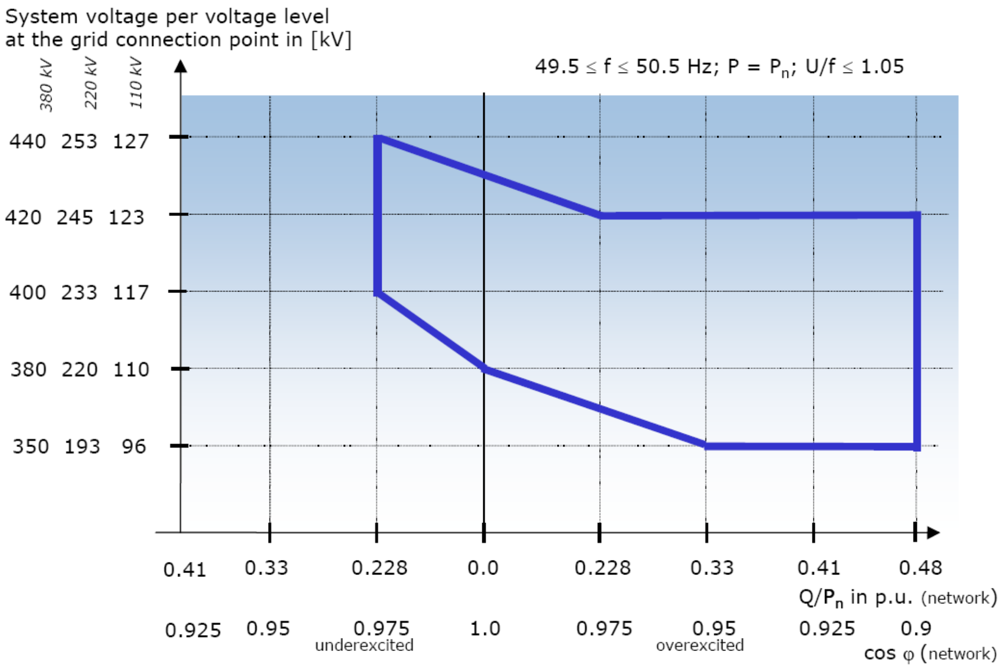


Figure 2.2: Basic requirement upon the network-side supply of reactive power from generating units to the network [22].

Additionally the German grid codes request the WPP to exchange the reactive power with the grid also below the rated active power production level. Figure 2.3 presents the largest reactive power range, which should be covered, along with the associated voltage band. The x axis displays the reactive power which should be supported in relation to the operational installed active power in percent. The y axis displays the instantaneous active power (in the consumer meter arrow system negative) in relation to the available installed active power in percent.

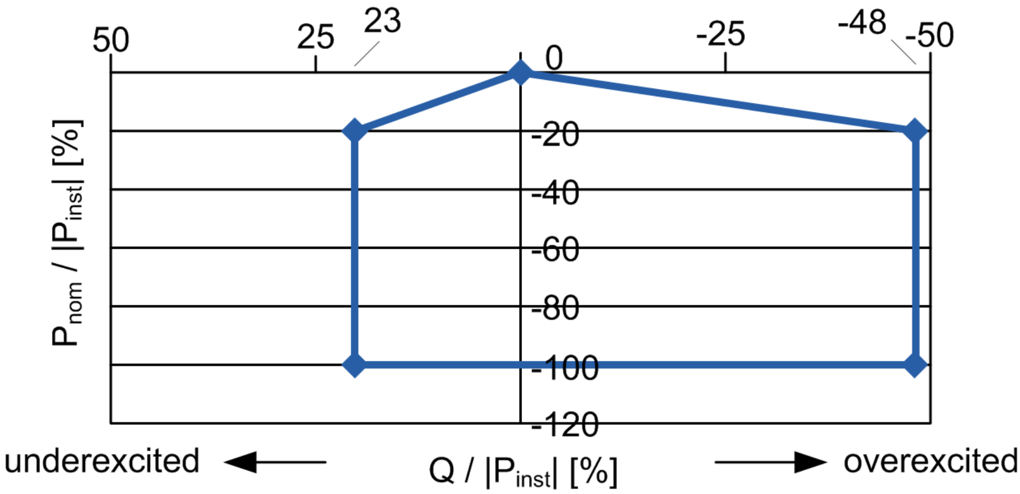


Figure 2.3: PQ diagram in the consumer meter arrow system for Figure 2.2 at 400-420 kV / 233-245 kV / 117-123 kV [22].

Some of the TSO's constrain the transition between operating set points with a certain time limit. For example in Germany E.On gives maximum time for getting to a new set point equal to 4 minutes [22].

### 2.1.3 Voltage quality

In every national grid codes a set of requirements are imposed to cope with problems arising due to rapid voltage changes/jumps, voltage flicker and harmonics. These requirements are more important on medium voltage levels, especially where the wind power penetration level is high.

Rapid voltage changes refer to sudden increase/decrease in the value of RMS voltage at the PCC. In the Danish grid codes a basic requirement for voltage jumps is that the deviation value cannot exceed 3.0% at the PCC[10].

Flicker is a term used for defining the unsteadiness of visual sensation in the light source, cause by voltage fluctuations. These variations occur due to switching of capacitors, lines, cables transformers etc. in the system. The voltage fluctuations in a Danish transmission system shall not exceed 3.0% in time frames of several hours and 1.5% in time frames of minutes.

For harmonic disturbance the indicator $D_n$ denotes the level of distortion for each individual harmonic:

$$D_n = \frac{U_n}{U_l} \times 100\% \tag{2.1}$$

Which should be less than 1.0% at PCC for every 1<n<51 The total harmonic effective distortion (THD) is defined as:

$$THD = 100\sqrt{\sum_{n=2}^{50}\left(\frac{U_n}{U_l}\right)^2} \quad \% \tag{2.2}$$

and it should have a value less than 1.5% at PCC.

### 2.1.4 Operation during grid disturbances

During the fault period WPP's are requested to restore the voltage level back to the nominal value at connection point by injecting required amount of reactive current. Modern WPP's are not allowed to disconnect during a grid fault as long as voltage at the connection bus is not lower than the voltage profile stated in the codes. In the Danish grid codes a description of the events for which WPP must remain connected to the grid is enumerated [10]. Parameters of interest are mentioned in [10] to be RMS values of current, active and reactive power in the PCC and the voltage variations. The reactive power regulation system is required to change from normal voltage to maximum voltage support during a grid fault.

The German TSO (E.ON) gives the maximum time of 1.5 seconds for the voltage recovery up to 90% of its rated value. E.On states that in symmetrical three-phase faults with high voltage dips, at least 1.0 pu. reactive current should be achievable [22].

## 2.2 Wind turbines capabilities with respect to grid codes

There are four basic wind turbine topologies on the market (Figure 2.4). Each of them can be categorized into either fixed speed wind turbines or variable speed wind turbines. The advantages and disadvantages of each topology in respect to grid connection are highlighted below.

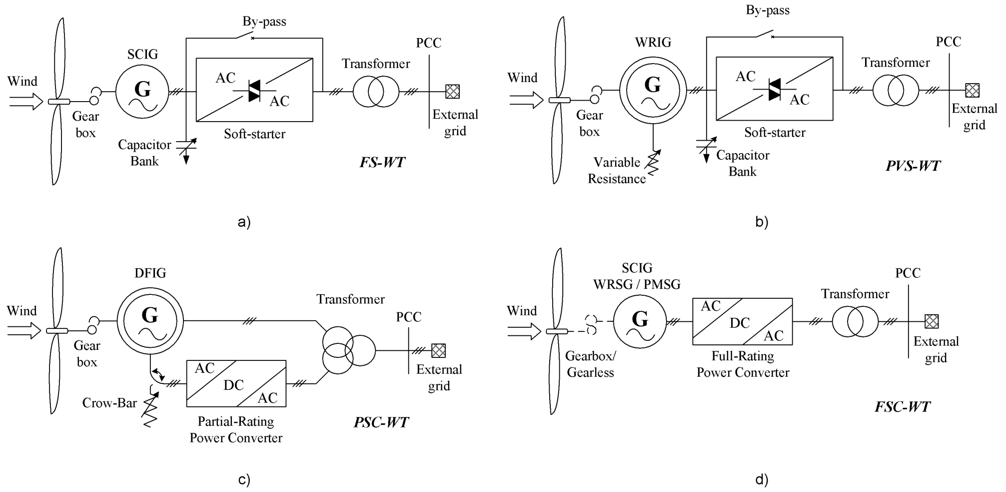


Figure 2.4: Wind turbine concepts a)FSWT b)PVS-WT c)DFIG d)FRPC [9].

Fixed Speed Wind Turbine ((FSWT in Figure 2.4a) is a concept that uses a Squirrel Cage Induction Generator (SCIG) directly connected to grid. Therefore the speed of this WT is fixed by the grid frequency. Due to this fixed speed, the wind fluctuations are converted in power fluctuations which will cause voltage variations in weaker grids. Having large numbers of FSWT in a wind farm connected to grid, the reactive power consumption will be large. This reactive power can be compensated by adding capacitor banks to each individual WT, for achieving a PCC power factor close to unity. This type of WT lacks power electronic interfaces, therefore reactive power control is not possible. The tracking of optimum active power and assuring power quality cannot be fulfilled. In case of a grid fault there is a large amount of fault current contribution, thus the turbines need to rely on protection devices (overcurrent, over- and undervoltage, over- and underfrequencies). As a result FSWTs cannot meet grid code demands without any form of external support such as FACTS devices.

Second type of wind turbine is the Partial Variable Speed Wind Turbine (PVS-WT in Figure 2.4b) with a variable rotor resistance. The generator for this turbine topology is a Wound Rotor

Induction Generator (WRIG) and like in the previous case, it is connected directly to the grid through a soft-starter. As a result, this type of wind turbine offers again low performances with regards to grid codes. A small improvement can be noticed during grid disturbances by connecting the variable resistance in series with the rotor winding. This will allow the increase of speed in the range of 0-10% above synchronous speed. A grid code problem regarding flicker is significant for the first two WT topologies, especially if the WPPs are connected to weaker grids.

The third wind turbine concept is the Variable Speed Wind Turbine (VSWT) with Partial Scale Power Converter (PSPC) shown in Figure 2.4c. It uses a Doubly Fed Induction Generator (DFIG) with the stator connected to the grid and the rotor speed is controlled by a partially scaled power converter (often a bidirectional power converter). This capability will allow a speed variation in the range of +/- 30% of the synchronous speed. Here the reactive power exchange is controlled by the grid-side converter, but the control is limited due to the partial rating of the converter. Therefore, in large WPP based on this concept if the grid is not stiff enough, additional reactive power support will be required from external sources. This concept in case of grid faults contributes to the fault current but for very short period because the control of the converter detects fast the voltage drop and disconnects the unit.

The last wind turbine concept is the VSWT with Full Scale Power Converter (FSPC) shown in Figure 2.4d. More than one generator type can be supported by this concept, in any case the controllability is much improved, being able to control active and reactive power in widest ranges. The variable speed WT do not contribute to the fault currents due to the converter topology. One drawback which can be mentioned for both third and fourth WT concepts is that with the use of power converter, they will be the main source of harmonics, therefore filtering devices are needed. In VSWT flicker is not a problem due to the existence of the energy buffer between generating unit and grid. As a conclusion this type of wind turbine will be capable of meeting the most severe grid codes issued by TSO's.

## 2.3 Summary

In this chapter a review of grid codes for wind power in Denmark and Germany was made, highlighting the important requirements relevant to reactive power control and power quality. These requirements shall be met by modern WPPs or by installing an external reactive power compensation device. The report focuses on the German grid codes because they impose stringent requirements on connected WPPs.

Grid impacts of each of the main four WT topologies in the market were discussed. The report chooses the fourth topology of FSPC with PMSG. This is a new and still improving topology, and so far the literature has not covered the impacts of large FSPC based WPPs with STATCOM on grid stability.

Chapter 3

# Overview of FACTS controllers for WP Technology

The basic limitations in power system transmission such as distance, stability, effective power flow and cable loading limits led to the investigation of power electronic devices into power systems and their impact on reactive power compensation. Thus Flexible AC Transmission System (FACTS) devices were introduced as a solution for ameliorating the power system performance. Development of this technology was based on the same principle as in traditional power system controllers (i.e. phase shifting transformers, passive reactive compensation, synchronous condensers etc.)[7].

Growing capabilities of power electronic components resulted in creation of controllers with much faster response times, due to their lack of mechanical switch inertias. Lower transient overvoltages are accomplished when using semiconductor devices, also a smooth, gradual change in var output is made, compared to the large discrete steps that arise from mechanically switching in capacitor and/or reactor banks. FACTS controllers using semiconductor devices are the fastest option for obtaining maximum system benefits. Also the usage of semiconductor switches instead of mechanical switches, led to an increased life-time of the system by less maintenance. The drawback of this technology is that it is more expensive than the traditional methods.

As can be seen in Fig. 3.1 FACTS devices can be divided into two subgroups. Old generation was based in thyristor valve idea and the new generation focuses on using the voltage source converter. In both cases corresponding solutions provide similar services. The main difference between those two categories is that VSC technology is much faster and has a bigger range of control [8].

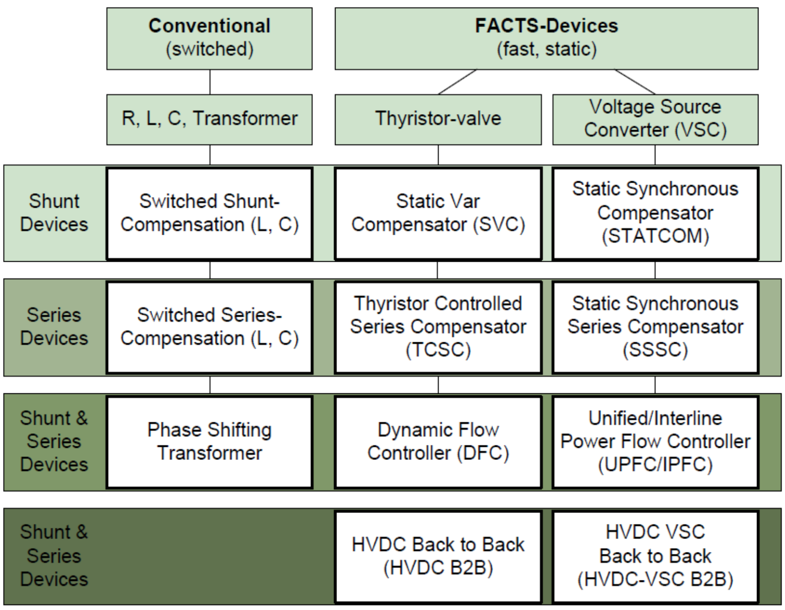


Figure 3.1: Overview of major FACTS devices [8].

Eventually FACTS devices found applicability in the wind power industry. It was found that providing earlier WPP's with some external reactive compensation devices such as SVC or STATCOM, the grid compliance can be met, and thus the WPP's could remain connected to the power system without stability risks.

Different way to categorize the FACTS controllers is to group them in a way that they are connected to the power system:shunt, series or shunt-series connection. This project focuses on FACTS device applicable for Wind Power(WP) technology. In the following section the shunt FACTS controllers used for Wind Turbines are presented.

## 3.1 Static Var Compensator - SVC

SVC's being dated from early 70's, have the largest share among FACTS devices. They consist of conventional thyristors which have a faster control over the bus voltage and require more sophisticated controllers compared to the mechanical switched conventional devices. SVC's are shunt connected devices capable of generating or absorbing reactive power. By having a controlled output of capacitive or inductive current, they can maintain voltage stability at the connected bus.

Figure 3.2 shows these configurations: the Thyristor Controlled Reactor (TCR), the Thyristor Switched Reactor (TSR) and the Thyristor Switched Capacitor (TSC) or a combination of all three in parallel configurations. The TCR uses firing angle control to continuously increase/decrease the inductive current whereas in the TSR the inductors connected are switched in and out stepwise, thus with no continuous control of firing angle.

Usually SVC's are connected to the transmission lines, thus having high voltage ratings. Therefore the SVC systems have a modular design with more thyristor valves connected in series/parallel for extended voltage level capability.

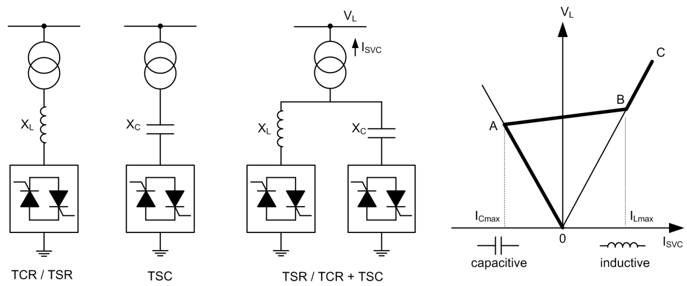


Figure 3.2: SVC configurations and its $I - V$ characteristic.

To provide the needed reactive power generation/consumption in the network SVC's adjust the conduction periods of each thyristor valve. For an SVC consisting of one TCR and one TSC, assuming that both reactor and capacitor have same pu. ratings then the following scenarios can occur:

- Reactive power is absorbed when the thyristor valve on the reactor leg is partially or fully conducting and the capacitor leg switch is off.
- Reactive power is generated when the thyristor valve on the reactor leg is in partial or no conduction mode and the capacitor leg switch is on.
- No reactive power is generated/absorbed if both the thyristor valve is not conducting and the capacitor switch is off.

The voltage-current (V-I) characteristic of an SVC with the two operating zones is shown in Figure 3.2. A slope around the nominal voltage is also indicated on the V-I characteristic, showing a voltage deviation during normal operation, which can be balanced with maximum capacitive or inductive currents. As the bus voltage drops, so does the current injection capability. This linear dependence is a significant drawback in case of grid faults, when large amount of capacitive current is needed to bring back the bus nominal voltage.

The technology of SVC with thyristor valves is becoming outdated mainly due to the slow time responses, of injected current dependence on bus voltage and low dynamic performance. Their replacements are called Static Synchronous Compensator's (STATCOM) and will be discussed in the following section.

## 3.2 Static Synchronous Compensation - STATCOM

Another way to enhance a Wind Power Plant with ability to deliver or absorb reactive power from the grid is to use Static Synchronous Compensation. STATCOM can be treated as a solid-state synchronous condenser connected in shunt with the AC system. The output current of this controller is adjusted to control either the nodal voltage magnitude or reactive power injected at the bus. STATCOM is a new breed of reactive power compensators based on VSC. It has a characteristics similar to a synchronous condenser, but because it is an electrical device it has no inertia and it is superior to the synchronous condenser in several ways. Lower investment cost, lower operating and maintenance costs and better dynamics are big advantages of this technology [8].

### 3.2.1 Power semiconductor devices

STATCOM consists of one VSC with a capacitor on a DC side of the converter and one shunt-connected transformer. Voltage Source Converter is usually built with Thyristors with turn-off capability like Gate Turn-Off (GTO) or today Integrated Gate Commutated Thyristors (IGCT) or with Insulated Gate Bipolar Transistors (IGBT) based converter. Configuration of the STATCOM circuit is presented on Fig. 3.3.

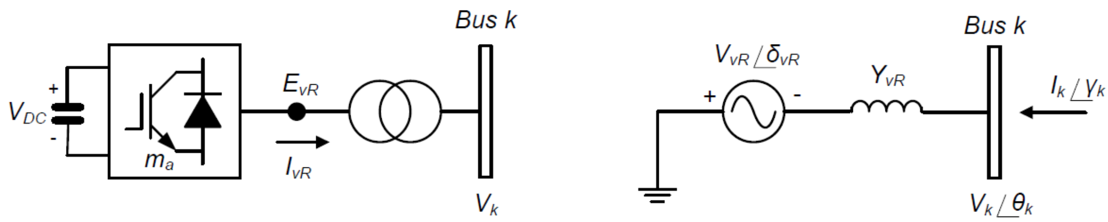


Figure 3.3: STATCOM scheme with equivalent circuit representation.

### 3.2.2 Operation principle

As it was mentioned before STATCOM can be treated as a synchronous voltage source, because its output voltage can be controlled as desired (Fig. 3.3). Assuming that no active power is exchanged between STATCOM and the grid (lossless operation) the voltage of the controller is in phase with the grid voltage. If the compensator voltage magnitude is smaller than the voltage at the connection node current will flow from the grid to STATCOM. In this case the reactive power will be consumed. If the situation is opposite the reactive power will be delivered to the grid. Schematic representation of this principle is presented using phasor diagrams on Fig. 3.4

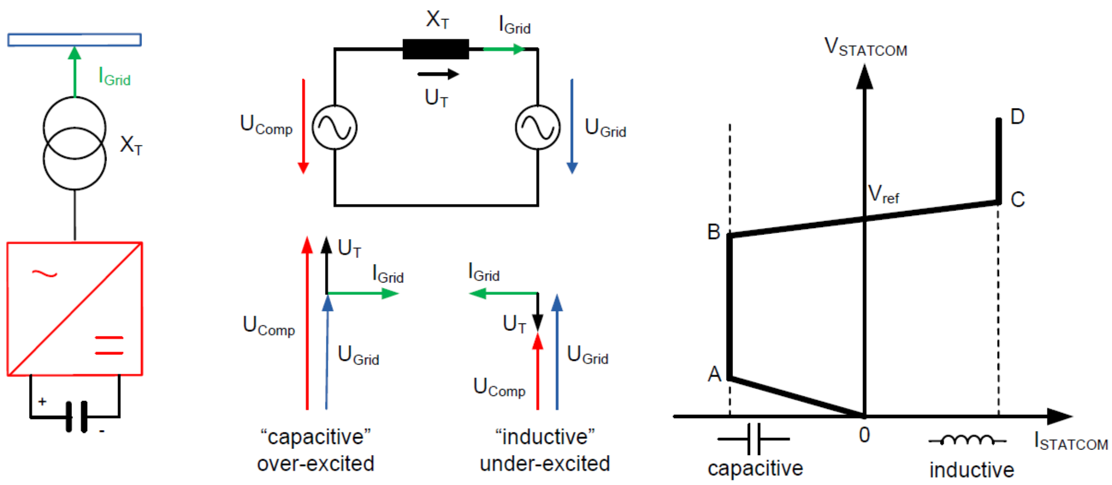


Figure 3.4: Schematic representation of working principle of STATCOM.

A STATCOM injecting reactive current is supporting the grid voltage. Comparably when STATCOM is absorbing reactive current it is decreasing the grid voltage. In the first case controller behaves as an overexcited generator or capacitor and in the second case STATCOM behaves as an under excited generator or inductor. According to [8] the power flow constraints of STATCOM are:

$$P_{sh} = V_i^2 g_{sh} - V_i V_{sh}(g_{sh} cos(\theta_i - \theta_{sh}) + b_{sh} sin(\theta_i - \theta_{sh})) \tag{3.1}$$

$$Q_{sh} = -V_i^2 b_{sh} - V_i V_{sh}(g_{sh} sin(\theta_i - \theta_{sh}) - b_{sh} cos(\theta_i - \theta_{sh})) \tag{3.2}$$

where $V_i$and $\theta_i$ are the voltage and the angle of the bus to which STATCOM is connected, $V_{sh}$ and $\theta_{sh}$ are the voltage and the angle of the synchronous voltage source (STATCOM) and $g_{sh} + jb_{sh} = 1/Z_{sh}$.

### 3.2.3 Control modes

The control of reactive power flow provided by STATCOM can be realized in one of the following control modes.

#### Reactive power

This type of control strategy focuses on reactive power injection to the local bus, to which the STATCOM is connected, according to a reference from the wind park controller. Mathematically, such a control constraint is described as follows:

$$Q_{sh} - Q_{sh}^{Spec} = 0 \tag{3.3}$$

where $Q_{sh}^{Spec}$ is given reference signal, $Q_{sh}$, which is described by equation (3.2) is the actual reactive power.

#### Voltage droop characteristic

In this type of operation STATCOM works in a way to fulfill a voltage/reactive power slope characteristics. This is done by setting a target voltage accepted from wind park controller at the PCC. The control constrain goes as follows:

$$V_i - V_i^{Spec} = 0 \tag{3.4}$$

where $V_i^{Spec}$ is a control reference signal.

**Power factor**

This mode provides control of the power factor at e.g the point of connection of the WPP. This done by realizing control constrain as follows:

$$Q_{ref} - Q_{PCC} = 0 \tag{3.5}$$

Where $Q_{PCC}$ is the measured reactive power at PCC, and $Q_{ref}$ is the reference signal calculated form equation presented below:

$$Q_{ref} = \sqrt{S^2 - P_{PCC}^2} = \sqrt{\frac{P_{PCC}^2}{cos^2\phi_{ref}} - P_{PCC}^2} \tag{3.6}$$

where $P_{PCC}$ is active power at the point of common coupling and $cos\phi_{ref}$ is desired reference power factor.

## 3.3 Applications

The growing penetration of produced wind power (size growth of wind farms) forced the TSO and DSO to develop more strict and detailed grid codes for wind turbines. The new grid codes specify new requirements for WPP regarding such issues as frequency control, voltage control and fault ride-through behavior. This thesis deals with reactive power compensation, which in practice influences the voltage control. Besides its main role, which is voltage regulation, STATCOM applications include the following:

- stabilization of weak system voltage
- reduced transmission losses
- enhance transmission capacity
- power oscillation damping
- improve power factor
- reduce harmonics
- flicker mitigation
- assist voltage after grid faults

### 3.3.1 Retrofitting case

STATCOM can be widely used for retrofitting old wind turbines or WPP which are not able to comply with new strict grid codes. This can be done by adding static synchronous compensation alone or with a battery storage.

### 3.3.2 New WPP case

In case of new WPP reactive power control can be done to some extend by single wind turbines. However, even new designs are limited with the respect to the newest requirements given in grid codes. Therefore some additional reactive power compensation is needed. STATCOM is a good example of such additional control.

## 3.4 Summary

The following table summarizes the main characteristics of the most important shunt Var compensators. The significant improvements observed in the STATCOM devices, makes them a first choice for improving the performances in AC power systems.

| | SVC | | |
|---|---|---|---|
| | **TCR** | **TSR (+TCR)** | **STATCOM** |
| Compensation Accuracy | Very Good | Good (very good with TCR) | Excellent |
| Control Flexibility | Very Good | Good (very good with TCR) | Excellent |
| Reactive Power Capability | Lagging/Leading indirect | Leading/Lagging indirect | Leading/Lagging |
| Control | Continuous | Discontinuous (cont. with TCR) | Continuous |
| Response Time | Fast, 0.5 to 2 cycles | Fast, 0.5 to 2 cycles | Very Fast |
| Harmonics | Very high (large size filters are needed) | Good (filters are necessary with TCR) | Good, but depends on switching pattern |
| Losses | Good, but increase in lagging mode | Good, but increase in leading mode | Very good, but increase with switching frequency |
| Phase Balancing Ability | Good | Limited | Very good with 1-f units, limited with 3-f units |
| Cost | Moderate | Moderate | Low to moderate |

Table 3.1: Comparison between SVC and STATCOM [34].

Chapter 4

# System modeling and Control

*In this chapter a description of investigated systems is presented. Two systems models were developed - the small scale system model and the large scale system model. Afterwards the control principles for STATCOM and WPP are presented and discussed. Next section describes the Q-capability performance of a WPP with regards to the grid codes. The last part of the chapter explains the developed reactive power distribution algorithm.*

## 4.1 Small scale system model

Small scale model is created for having a possibility to perform experimental verification of investigated ideas. It is built in MATLAB Simulink using the PLECS toolbox and after validation it is implemented in laboratory. This model is simplifying the concept of WPP and STATCOM. The approaches taken into consideration are presented below.

### 4.1.1 Wind Power Plant

For small scale system WPP was modeled as an VSC with IGBT switches. The VSC is supplied from a constant DC source and the output active power is set to a constant value. An LC filter is placed at the output of the converter. The use of an VSC with an LC filter allows you to generate sinusoidal voltages at the output with low harmonic distortion. All the details regarding the model are presented in the Appendix A.1.

### 4.1.2 Transformer and cable

The model of the transformer is simplified to an inductance and resistance. This is due to the fact that in the simulation and in experimental setup the PCC was placed on the primary windings of the transformer. The cable emulating line connection of the WPP to the PCC is modeled as a variable inductor placed between the output of WPP filter and primary winding of the transformer. A detailed description of the model can be found in Appendix A.2.

### 4.1.3 Grid model

For the simulation purposes grid is modeled as a controlled three-phase voltage source having small inductance and resistance. A detailed description of the model can be found in Appendix A.3.

### 4.1.4 STATCOM model

For small scale system STATCOM is modeled as an VSC with IGBT switches. The modeling is done in the same manner as in case of WPP small scale system model. The only difference is that STATCOM is not supplied from a DC source, but it has an internal capacitor which has to be charged at the beginning. All the details regarding the model are presented in the Appendix A.1.

## 4.2 Large scale system model

Large scale model is a representation of actual large WPP system. In this approach focus is emphasized on modeling of every component of a single wind turbine. The rated power of the turbine is set to 2 MW and the rated power of STATCOM was set to 2MVAr. The parameters used for modeling of the turbine are taken from the data sheet of VESTAS V80 2 MW turbine. After validating the modeled WT an aggregation was performed according to the method presented in [11].

### 4.2.1 Wind Turbine Model

For WT modeling, a turbine with PMSG is chosen. This model is based on the fourth WT topology presented in the Figure2.4 in the section 2.2 The built WT model consists of several elements: wind, rotor, drive train, generator, full scale converter. Short description of each element is presented below.

#### Wind model

The wind model developed for purpose of simulation of Wind Power Plant is based on [11] and [12]. A model that can generate wind speed sequences, with characteristics to be chosen by the user is developed. The ability that allows to choose the data for the main wind components makes this model flexible. A detailed description of the model can be found in Appendix A.4.

#### Rotor model

Created rotor model has a property to be a model for VSWT or a model for FSWT. Most of the rotor model are using lookup tables with power coefficient curves. This one is using a general approximation of the power curves based on mathematical equation. A detailed description of the model can be found in Appendix A.5.

#### Drive train model

The drive train is modeled as a two-mass model with a single stage gearbox. The model itself is a simplified two-mass model with several assumptions. A detailed description of the model can be found in Appendix A.6.

#### Wind Turbine Generator

WTG as a core in a wind energy conversion system has to be chosen very carefully. As it is explained before in section 2.3 the chosen machine was a PMSG with a full scale converter. A detailed description of the model can be found in Appendix A.7.

#### Full scale converter model

According to [20] the wind turbines with a full-scale power converter between the generator and the grid give a better technical performance. Nowadays back-to-back Voltage Source Converter (VSC) is the most used topology in the wind turbine industry. Although there are several possible systems incorporating a full scale converter, this project is only interested in architecture involving a PMSG. A detailed description of the model can be found in Appendix A.8.

#### Aggregated WPP model

Aggregated WPP model containing collective response of the many wind turbines at rated operation will be represented by a single machine equivalent operating at the optimum set point [11]. A detailed description of the model can be found in Appendix A.9.

### 4.2.2 Grid model

For modeling the grid a symmetrical three-phase voltage source having an inductance and resistance is used. A detailed description of the model can be found in Appendix A.10.

### 4.2.3 STATCOM model

STATCOM was modeled as VSC based on signal model presented by [12]. The approach is very similar as in case of modeling of full scale converter for WT. A detailed description of the working principle can be found in Appendix A.8.

## 4.3 Wind turbine control

The project deals with a variable speed, variable pitch FSPC WT. The main circuit and control block diagrams for the chosen WT topology, are presented in Figure 4.1. For variable speed operation, the WT uses a full scale back-to-back converter. The generator side converter is controlling the speed of the generator for maximum power extraction. The grid side converter controls the voltage on the DC-link and also the reactive power flow between the WT and grid. Another control for the WT is the pitch control. It is applied to the rotor blades and modifies the angle of attack of the blades so that the output power can be controlled during high wind speeds.

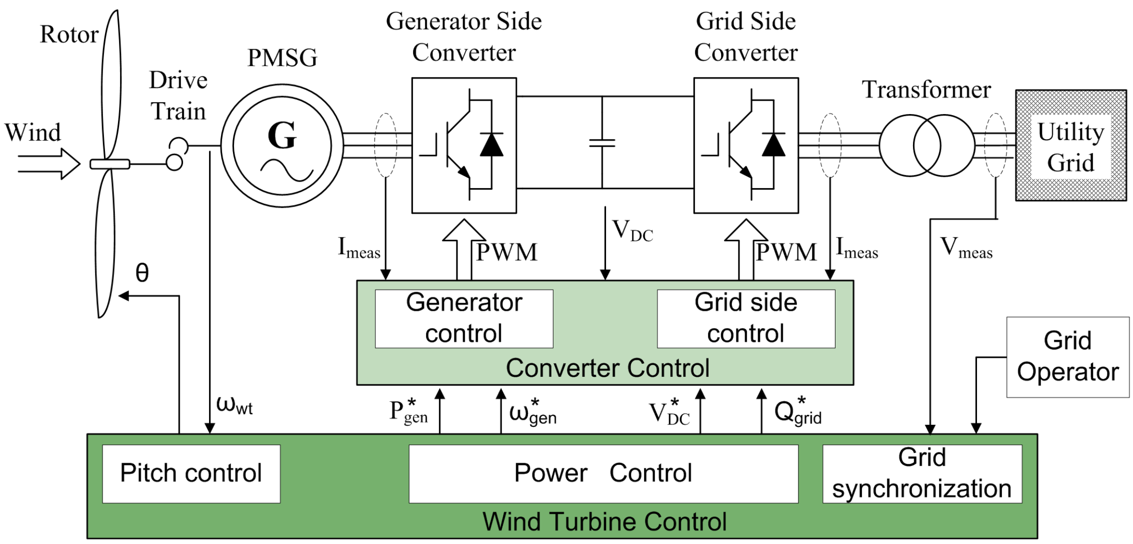


Figure 4.1: Control scheme of WT.

### 4.3.1 Generator side converter control

The generator side converter is controlled with the Field Oriented Control (FOC) strategy. The control scheme of this strategy is presented in Figure 4.2. Since this part of wind turbine control was the focus of last semester project, it will be only briefly described here. FOC is the most popular vector control method in electrical machines. In case of a PMSG, the electrical equations are transformed into a coordinate system which will rotate in synchronism with the permanent magnet flux vector $\Psi_{PM}$. The position information of the PM flux is required, which can be easily obtained by monitoring the rotor angle or speed, using an optical encoder.

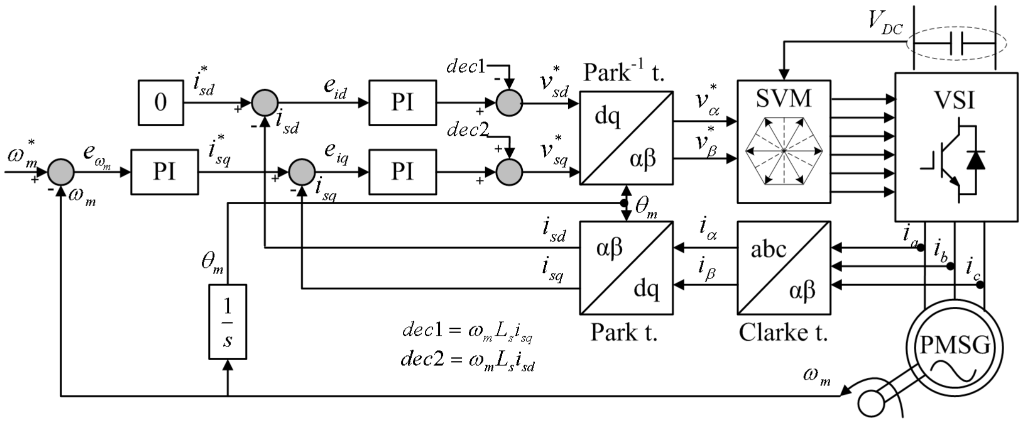


Figure 4.2: The Field Oriented Control for Generator Converter

FOC uses a current control method in the $dq$ synchronous reference frame and adjusts the generator speed to suit the wind speed. There are three PI controllers used in the strategy. Two of the controllers, which form the inner loops, regulate the $d$ and $q$-axis of the stator currents. The third controller in the external loop sets the speed reference. This reference is calculated from the optimal rotor tip speed ratio for getting maximum output power from each wind speed. To improve the accuracy of the control and obtain better performance, the $i_d$ and $i_q$ currents are decoupled. The outputs from the two current controllers are the $d$ and $q$-axis stator voltage references, which are sent to the space vector modulation (SVM) block. The SVM will generate the switching signals required by the transistors inside the converter.

### 4.3.2 Grid side converter control

The aim of the grid side converter control is to supply a reliable electric power to the consumers, following a specific set of parameters such as voltage, frequency and harmonic levels.

The developed control strategy is called Voltage Oriented Control (VOC) and the scheme of this strategy is presented in Figure 4.3. and as in Field Oriented Control strategy the transformation of $abc$ reference to $dq$ synchronous reference is implemented for an easier control. Also VOC control contains two cascaded loops. The inner loops independently control the grid $i_d$ and $i_q$ currents, while the outer loops control the DC-link voltage and the reactive power. The PI controllers are tuned using the method explained in Appendix C.1.

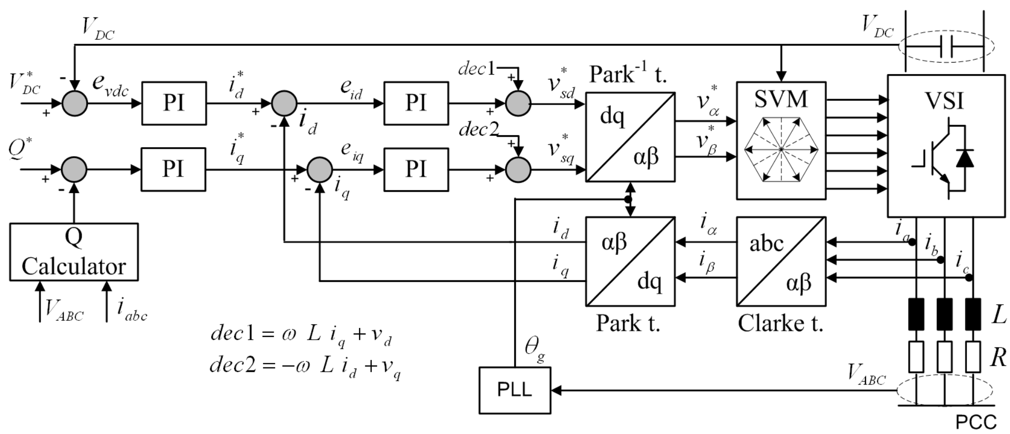


Figure 4.3: The Voltage Oriented Control for Grid Inverter

The grid side converter has to keep the DC-link voltage constant and control the power factor of the output electricity by adjusting the reactive power. Under normal conditions the wind turbine's reactive power output is controlled in +/- 0.1 pu. range (according to the Danish grid codes). In situation with grid disturbances the grid operator requires reactive power compensation and thus it can send a reactive power reference signal to the inverter control. As well as in FOC, at the outputs of the current controllers, the cross-coupling terms and voltage feedforward are added for improving the system performance. The resulted signals will be the $v_d^*$ and $v_q^*$ voltage references for the SVM method.

### 4.3.3 Grid synchronization

For synchronizing the output of the full scale converter of wind turbine Phase Locked Loop (PLL) algorithm is used. In the state of the art this is one of the most common techniques for phase detection. It has to be stated that there are many variations of this method. The algorithm presented below was used because it is suited for the synchronous $dq$ reference frame current control strategy (which was used for performing the experiments in the laboratory). The block diagram of the PLL implemented in Simulink is presented on the Figure 4.4:

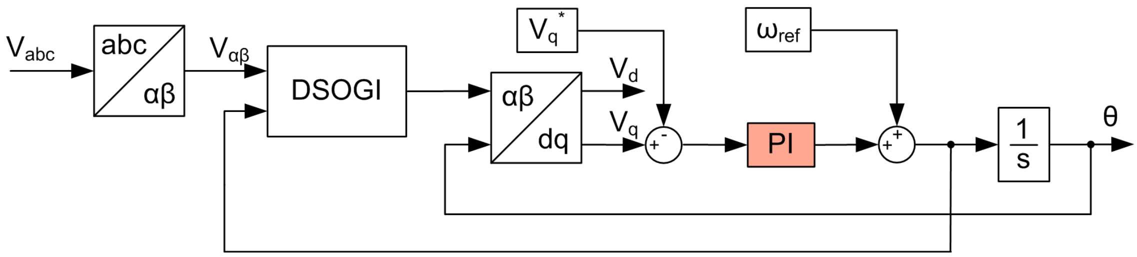


Figure 4.4: The structure of PLL.

The PLL makes use of a transformation module ($abc \rightarrow \alpha\beta$) and a structure based on two Second Order Generalized Integrators ($SOGI$) [13], [14], [15], [16], [17]. The structure of SOGI is presented in [18], [19].

The property of SOGI structure is filtering. As can be seen in Figure 4.4 the frequency signal provided by locking loop is fed back to SOGI, which leads to having a self adapting algorithm [17]. The dynamic of the PLL is strongly related to the bandwidth of the SOGI filter.

After filtering the orthogonal components of the voltage the signals are coming into a block that makes the Park transformation ($\alpha\beta \rightarrow dq$). The $q$ component is used of the Park transformation block. This case implies aligning the voltage vector with the $d$ axis. One could align the voltage vector with the $q$ axis using only the $d$ component of the voltage. The difference between this two possibilities lies in the application. In the case of grid connected inverters $d$ axis alignment is preferred. In the case of electrical machines control, the $q$ axis alignment is more desirable [13]. From the $q$ component, the reference component $V_{q\_ref}$ must be stated in order to obtain an error signal that is introduced in a PI controller. The output of the PI controller is added to a block which represents the pulsation of the fundamental signal ($2\pi50$). This feed forward makes the presented PLL algorithm much faster and thus more reliable. After that the signal is integrated what results in getting the angle ($\theta$) of the voltage. Angle $\theta$ is used for further transformation of signals in different reference frames. The obtained results can be seen in Figure 4.5.

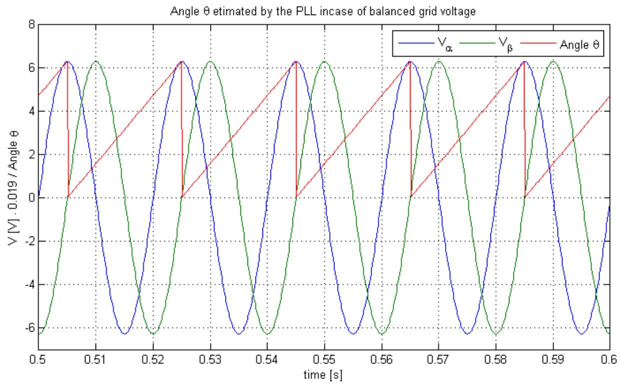


Figure 4.5: The estimated grid voltage angle $\theta$ in case of balanced grid

### 4.3.4 Pitch control

For the purpose of limiting the produced power, when wind speeds rise above rated, a pitch control mechanism was implemented. The control uses a proportional (P) gain after the obtained error between measured generator power and rated WT power. Because this method was treated in the previous project it will not be further explained. Details and results obtained for the pitch control can be found in [31].

## 4.4 STATCOM reactive power control

### 4.4.1 STATCOM control

The control of reactive power is based on the scheme presented in Figure 4.6. Control is divided in two sections. First one is responsible for controlling the DC-link voltage of STATCOM. It is keeping the DC voltage at the desired value. The lower branch is responsible for actual STATCOM control. The figure shows two strategies that were implemented. The first one (highlighted in blue) is a voltage droop characteristic control. It allows to control the voltage level at PCC according to the voltage-droop characteristics with a desired slope (X). The strategy highlighted in green allows to inject or absorb reactive power according to the TSO demands. Those strategies were based on [26], [27]. The reference current calculation is based on instantaneous active-reactive control theory based on [27], [28]. For detailed control strategy description see the Appendix C.2.

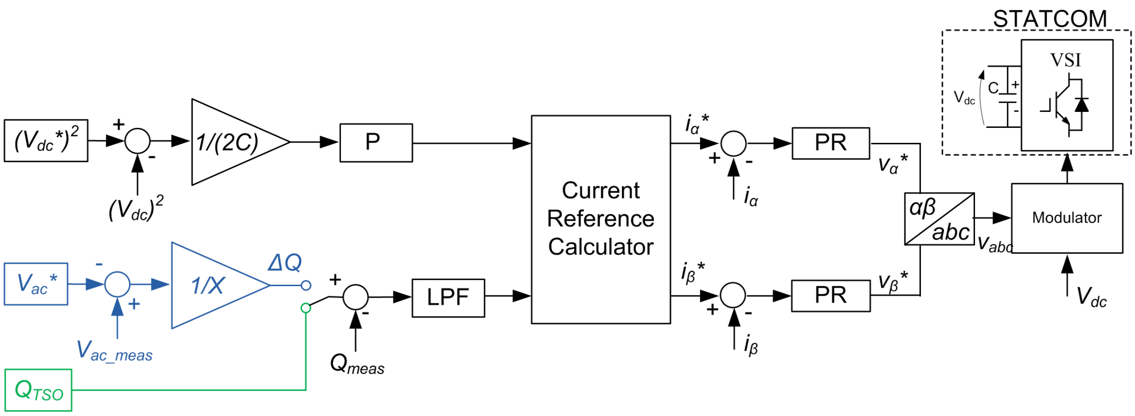


Figure 4.6: STATCOM control scheme

### 4.4.2 Control of the emulated system

As it was described in section 1.3 to emulate the WPP with STATCOM connected to the grid a simple model, which contains two grid connected inverters, was applied in the laboratory. The overall control structure is presented in the Figure 4.7. Reference currents for Inverter 1 (WPP) are calculated from the power delivered by simulated model of WPP. The reference currents for Inverter 2 (STATCOM) are calculated according to one of the chosen STATCOM control strategy which where described in section above. For detailed control strategy description see the Appendix C.3.

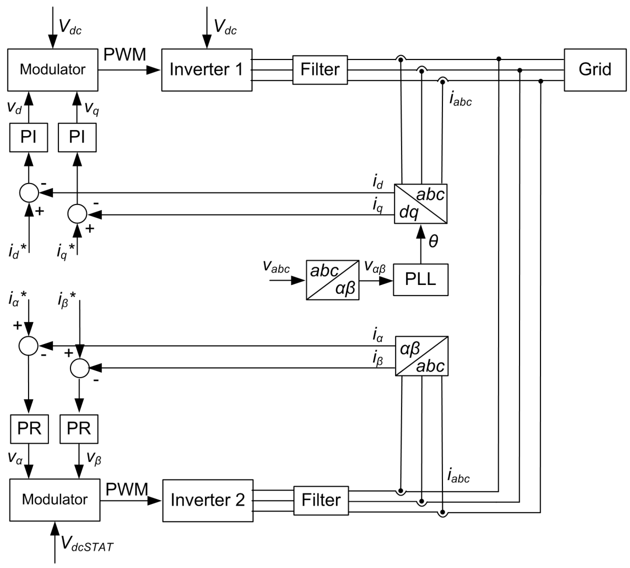


Figure 4.7: Control diagram for the system in laboratory

## 4.5 Distribution of reactive power between WPP and STATCOM

Wind farms can deal with provision of reactive power support to the grid in two ways. They can use only the capability of WT from a WPP or they can use additional reactive power support devices. As it was mentioned before commonly used device for that purpose is STATCOM. One of major tasks when having two power support points is to distribute the reactive power in an efficient way. It means if the WPP is able to deliver required amount of reactive power STATCOM should not interfere. It should work only when WPP reactive power capability is not enough to fulfill the requirements. The next problem is that usually there is a line between WPP and PCC, which can result in reactive power losses. If it goes for STATCOM it is usually installed at PCC. This section describes the algorithm for reactive power distribution between WPP and STATCOM.

### 4.5.1 WPP reactive power capability curve

This section is based on [29]. The scope of the project focuses on a WPP created from VSWT with full-scale power converter. Such WPP system is presented on Figure 2.4d. The $V_g$, $P$ and $Q$ are voltage, active and reactive power at PCC. $V_c$ represents the converter voltage, which is determined by the $V_{dc}$ voltage of a power converter, the amplitude of the modulation index and the modulation technique itself [30]. When one is considering a given hardware setup, converter voltage has a certain maximum value. The reactances on the figure are described as follows: $X_1$ stands for the total inductance of a WT's step-up transformers and grid filters, while $X_2$ represents the transformer reactance for transforming the WT medium voltage to high voltage bus.

For getting the maximum possible reactive power from WT on has to impose limiting factors.

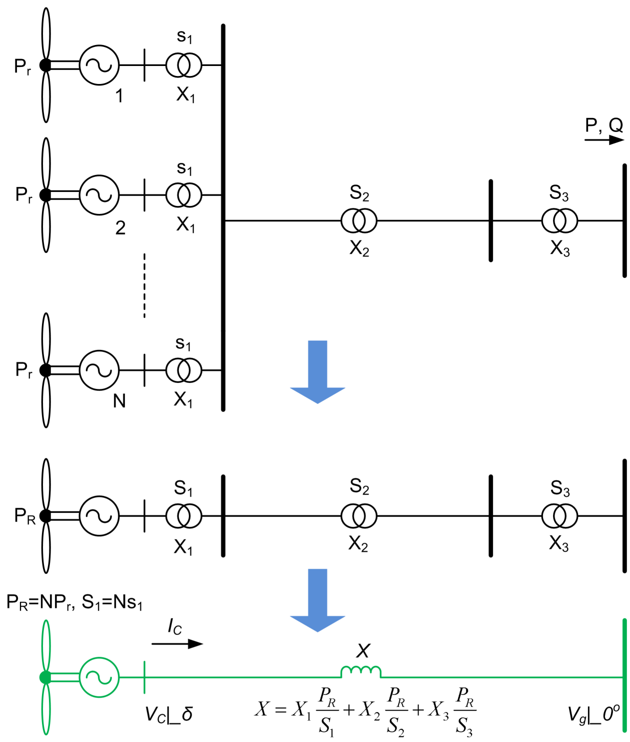


Figure 4.8: Considered wind park.

First of the imposed limits is the grid side converter maximum current-carrying capacity. The equation describing the relation between $P$, $Q$ and and limit of the converter current is shown below:

$$P^2 + Q^2 = (V_g I_c)^2 \tag{4.1}$$

where $I_c$ is the converter current. In $PQ$ plane the graphical limitation will be similar to armature current limits of a synchronous generator [29].

The next limit is a result of converter voltage limitation. It is similar to field current limit of a synchronous generator. Knowing that one can state the relationship between $P$, $Q$ at converter voltage limit is given by the equation:

$$P^2 + (Q + \frac{V_g^2}{X})^2 = (\frac{V_c V_g}{X})^2 \tag{4.2}$$

where X is the total equivalent reactance from the wind turbine low-voltage terminal to the PCC (formula describing X is presented in Figure 4.8).

As it was mentioned before, many grid codes require WPP to be able to operate continuously at the rated power with a requested power factor in a specified voltage and frequency band. Referring to the German grid codes [22] the upper and lower values can be defined for voltage and frequency: $V_{g,max}$=1.12, $V_{g,min}$ = 0.9, $f_{max}$=1.01, $f_{min}$=0.98 and the rated power factor as $cos\theta_R$, where $\theta_R$ is the rated pf angle of WPP. These values can be used in design process to determine the maximum values for the converter voltage and current. The design procedure for $Q-capability$ curve will be shown below.

The converter current can be obtained from the equation:

$$I_c = \frac{\sqrt{P^2 + Q^2}}{V_g} \tag{4.3}$$

The maximum current of the converter is determined when the reactive and active power from the WPP at their rated values, and the grid voltage is at minimum, which yields:

$$I_{c,max} = \frac{\sqrt{P_R^2 + Q_R^2}}{V_{g,min}} = \frac{\sqrt{P_R^2 + (P_R tan\theta_R)^2}}{V_{g,min}} \tag{4.4}$$

Taking $P_R$ as a mega volt ampere base of the system the previous expression can be reduced to an pu. equation:

$$I_{c,max} = \frac{\sqrt{1 + tan^2\theta_R}}{V_{g,min}} \tag{4.5}$$

To find the converter voltage one can use the relation:

$$\left(\frac{V_c V_g}{X}\right)^2 = P^2 + \left(Ptan\theta + \frac{V_g^2}{X}\right)^2 \Rightarrow V_c = \frac{X}{V_g}\sqrt{P^2 + \left(Ptan\theta + \frac{V_g^2}{X}\right)^2} \tag{4.6}$$

The maximum voltage of the converter can be determined when the reactive and active power from the WPP at their rated values, and the grid voltage and frequency are at maximum:

$$V_{c,max} = \frac{Xf_{max}}{V_{g,max}}\sqrt{1 + \left(tan\theta_R + \frac{V_{g,max}^2}{Xf_{max}}\right)^2} \tag{4.7}$$

To calculate the maximum reactive power injection capability one can use the formula:

$$Q = min(Q_c, Q_v) \tag{4.8}$$

where $Q_c$ and $Q_v$ are converter-current-rating and converter-voltage-rating limits given at certain level of active power production. They are described by the formulas:

$$Q_c = \sqrt{(V_g I_{c,max})^2 - P^2} \tag{4.9}$$

$$Q_v = \sqrt{\left(\frac{V_{c,max} V_g}{X}\right)^2 - P^2} - \frac{V_g^2}{X} \tag{4.10}$$

The $PQ$ curves showing $Q-capability$ of WPP may be graphed for different pf requirements at the PCC. Table 4.1 presents different design cases for system emulated in the laboratory. The design parameters for the laboratory system are presented in Appendix D in Table D.

Table 4.1: $I_{c,max}$, $V_{c,max}$, $P_{c,max}$ for different PF

| | pf=1 | pf=0.95 | pf=0.9 |
|---|---|---|---|
| $I_{c,max}$ [pu] | 1.11 | 1.17 | 1.24 |
| $V_{c,max}$ [pu] | 1.139 | 1.206 | 1.2379 |
| $S_{c,max}$ [pu] | 1.2643 | 1.411 | 1.535 |

Figure 4.9 presents the actual $Q-capability$ curves for system implemented in the laboratory designed for having a pf=1 at the PCC. As it was described above the curves were plotted for three operating points. Namely for $V_g = 0.9$, $V_g = 1$ and $V_g = 1.11$. The grid code requirements from Figure 2.3 are incorporated on the figure below (red lines). It can be easily notice that for a

steady state with voltage equal to 1 pu. the WPP is able to comply with the grid codes without need for any external reactive power delivery. However, in case of having voltage at level of 1.12 pu. WPP is able to fulfill the requirements only for supporting the voltage at PCC. In case of having the PCC voltage at 0.9 pu. the WPP will have problems with complying with grid codes when it is asked for supporting the grid voltage, when it is working around its rated active power. One should also note than this curves are considering that the WPP injects the reactive power directly at the PCC. It means that for having long connection line between the WPP and PCC one should consider having a reactive power compensation at PCC.

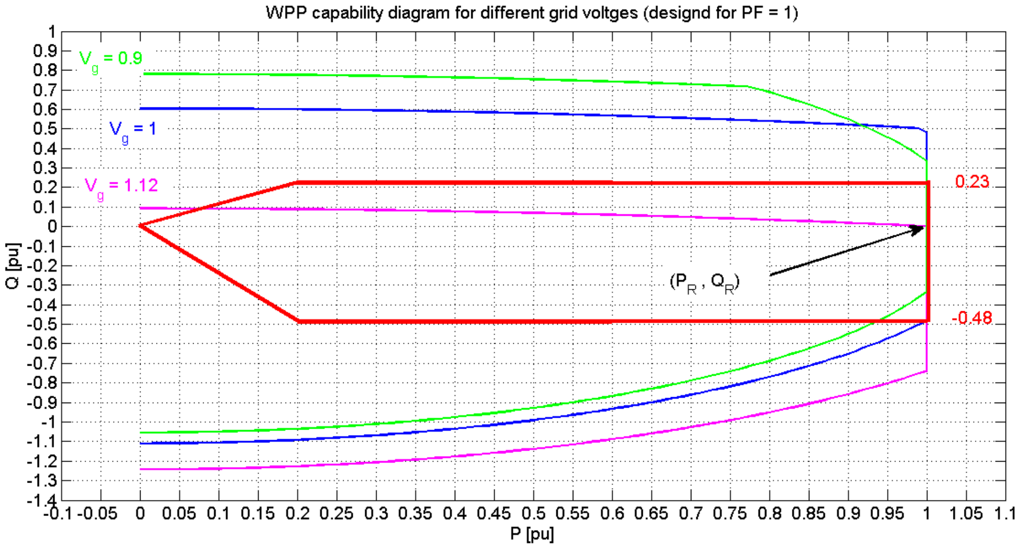


Figure 4.9: Q-capability curves for different grid voltage levels.

### 4.5.2 Reactive power distribution algorithm

Having the ability for providing the reactive power by WPP is not always enough. For WPP with long connection cables the line losses can significantly influence the availability of reactive power at PCC. One of the possible solution is to use STATCOM at the PCC. The challenge lies in building a good communication and distribution algorithm, for both WPP and STATCOM. This section proposes a simple solution. Figure 4.10 presents the idea:

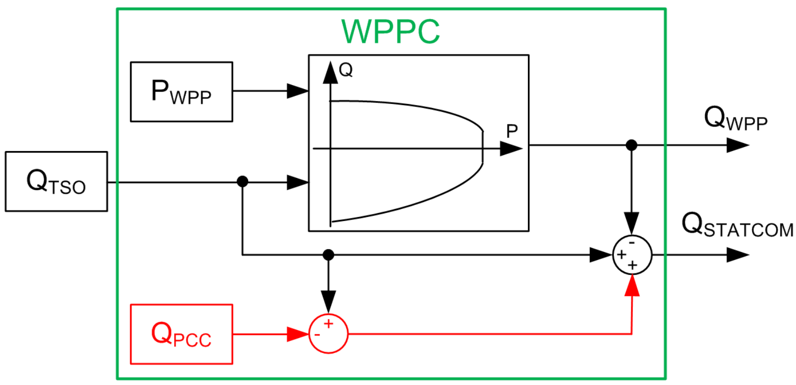


Figure 4.10: Simple reactive power distribution algorithm for WPP with STATCOM.

The algorithm works as follows: first the Wind Power Plan Controller (WPPC) gets the reactive power reference signal from TSO. Then depending on the produced active power WPPC gets the available reactive power from WPP. If the TSO requirement is not fulfilled a reactive power reference signal is send to STATCOM controller. This signal is built as a difference between the required reactive power at PCC and reactive power produced by WPP. In case of having a connection line between the WPP and the PCC additional reference signal component for STATCOM is defined. This signal is built as a difference between required reactive power at PCC and actual measured reactive power at PCC.

### 4.5.3 Summary

In this chapter system modeling and used control strategies are presented. The development and explanation of each element of the proposed system is demonstrated. The control methods include WT control, for WT with full scale back-to-back converter, STATCOM reactive power control and reactive power distribution algorithm. The WT consists of:

- generator side converter control (Field Oriented Control)
- grid side converter control (Voltage Oriented Control)
- gird synchronization (Phase Locked Loop)
- pitch control

The STATCOM control consists of:

- QU slope control strategy
- demanded Q strategy
- emulated laboratory system control

The reactive power distribution algorithm takes into account the WPP Q-capability curve. It is investigated how the WPP can comply with the grid codes in terms of reactive power injection/absorption.

Chapter 5

# Simulation and experimental results

*This chapter presents the obtained results. First section describes the laboratory setup, which includes the explanation of used software and hardware. The next part of the chapter shows the simulation and laboratory results for small scale system model. It contains several test cases and summary in which comparison of results is concluded. The next section demonstrates how the simulations for large scale system model are performed. Several test cases are taken into consideration. The last part of this chapter summarizes all the obtained results.*

## 5.1 Laboratory setup

A dSPACE DS1103 platform is used for implementing the small scale setup. Since the modeling and controller design is accomplished in MATLAB/Simulink environment special system for communicating between the dSPACE platform and Simulink is required. This is done by Real-Time interface (RTI). RTI allows user to build Simulink models with the dSPACE PowerPC processor. It also adds a new library to Simulink which give the opportunity to have access to corresponding blocks with I/O of the board. This means access to timers, PWM generators, interupts etc. The RTILIB interface is presented in the figure below:

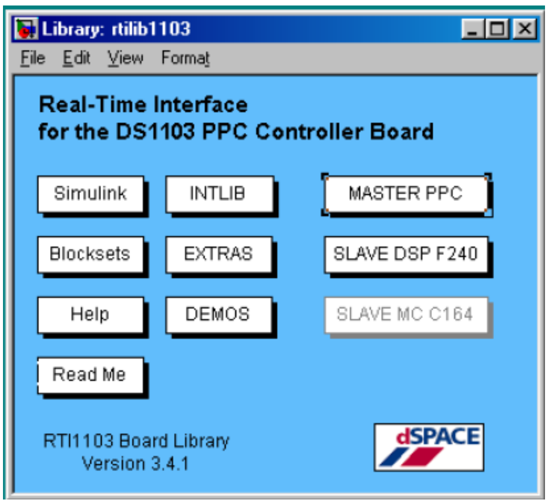


Figure 5.1: RTILIB library.

For easy monitoring of the experiments, adequate maintenance and management Control Desk Studio software is used. It allows the user to link the actual measurements with its virtual instruments. This feature allows to display the gathered data in attractive form. The display can be presented as a user made control panel, including sliders, indicators, buttons and scopes. Moreover, the Drag&Drop technique makes the work intuitive and easy. Taken measurements displayed on PC screen can be exported to MATLAB for further analysis. Experiment layout is shown in Figure 5.2.

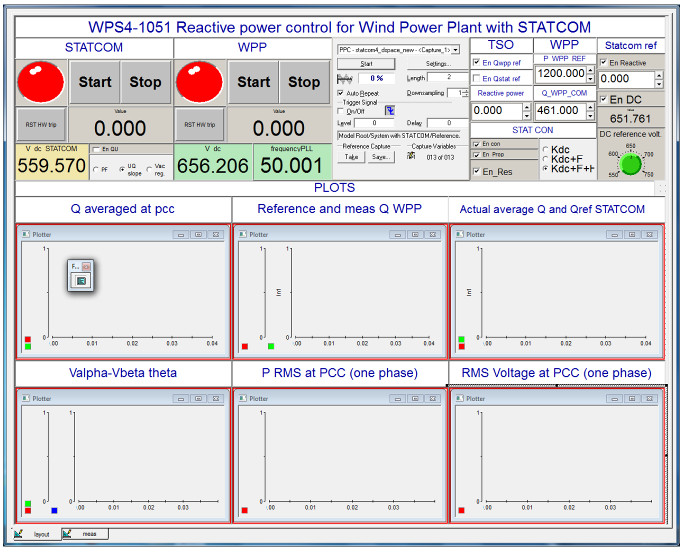


Figure 5.2: Control desk studio layout.

The hardware implementation used for experimental work consists of DS1103 dSPACE platform,transformer for grid connection, two Danfoss FC302 inverters, LEM measuring modules, two DC supplies connected in series for supplying the emulated WPP inverter and PC. Detailed information about each of the hardware elements can be found in Appendix E. The experimental setup with indication of each element is presented in Fig.5.3.

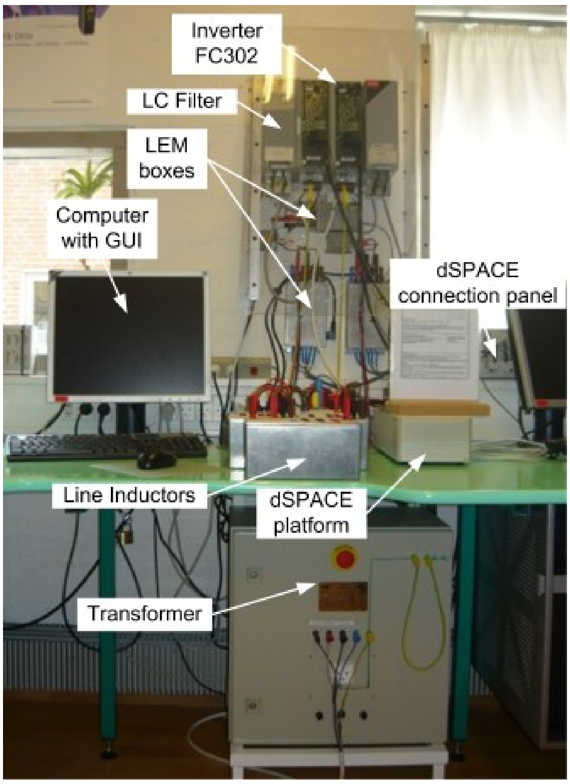


Figure 5.3: Experimental setup in the lab.

## 5.2 Study cases for small scale model

Study cases for small scale model include investigation of how the distribution algorithm behaves and how can it be affected by having a line between WPP and PCC. The third section of the studies presents the QU-slope characteristics for STATCOM. Having a distinct difference between sending and receiving ends, when talking about absorbing or generating reactive power the sign conventions must be stated. In this project following convention are used for generating and absorbing reactive power:

Table 5.1: Generating and absorbing reactive power: sink and source conventions [32]

| Convention | Lagging PF (I lags V) | Leading PF (I leads V) |
|---|---|---|
| Load (sink) | $Q_r > 0$ Absorbing VArs | $Q_r < 0$ Generating VArs |
| Generator (source) | $Q_s > 0$ Generating VArs | $Q_s < 0$ Absorbing VArs |

For small scale model the load convention is used and in case of having the large scale model the generator convention is used.

### 5.2.1 Simulation results

Simulations were carried out using MATLAB Simulnik software with PLECS toolbox. Simulation model is built in a way to reproduce as close as possible, though including some simplifications, the laboratory conditions.

#### Q distribution

The algorithm presented in section 4.5.2 is implemented in simulations and tested. In this test case the TSO requests the reactive power as steps in power. The active power coming from WPP is set to 0.64 pu (1.4 kW). This power limit is appearing due to the laboratory setup limitations.

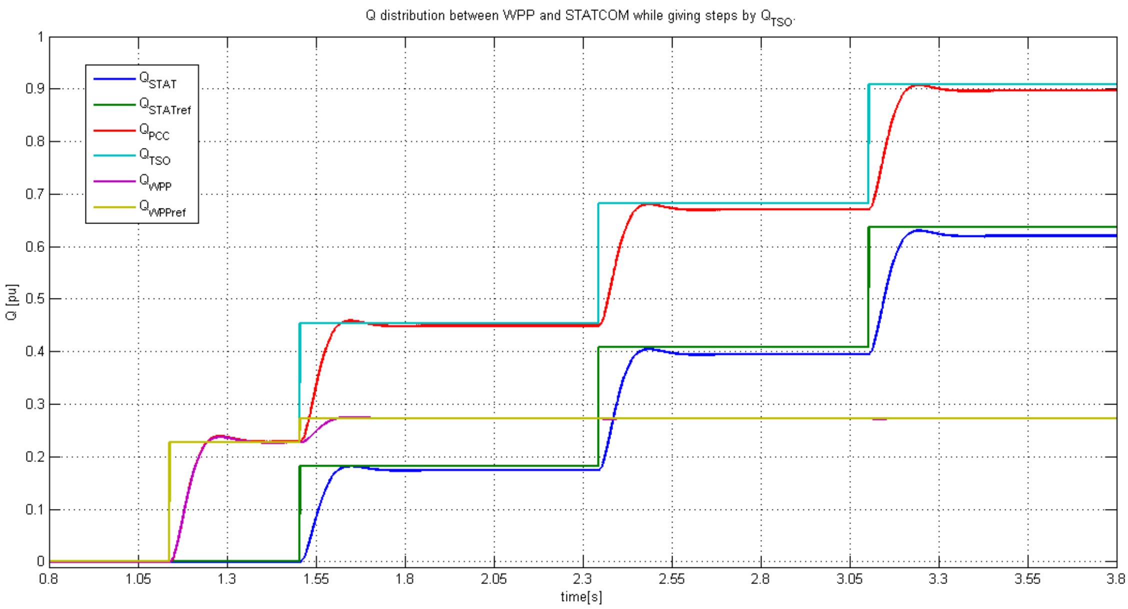


Figure 5.4: Steps in reactive power for $Q_{TSO}$.

Trying to use higher power in the laboratory resulted in having an overcurrent warning on the DC source, so for sake of the setup power of 1.4 kW is used. To reproduce the same conditions in simulation the same power level is used and according to the Figure 4.9 from section 4.5.1 the WPP is able to produce reactive power of 0.58 pu (1.276 kVAr)at maximum. Having a LC filter at the output of the inverter emulating the WPP is drawback having a significant impact on available reactive power production. For having a $Q_{PCC} = 0$ at steady state compensation of the filter reactive power production must be taken into account. Due to the fact that filter capacitors produce a reactive power the WPP converter has to absorb this amount of reactive power. This results in having only 0.273 pu (600 VAr) available reactive power from WPP. It means that WPP absorption capability is significantly reduced. Applied $Q_{TSO}$ steps and resulting reactive power distribution are presented in the figure above. As can be seen in the Figure 5.4 the distribution algorithm is working in a good manner. In the beginning when the demanded power at PCC is zero there is no reactive power absorption. Then, when the requested reactive power rises in as steps one can observe that WPP starts to absorb the reactive power following the demanded value. Then when the WPP reaches it limit the signal is sent to STATCOM, which provides an extra requested reactive power absorption. One can observe that having a step request of reactive power the controller is able to reach the desired level of power with a speed of 200 ms (for both WPP and STATCOM). Such fast response can satisfy with ease the grid codes from different TSO's.

### Q distribution - line impact

When having a large WPP one should consider the influence of having a connection cable between a WPP and the PCC. For simulation purposes analysis, containing emulation of line as additional phase inductor, is conducted. Different line lengths are investigated. Figure 5.5 presents the case when a 5.4 mH (emulating 4.15 km) inductor is used.

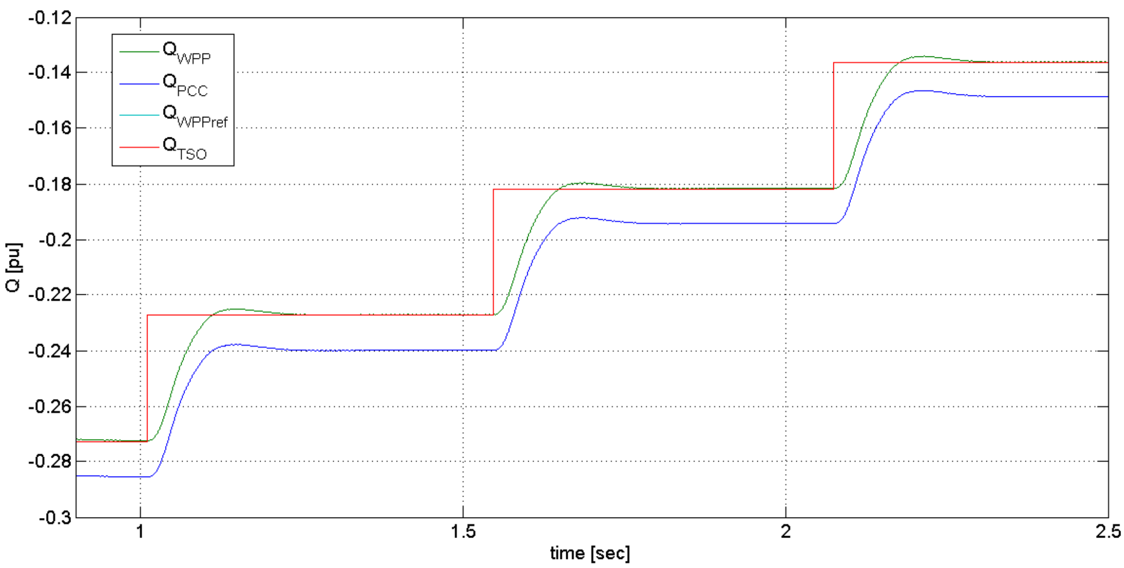


Figure 5.5: Line impact on the delivered reactive power - STATCOM compensation not active.

Looking at the figure above one can see that having a line between the WPP and PCC introduces reactive power losses. The reason for that the $Q_{PCC}$ is lower than the requested value of reactive power is that, the line which is modeled as inductor is absorbing reactive power. The difference between requested reactive power and between the actual delivered reactive power is 0.013 pu. This can be seen in the next figure.

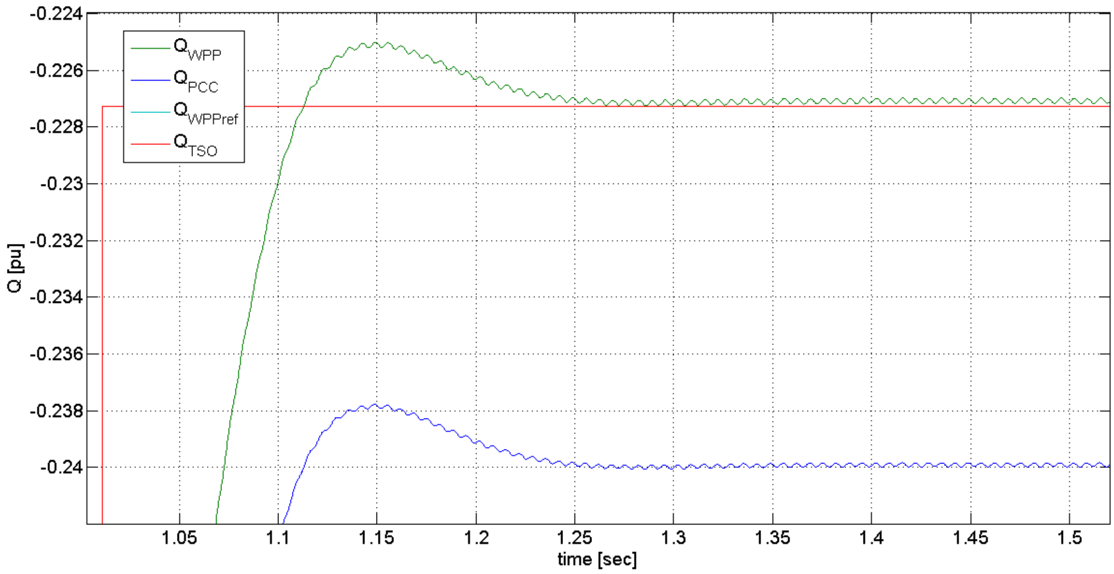


Figure 5.6: Line impact on the delivered reactive power(ZOOM).

As it was explained above having a line between the WPP and the PCC results in difference between requested reactive power and between the actual delivered reactive power. Algorithm presented in Figure 4.10, in section 4.5.2 takes into account such scenario. It copes with line losses using STATCOM for compensation at PCC. The results of compensation can be seen in the next figure.

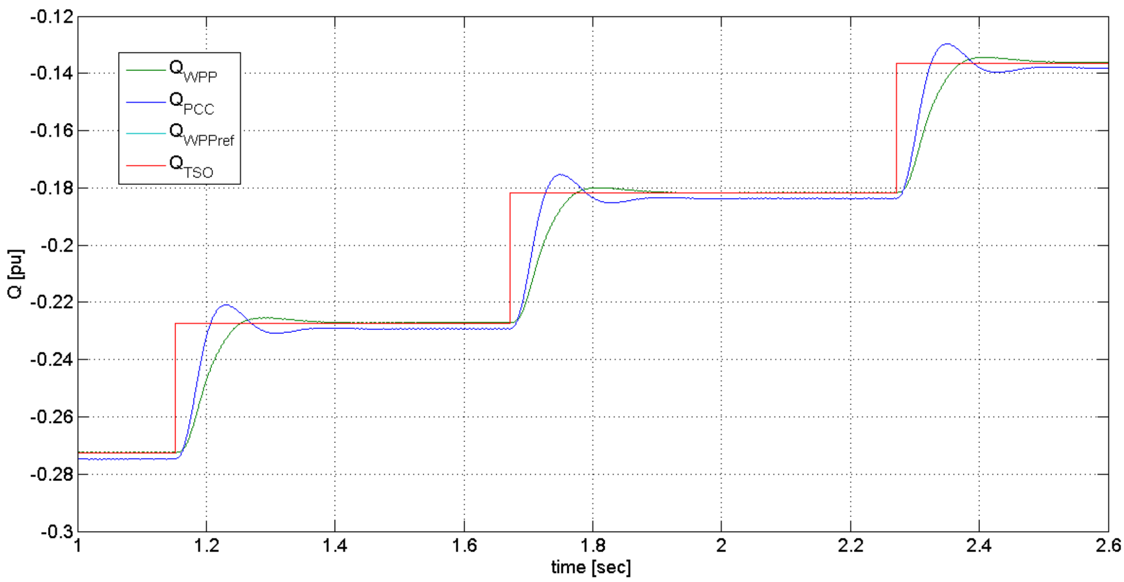


Figure 5.7: Line impact on the delivered reactive power - STATCOM compensation .

Looking at figures 5.6 and 5.8 one can clearly see the difference between the demanded and delivered reactive power is smaller. However, one can notice that control is not removing all the steady state error. This is due to the fact that gain of the PR controller were chosen in way to get rid of oscillations in delivered reactive power and over-currents. More explanation can be found in section 5.2.2.

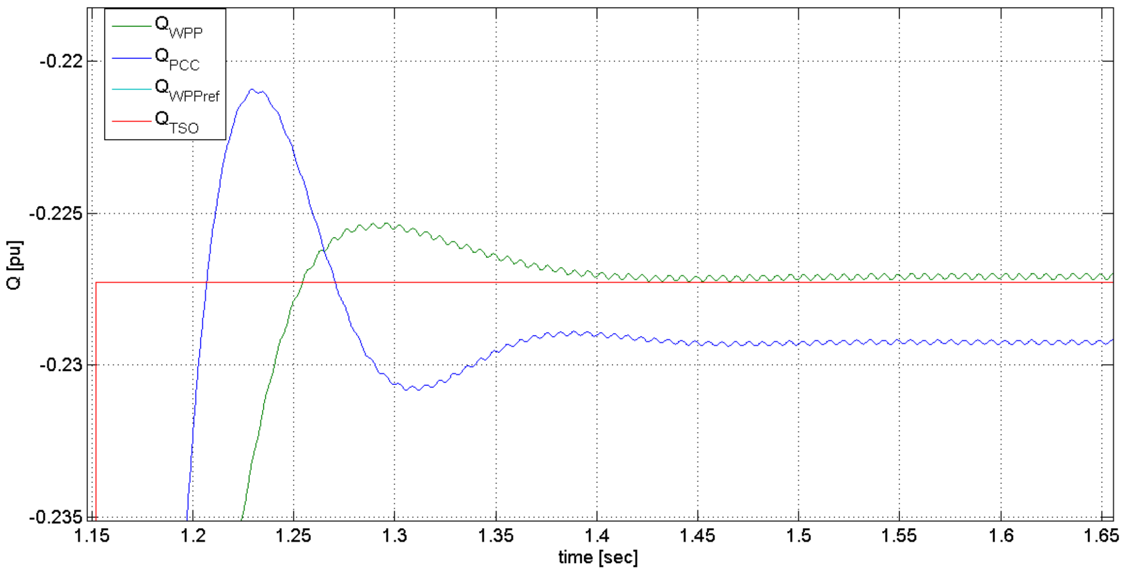


Figure 5.8: Line impact on the delivered reactive power - STATCOM compensation (ZOOM).

### QU-slope strategy

One of the applied methods for STATCOM is QU-slope strategy. Investigation is performed for whole range of available reactive power coming from STATCOM. Such linear characteristic is required in some of the grid codes [33].

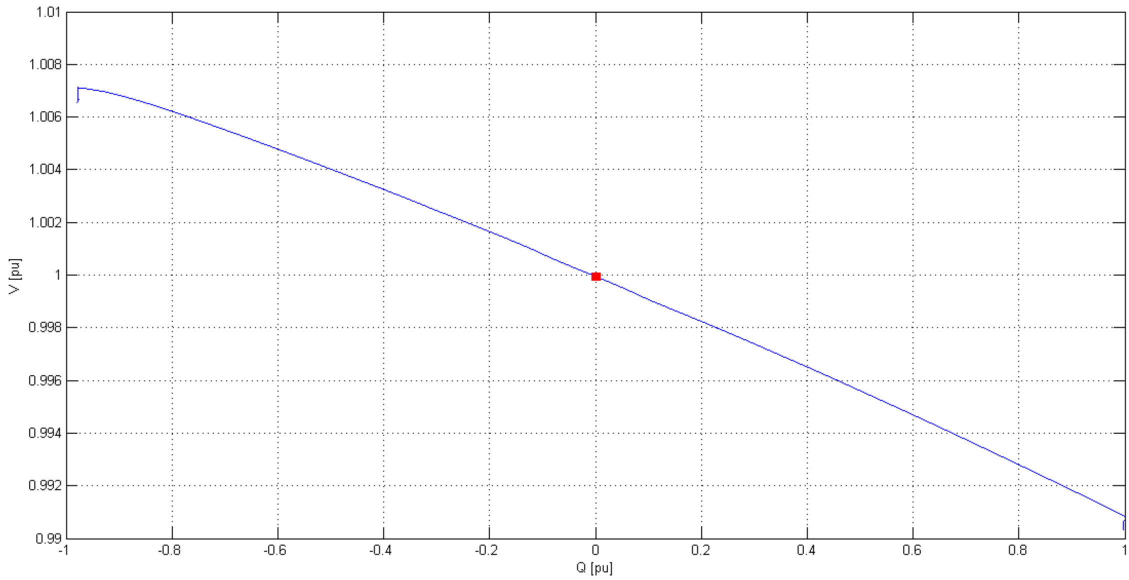


Figure 5.9: Obtained QU-slope.

Due to the fact that the grid was simulated as a stiff and stable (to reproduce the laboratory conditions) the slope obtained in the simulation analysis is around 0.7%. Despite this result, one has to state that as it was mentioned above some of the grid codes require such linear characteristic, but with a slope of at least 5%. In this case our STATCOM wouldn't comply with UK codes [33].

### 5.2.2 Laboratory results

Laboratory experiments are carried out in the same investigation manner like it is presented in the section above. The test cases taken into account: distribution algorithm examination, line impact on distribution algorithm, QU-slope characteristic determination.

#### Q distribution

The figure below presents the behavior of distribution algorithm in the setup implemented in the laboratory. In the beginning, when only the WPP is delivering required reactive power, one can see that STATCOM is injecting small amounts of reactive power. This happens during steps of demanded reactive power. The reason for that is the way that the reference signal for STATCOM is calculated.

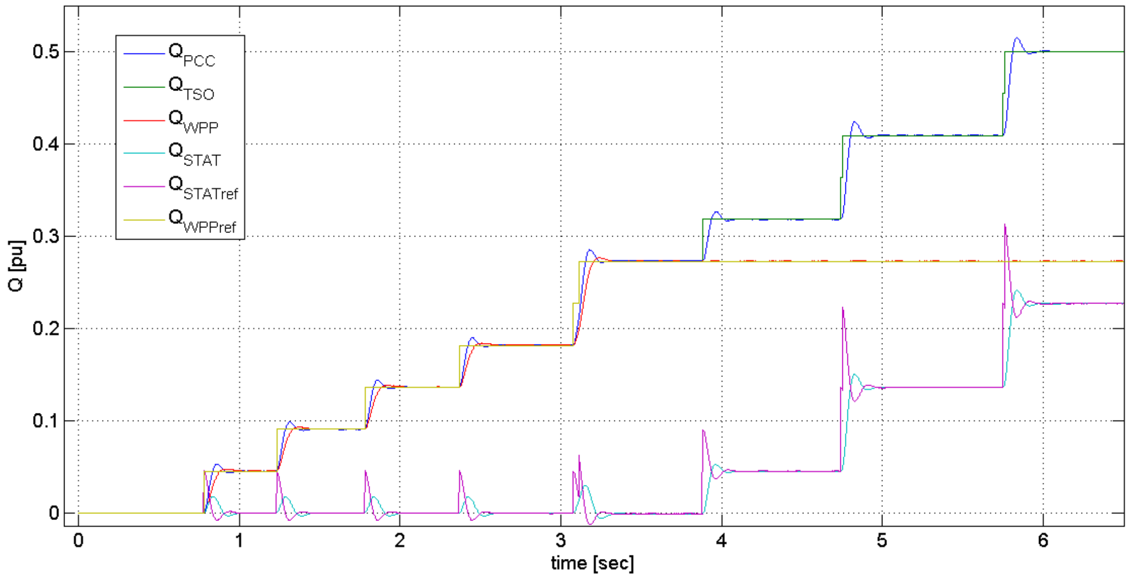


Figure 5.10: Performance of the distribution algorithm.

One of the components of STATCOM reference signal is connected with the measured $Q_{PCC}$. When a step is appleid in demanded reactive power, the reactive power at PCC will not immediately reach the desired level. In the figure above it can be seen that after each step reactive power injected by the WPP need around 40 ms to reach the steady state. However STATCOM is trying immediately reduce the difference causing the change in the reactive power decreasing faster. In the laboratory similar drawbacks to those considered in simulations are taken into account. This refers to the filter reactive power compensation. Also due to the DC source limitations maximum active power generated from the WPP is 1.4 kW.

#### Q distribution - line impact

For investigation the line impact on the distribution algorithm a 3-phase inductor is used. Different line lengths are investigated. Figure 5.11 presents the case when a 5.4 mH (emulating 4.15 km) inductor is used. As is can be seen in the figure below the similar situation is shown, as in the case of simulated test.

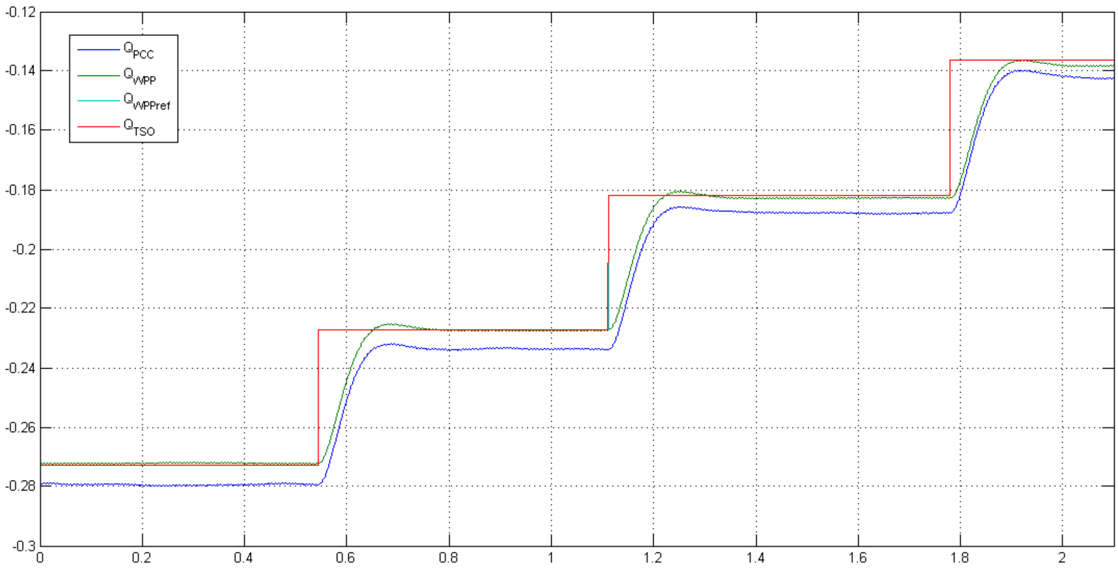


Figure 5.11: Line impact on the delivered reactive power.

The difference between requested reactive power and between the actual delivered reactive power is around 0.008 pu. This can be seen in the next figure.

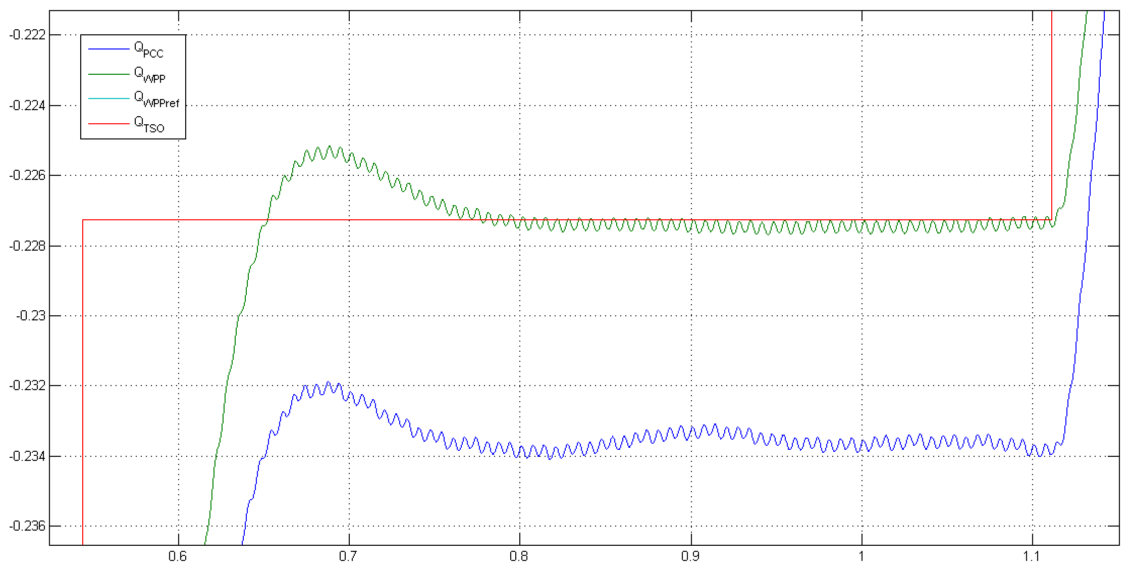


Figure 5.12: Line impact on the delivered reactive power (ZOOM).

For compensating for the line influence, again as it was described in the simulation section above, STATCOM is used. The delivered reactive at PCC with STATCOM compensation for line losses is presented below.

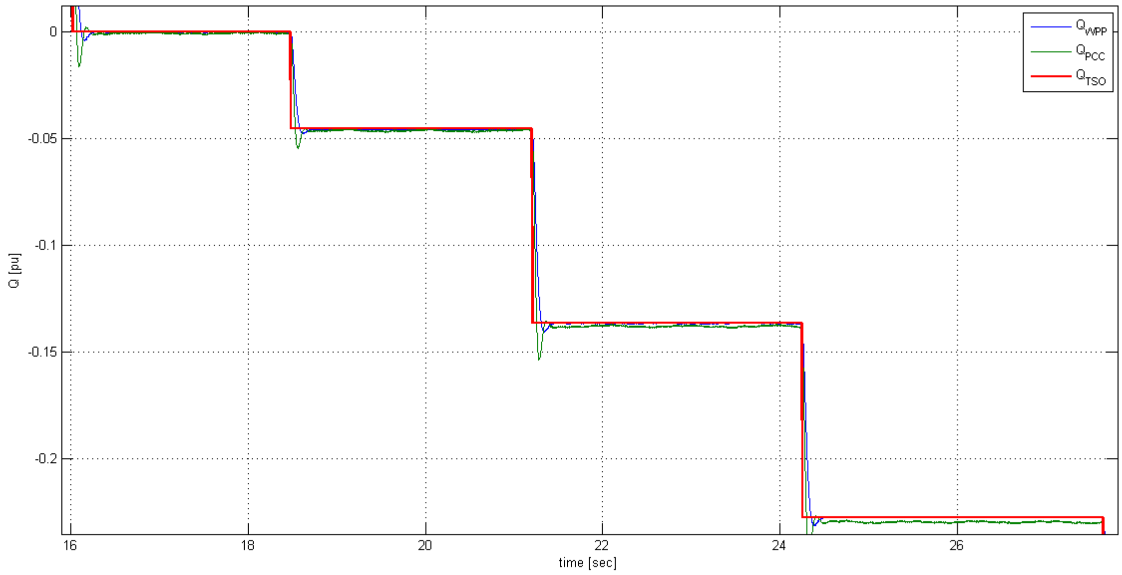


Figure 5.13: Line impact on the delivered reactive power - STATCOM compensation .

Looking at figures 5.12 and 5.14 one can clearly see that the difference between the requested reactive power and actual delivered reactive power decreased significantly (namely from 0.008 pu to 0.002 pu).

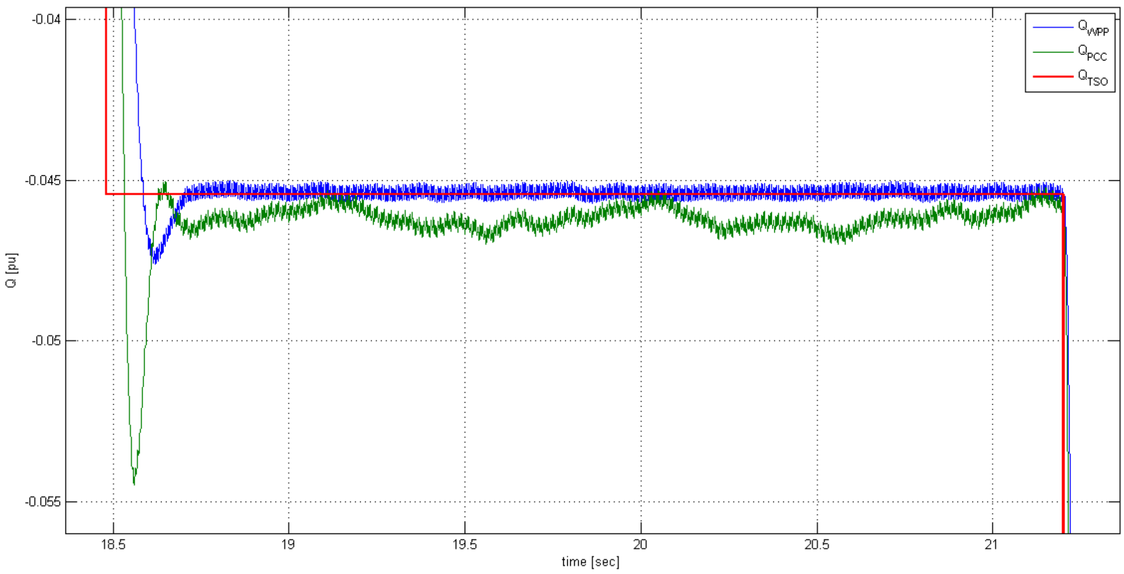


Figure 5.14: Line impact on the delivered reactive power - STATCOM compensation (ZOOM).

One can reduce completely the steady state error at the PCC by changing the gains of the controllers. However, there are some drawbacks that one has to take into account. Namely delivered reactive power oscillations at the PCC. This situation is showed on the figure below. Except that another disadvantage is having over-current spikes in STATCOM currents.

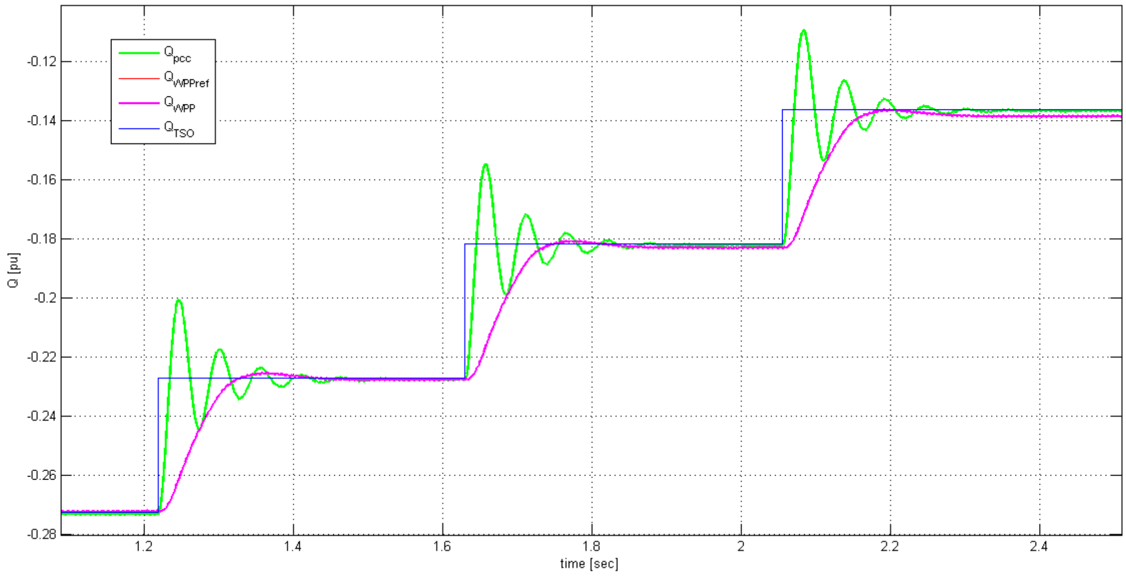


Figure 5.15: STATCOM compensation for reative power losses.

### QU-slope strategy

In this section the results of injecting/absorbing reactive power with desired slope are discussed. Due to acquisition data errors coming from dSPACE measuring system the measured voltage data is linearized. Obtained data is linearized in the way presented in Figure 5.16.

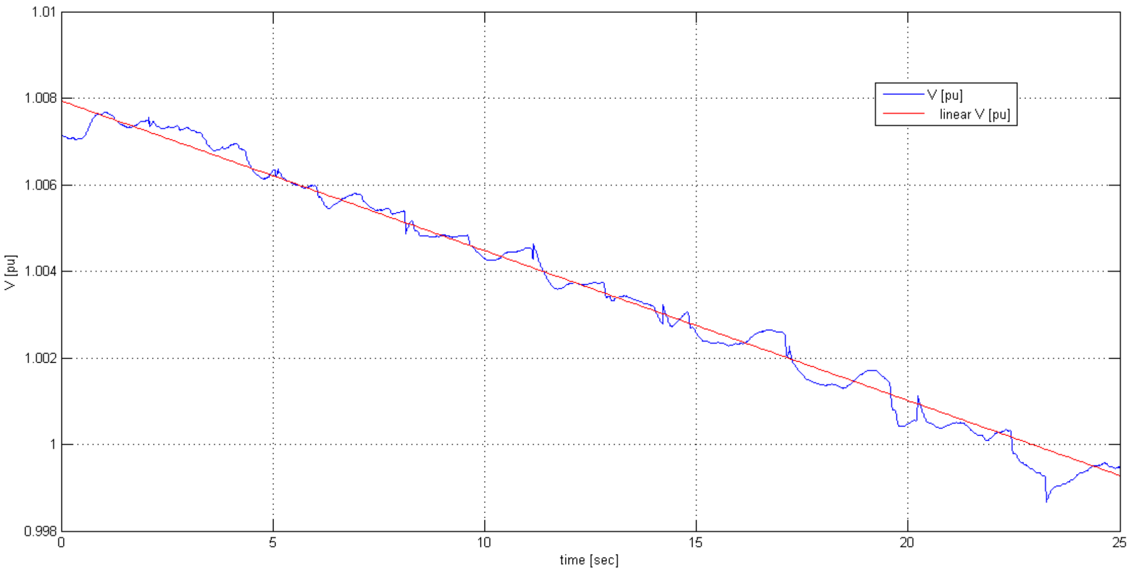


Figure 5.16: Linearization of obtained data.

Investigation of the voltage variation was done for whole range of reactive power injection/absorption by STATCOM. Obtained results are shown in a form of QU-slope characteristic presented below.

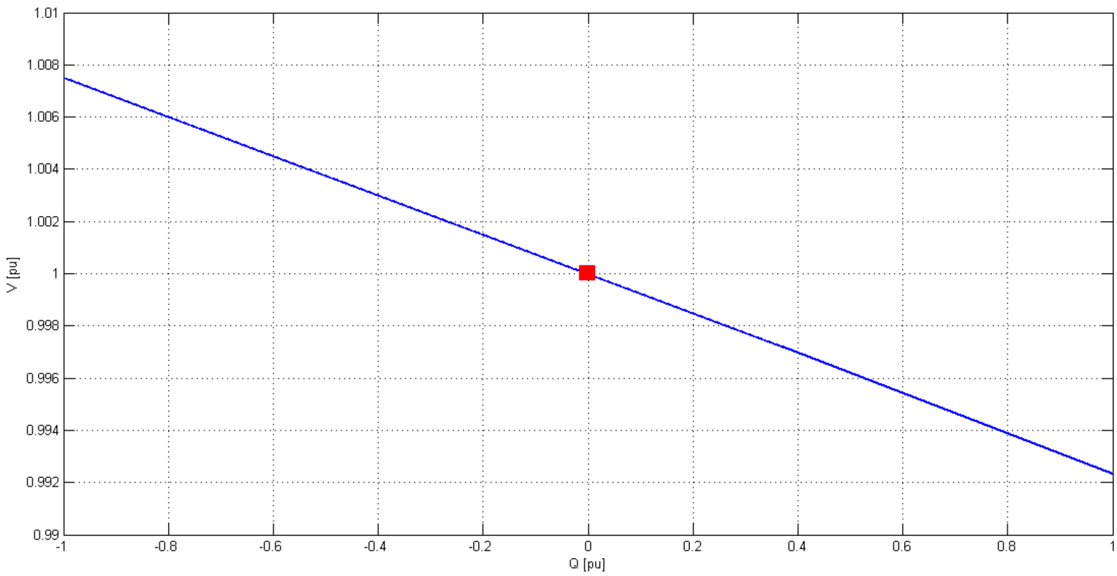


Figure 5.17: Obtained QU-slope.

The slope of the characteristic is equal to 0.7%. The fact that the obtained slope value is small is due to having a strong and stiff grid, and at the same time small power rating of the laboratory setup.

### 5.2.3 Summary

The obtained laboratory results fairly correspond to the results obtained in simulations. The difference between simulations and experimental results occurs due to several factors. In the first place it should be stated that simulations deal with ideal elements. Second factor having an influence on obtained results is that the transformer for simulations is modeled as an inductor and resistor connected in series, while in the laboratory setup the real transformer is used. Next is the impact of measuring devices used in laboratory. In simulations measuring error does not appear.

Having in mind all the above limitations one can still consider that the obtained results are matching. This leads to a conclusion, that the small scale model test cases can be expanded to a large scale model. In large scale model some additional properties of WPP are taken into consideration.

## 5.3 Study cases for large scale model

In this analysis the model of the large system is consisting of one 2MW WT unit and one 2MVAr STATCOM. The two blocks are modeled using mathematical equations in Simulink, both are using PI controllers in their control loops. Three different study cases have been performed to validate the well function of the system in steady state situations. The obtained results are plotted in pu. values. The base values for the WPP and STATCOM are presented in Appendix D in Table D.

### 5.3.1 Steps in active power from WPP, zero reactive power

In this first case, steps in the active power produced by the WT are considered, to simulate wind speed changes. It is assumed that no reactive power was demanded from TSO, as a result the references for WT and STATCOM reactive powers were set to zero. From the generator side control the DC-link current is obtained which will be an input for the grid side inverter. For an easier understanding and clear representation of results obtained the actual DC-link current coming from generator side converter is approximated with step functions. In reality, inertias of the WT rotor and generator masses will cause the speed to change in slower pace, which will be further propagated in the DC-link current (see Appendix D). Thus, the DC-link current from the rectifier (the reference) side and from the inverter side are plotted in Figure 5.18.

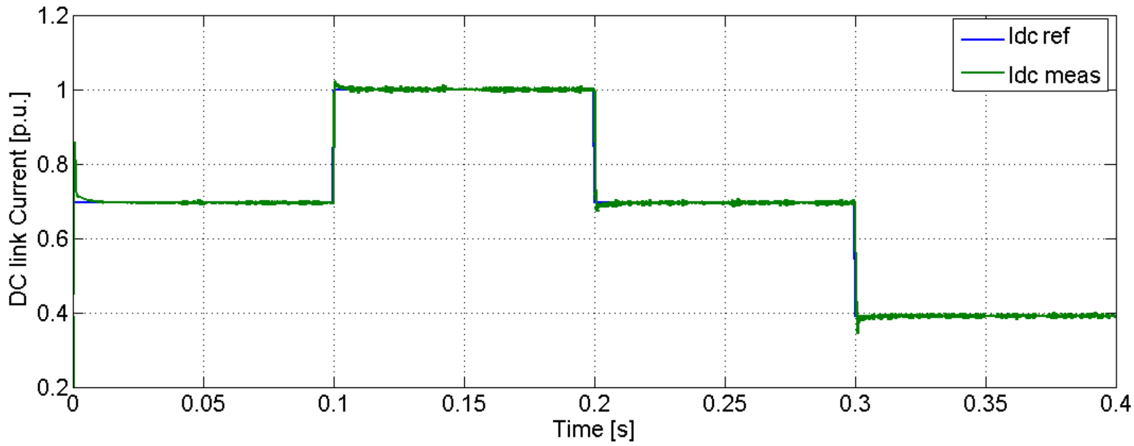


Figure 5.18: DC-link currents after the capacitor (blue) and to inverter (green).

The measured output DC-link current (green) is shown in the above figure with respect to input DC-link current (blue). The results in Figure 5.19 and Figure 5.20 indicate the active and reactive power flows between WT and PCC. The steps resulted in the active power produced (from Figure 5.19) are proportional to the DC-link current input to the inverter and are a consequence of steps in wind speed. Thus, at time 0.1s the active power rises from 0.7pu. to 0.95pu. (including inverter losses), which is equivalent to a wind step from 11m/s to 12m/s (the rated value). The simulation follows then at time 0.2s and 0.3s with two steps-down in the DC-link current, resulting in the decrease of active power produced from the WT.

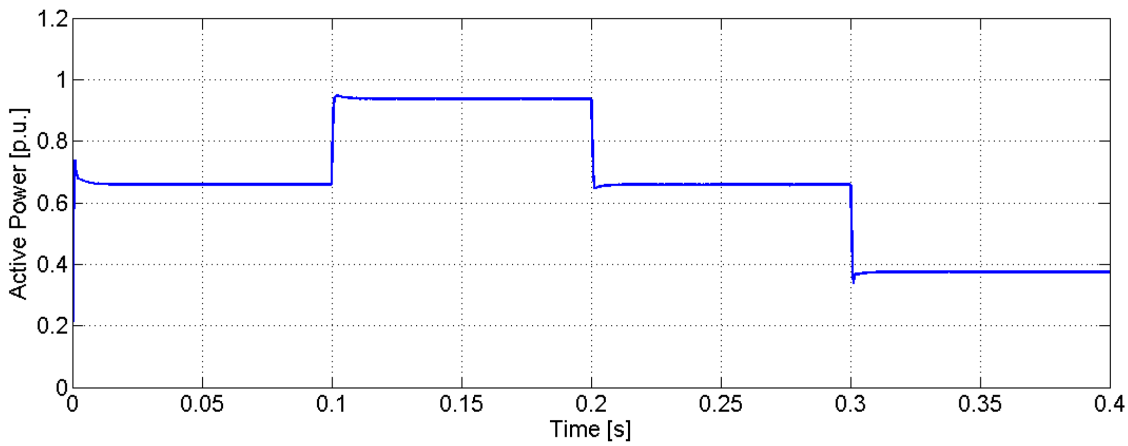


Figure 5.19: WT's Active Power Flow .

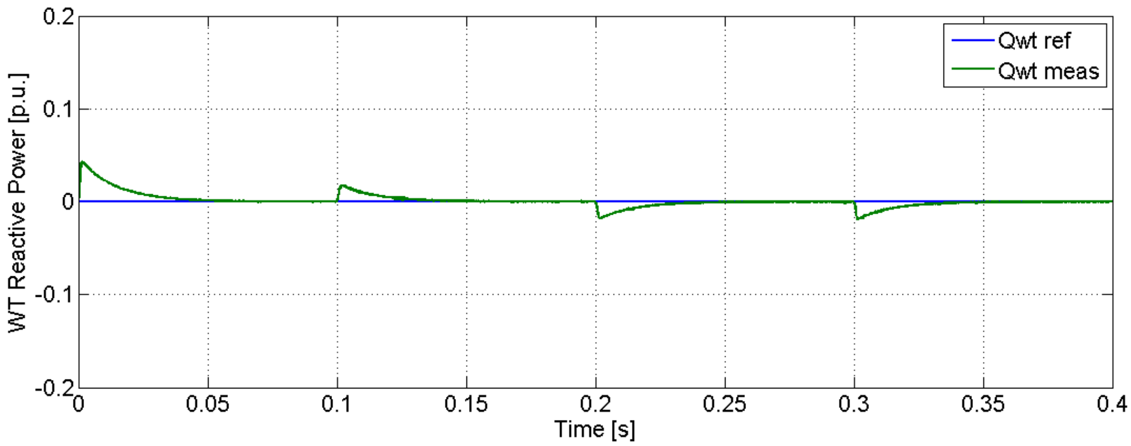


Figure 5.20: WT's Reactive Power Flow.

In Figure 5.20 small changes in reactive power are noticed at the moments of applying the steps. The deviations from the zero set point of reactive power are very small compared to the rated power (less than 5%). In Figure 5.21 the DC-link voltage measured across the capacitor shows the dynamics of the system during power flow. When more power is delivered to the grid the DC-link voltage tends to increase and when less power is given then the voltage tends to decrease. This is a consequence of current difference between rectifier and inverter which will charge the capacitor at time 0.1s and discharge it at time 0.2s and 0.3s. But the voltage controller responds very fast and puts back the voltage on the reference value, moment when the two currents become equal.

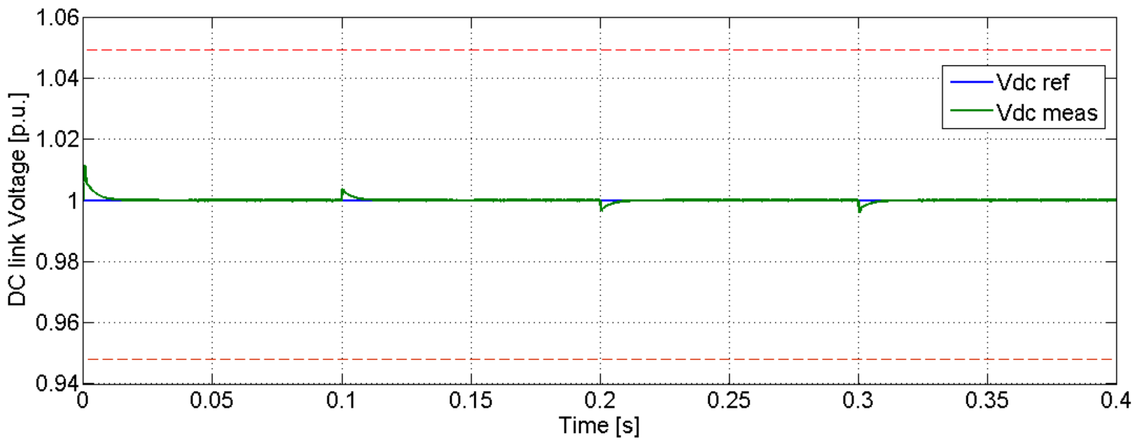


Figure 5.21: DC-link Voltage Transients.

The dashed red lines at 0.95 and 1.05 pu. indicate the +/-5% variation allowed in the DC-link voltage. This is the required dynamic performance and it is well accomplished by the obtained results. The relation between active power/reactive power and d-axis/q-axis current is made clear from Figure 5.22 compared to Figure 5.19 and 5.20.

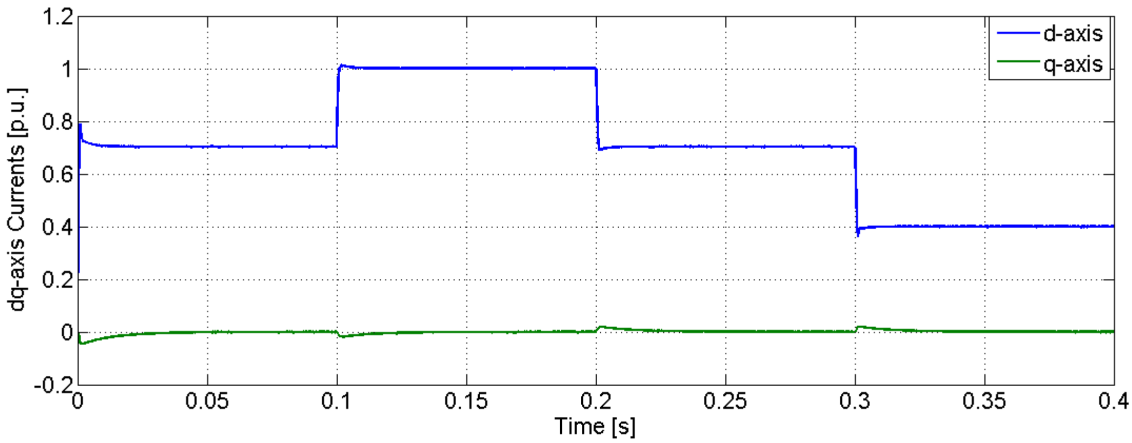


Figure 5.22: Inverter dq-axis Currents.

Because only active power is produced by the WT, the plot in Figure 5.23 shows that the voltage and current for phase a at the PCC are in phase as expected. Thus the unity power factor at the grid is achieved. The currents at the PCC are increasing / decreasing, following the current on the d-axis id from previous figure. When the rated power is reached by the WT, the currents also increase to 1.0pu. values.

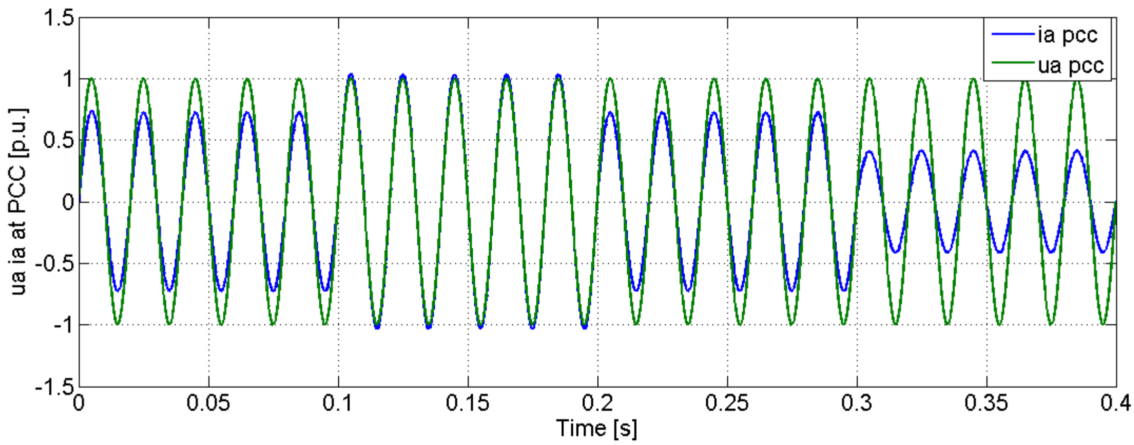


Figure 5.23: Phase a of PCC Voltage and Current.

Analyzing the result from the Figure 5.24, a slight phase angle shift is noticed between the PCC voltage and the WT inverter voltage. Because PCC voltage lags the inverter voltage it is proven that the active power produced by WT flows from the inverter to the PCC.

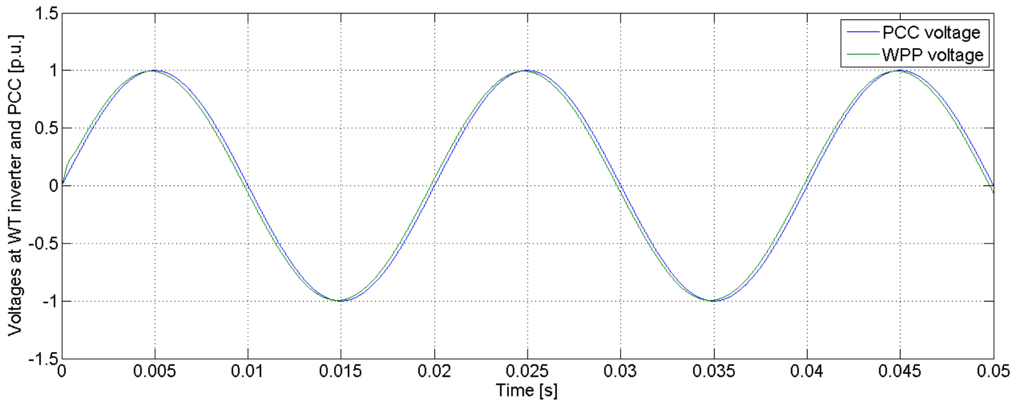


Figure 5.24: Phase a voltages for inverter and PCC.

### 5.3.2 Reactive power steps for WPP while active power set to rated

In this second analysis, TSO requests some amount of reactive power to be delivered by the WT. It is assumed that the wind speeds are of 12m/s or higher, thus the WT rated output power is produced (0.95 pu. if adding the losses). Figures 5.25 and 5.26 indicate the active and reactive power flow between WT and PCC.

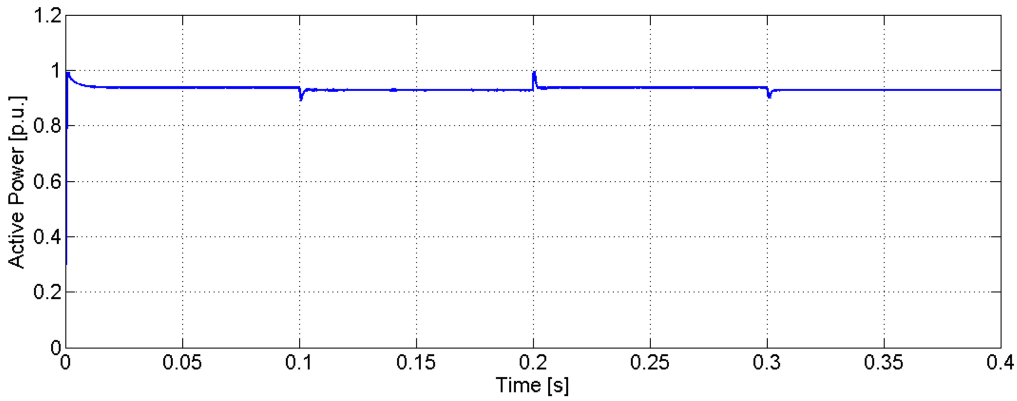


Figure 5.25: WT's Active Power Flow .

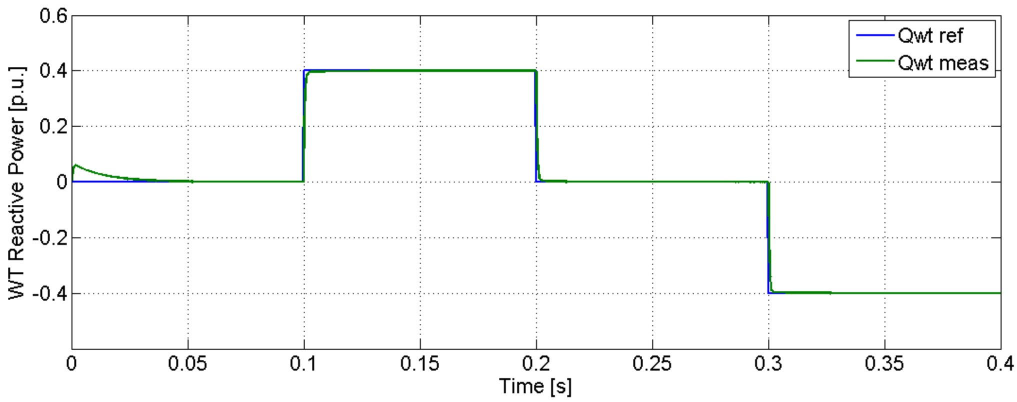


Figure 5.26: WT's Reactive Power Flow.

The reactive power steps vary from 0 to +/-0.4 pu. (meaning 40% from the total active power). These steps are applied as reference inputs to the inverter controller. It can be noticed the very good step responses in the reactive power. Fast time responses of less than 30ms are achieved and also no overshoot when stepping up from zero reactive to 0.5 pu. capacitive or inductive. Because of the small DC-link voltage variations from Figure 5.27 the active power shows some overshoots at the moment of steps in reactive power reference.

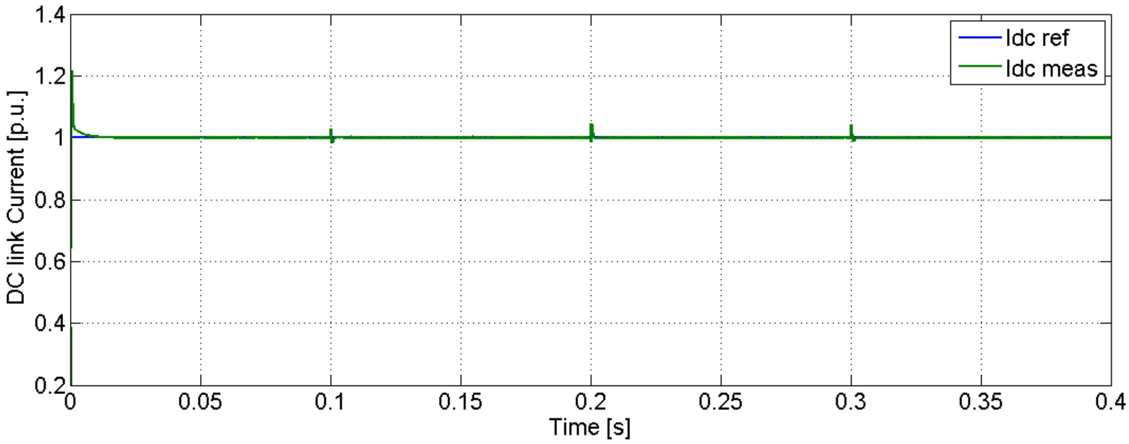


Figure 5.27: DC-link Currents from rectifier (blue) and to inverter (green).

The measured DC-link current is kept almost constant at rated value 1 pu.

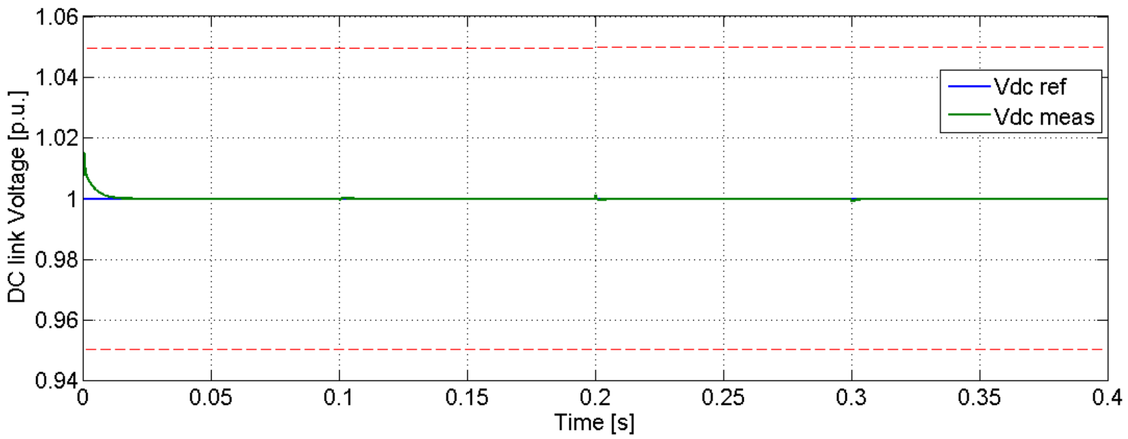


Figure 5.28: DC-link Voltage Transients.

The DC link voltage variations are very small, so it can easily satisfy the 5% dynamic performance (highlighted by the red lines).

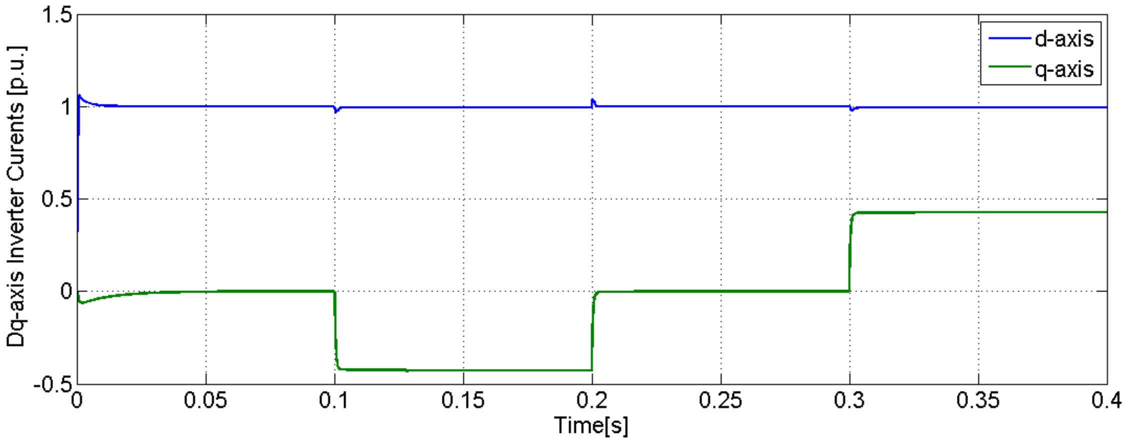


Figure 5.29: Inverter dq-axis Currents.

The small overshoots that appear in the measured d-axis current are a result of the applied steps in the reactive currents from the q-axis. Both PI controllers for the dq-axis currents work properly with response times in the order of few milliseconds and less than 5% overshoots.

Figure 5.30 and Figure 5.31 depicts the phase one in voltage and current at the PCC. It is observed that at simulation time of 0.1s the positive step in reactive power - which means that the WT gives the reactive power to the grid - the q-axis current becomes negative, therefore the current $i_{a,PCC}$ is lagging the voltage $u_{a,PCC}$. Also when a negative step in reactive power is applied at time 0.3s - which signifies that the WT inverter is absorbing reactive power - the q-axis current is now positive, therefore the current $i_{a,PCC}$is leading the voltage $u_{a,PCC}$.

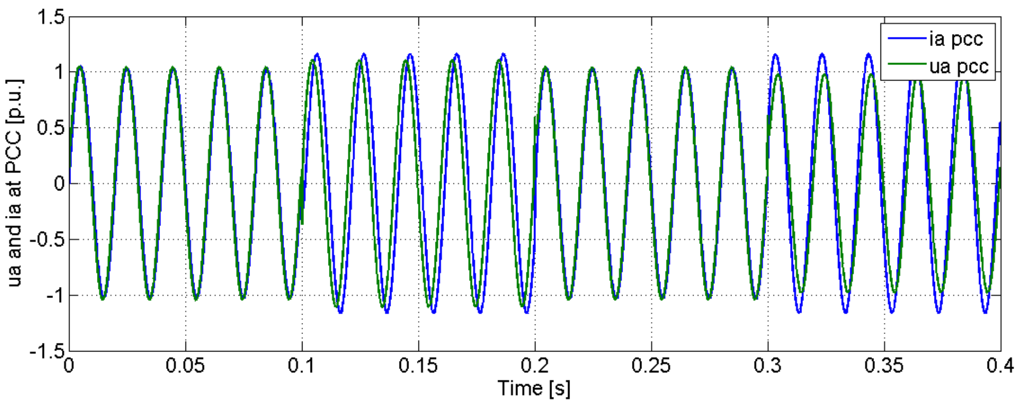


Figure 5.30: Phase one current and voltage at the PCC.

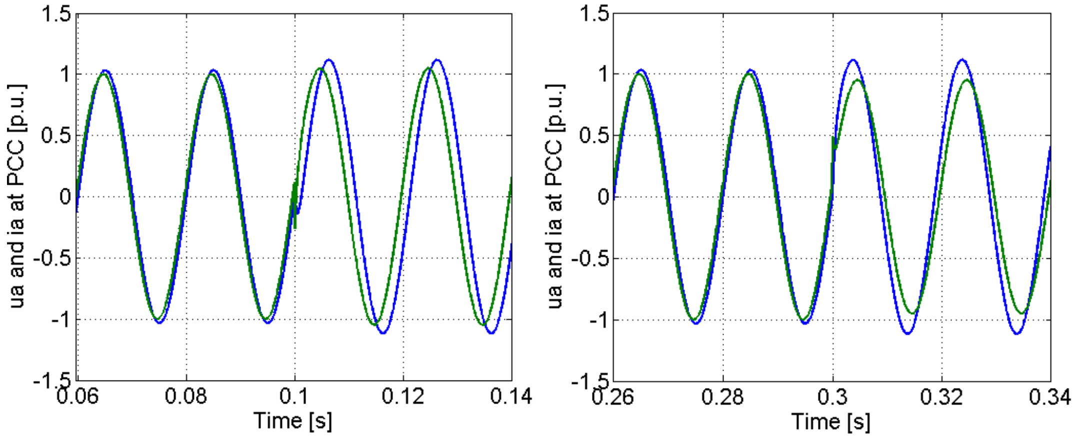


Figure 5.31: Lagging and leading phase one current.

From the following figure it is observed that when reactive power is either absorbed or generated by the WT, the amplitude in the three phase currents at the PCC are increasing. This is explained by the fact that q-axis current will no longer be zero and thus, contribution from both id and iq currents will give a rise in the PCC currents.

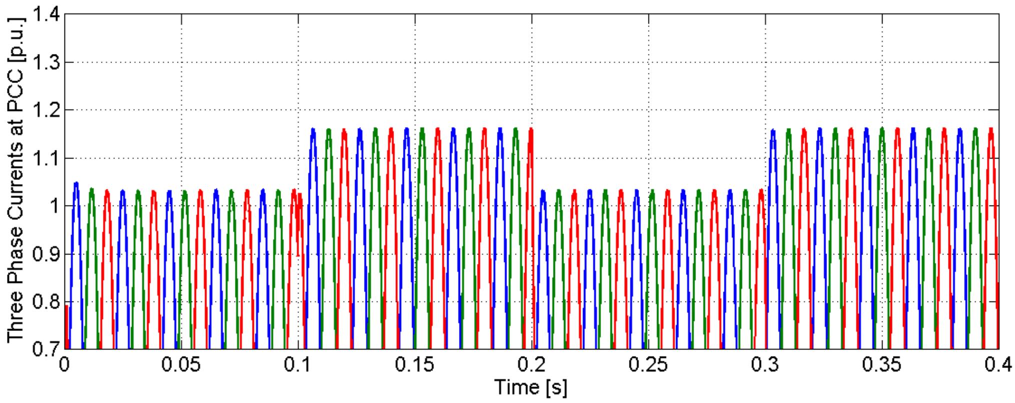


Figure 5.32: Three phase currents at the PCC.

The three phase voltages shown in Figure 5.33 indicate the impact of reactive power injection/absorption on the PCC voltage. It can be seen being able to control the reactive power by STATCOM, one can control the voltage at the PCC. In this case the range of +/-5% is achieved.

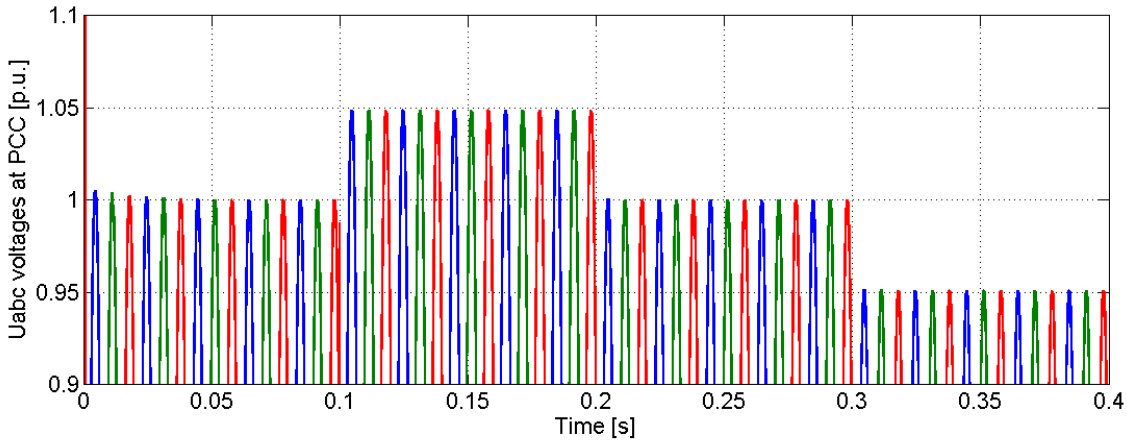


Figure 5.33: Three phase voltages at the PCC.

### 5.3.3 Reactive power steps for both WPP and STATCOM

In this third analysis, TSO requests reactive power to be delivered in steps as it is shown in Figure 5.34.

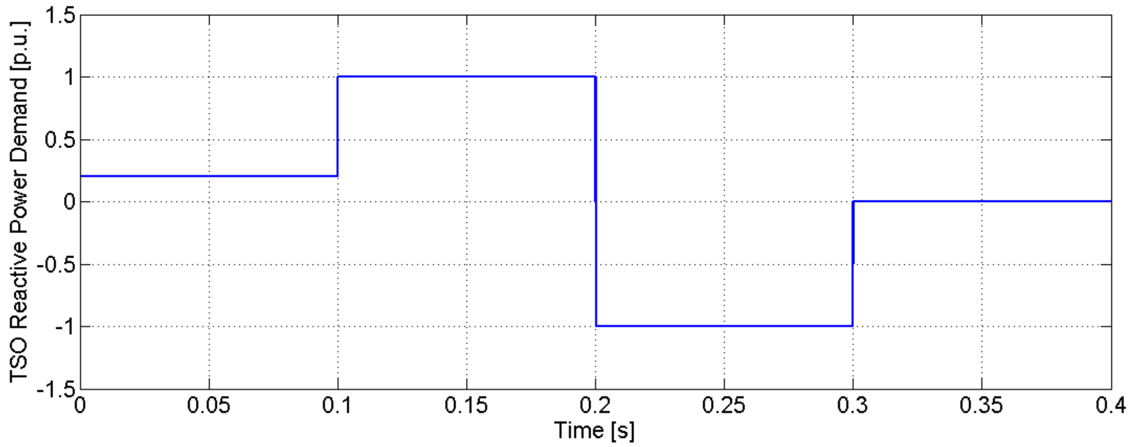


Figure 5.34: TSO's reactive power demand.

In the beginning the reactive power demanded is 0.2 pu. and it can be delivered by the WT alone. At simulation time 0.1s the demand is increased to 1.0 pu. According to the PQ capability curve of the WT, the maximum amount of reactive power to be generated / absorbed by the inverter is +/-0.48 pu. (in this case 1 pu. active power is considered) as stated in section 4.5.1 (indicated by the red dashed lines from Figure 5.35) and thus the WT is no longer able to fulfill the TSO demands. As a result the installed STATCOM will start working and deliver the difference in reactive power (0.52 pu.). At simulation time 0.2s the TSO suddenly changes its reference reactive power to -1.0 pu. which will cause both WT and STATCOM to shift their Q capability from inductive to capacitive.

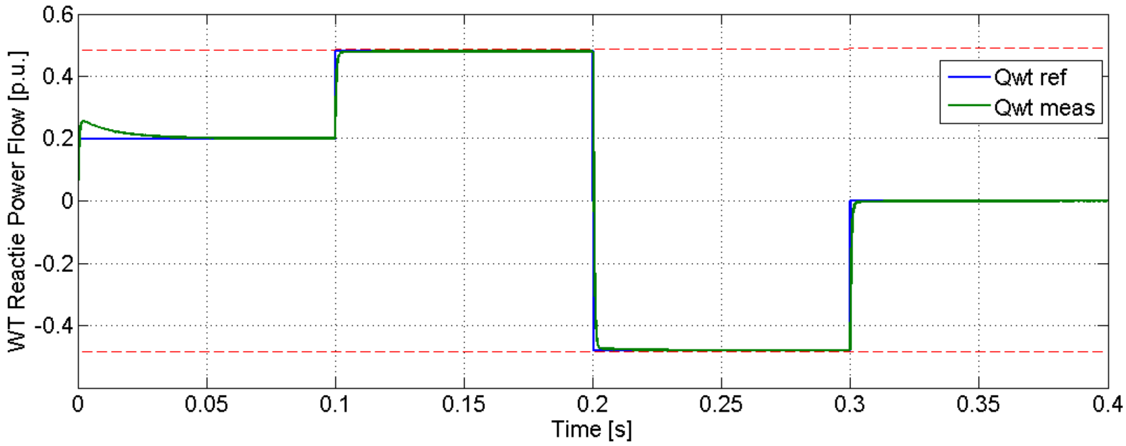


Figure 5.35: WPP's reactive power capability .

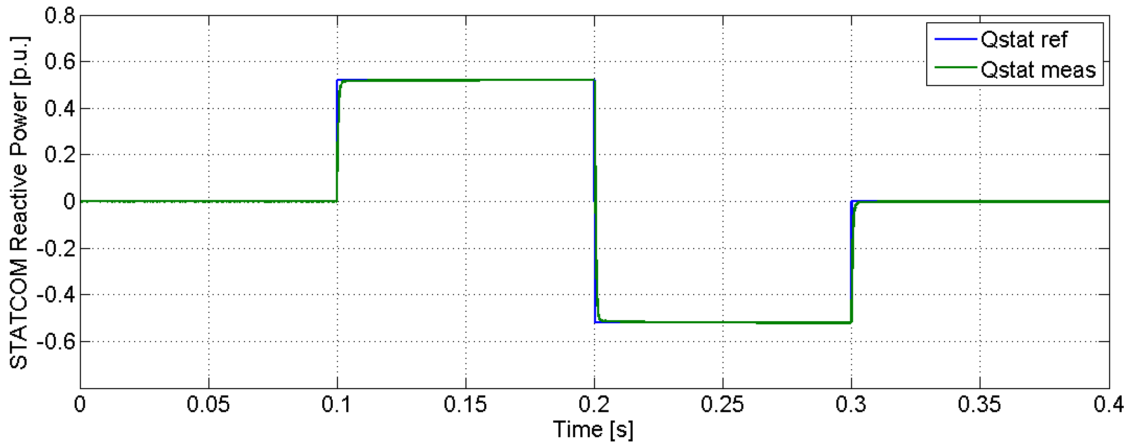


Figure 5.36: STATCOM's reactive power flow.

It is of importance to see that STATCOM's measured reactive power follows the reference from TSO with high speed and accuracy. The step applied at time 0.2s takes the STATCOM reactive current from 0.52 pu. inductive to 0.52 pu. capacitive in less than 10ms. Dynamic performance of a commercial STATCOM (From ABB reference) includes step responses of 30ms from fully inductive to fully capacitive reactive power generation. There are no oscillations after the applied step. Thus it complies with the most demanding E.ON requirement (which is 30ms response time and 60ms settling time).

It is assumed that the power delivered by the WT is the rated value. Figure 5.37 shows the active power variations, in which small overshoots appear due to changes in reactive power reference.

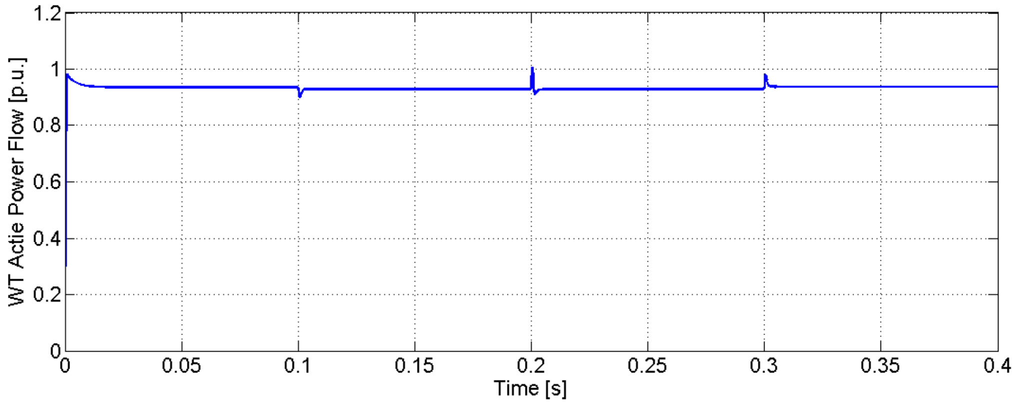


Figure 5.37: WPP produced active power.

Figure 5.38 indicates that the STATCOM's active power is zero at all times, not counting the very small overshoots at the moments of step in reactive power reference, which stabilize in less than 10ms.

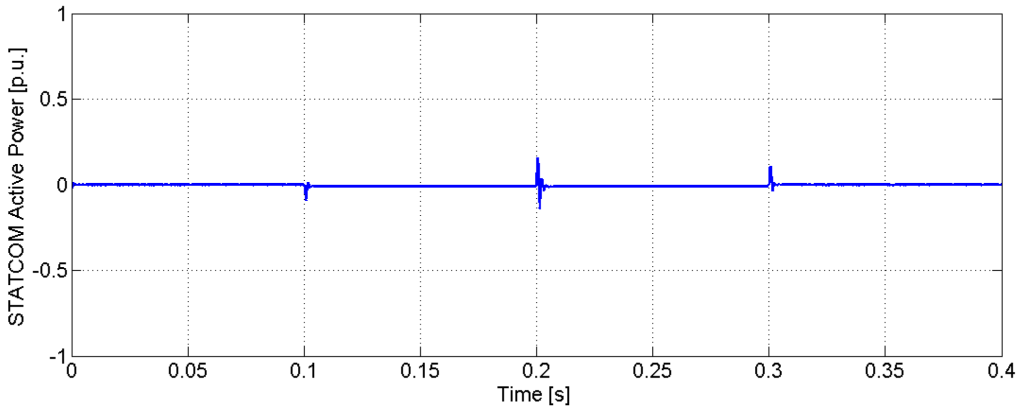


Figure 5.38: STATCOM's active power.

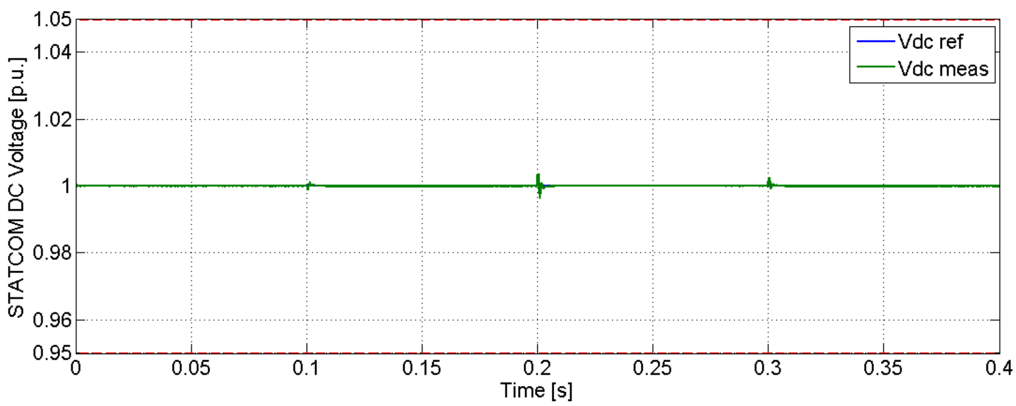


Figure 5.39: DC voltage for STATCOM.

In Figure 5.39 the response of DC link voltage is shown. The DC link voltage tracks the reference with high precision and the variations are very small, thus it can easily satisfy the 5% dynamic performance (highlighted by the red lines).

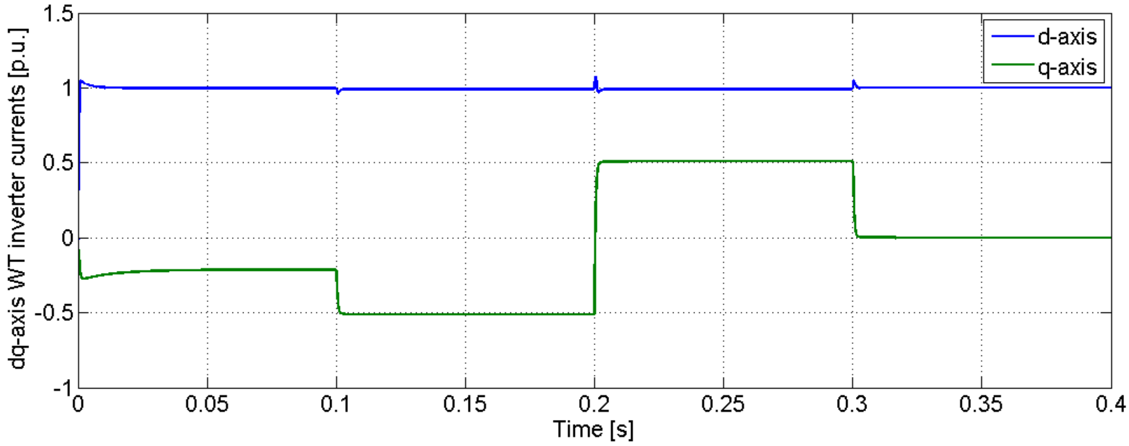


Figure 5.40: WT inverter dq-axis currents.

The relation between active power/reactive power and d-axis/q-axis current for the WT is made clear from comparison of Figures 5.40 to Figure 5.35 and 5.37.

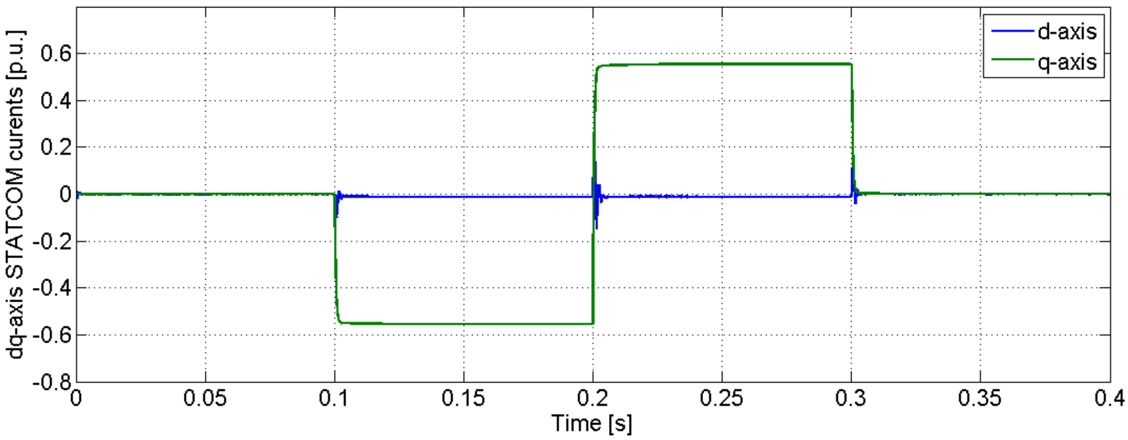


Figure 5.41: STATCOM dq-axis currents.

Also the STATCOM's dq-axis currents in Figure 5.41 are well correlated with the active and reactive powers from Figures 5.36 and 5.38. Figure 5.42 and Figure 5.43 depicts the phase one in voltage and current at the PCC. As it is explained in the previous test case, here the lagging or leading current in respect to voltage is behaving accordingly with the injected or absorbed reactive power to the PCC.

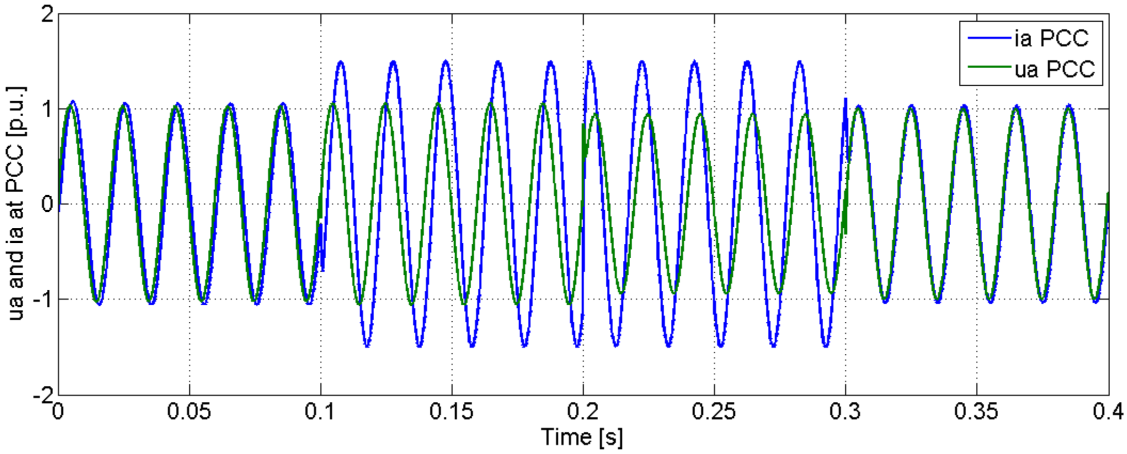


Figure 5.42: Phase one current and voltage at the PCC.

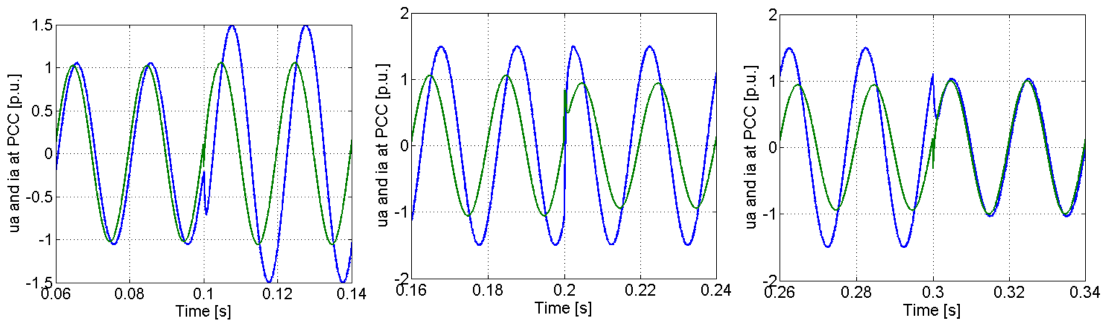


Figure 5.43: Transition from lagging to leading of phase one current.

Figure 5.44 indicates how the amplitude in the three phase currents at the PCC are increasing in respect to the amount of injected reactive power. The currents are increasing both in the positive and negative reactive power steps, however the difference is that the phase angle changes at time 0.2s from lagging to leading as shown in the previous figures.

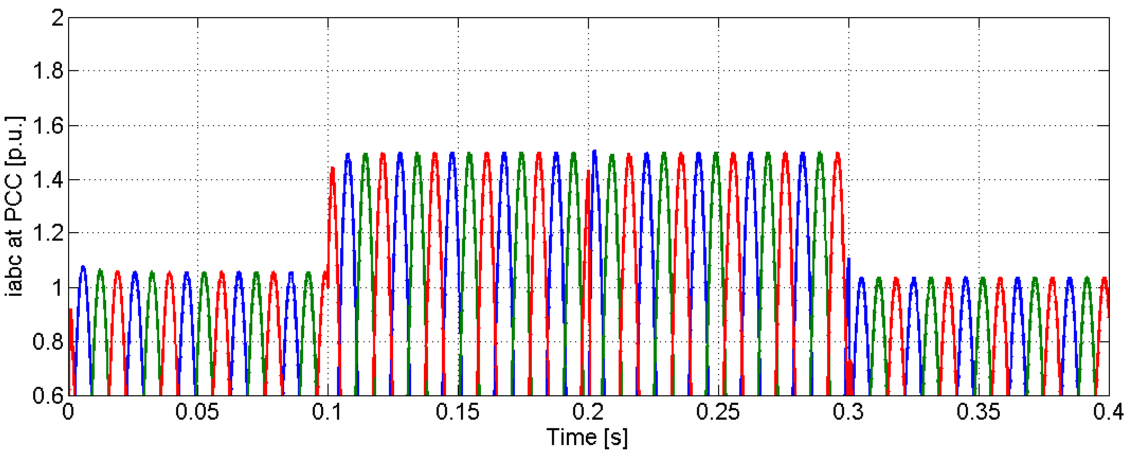


Figure 5.44: Three phase currents at PCC.

As explained in the previous test case, the injection or absorption of reactive power at the PCC affects the magnitude of the three phase voltages. For this case the contribution of WPP and STATCOM to the reactive power flow can increase or decrease the voltages by +/-5%. Therefore in case of voltage excursion in the 0.95 pu. range, they can reestablish the desired 1.0pu. voltage level at the PCC.

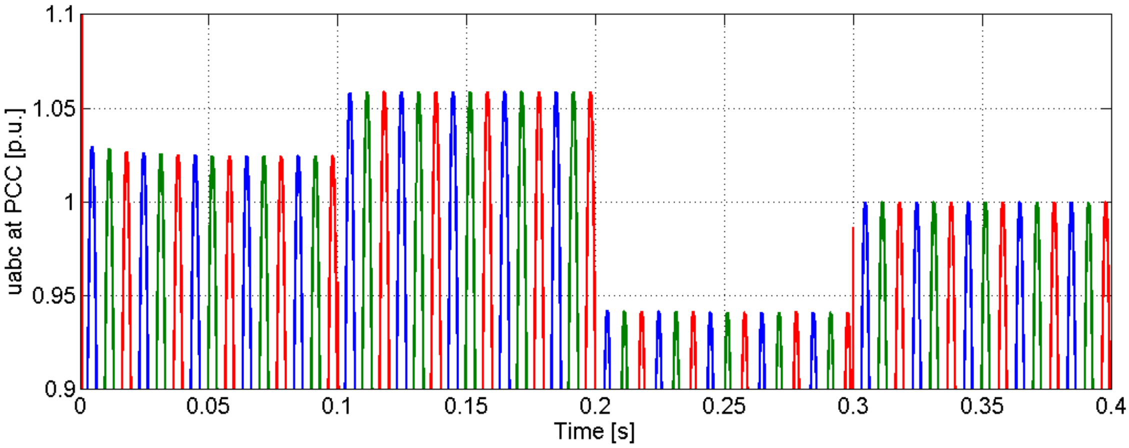


Figure 5.45: Three phase voltages at the PCC.

### 5.3.4 Q/U Slope

This last test case was performed with the outcome of obtaining the Q/U slope for the STATCOM. This case is investigated when the reactive power is produced only by STATCOM, only active power comes from WPP. In steady state reactive power supply or absorption, a reactive power set-point should be followed. This can be implemented by a linear reactive power versus voltage (Q/U) characteristic. The grid codes require such a voltage control (like in UK grid codes [33]), with slopes of 5%. Two simulations were performed and the following plots are obtained. In Figure 5.46 the blue slope has a high slope rate of 13%. In this case the rated STATCOM power was 2MVAr, the same rating as for the WT. This can explain the large changes made possible in the voltage in the range of 0.87 pu.<V<1.13 pu. But in the second simulation a power rating of 660kVAr is assumed (which is one third of the WT rating). Thus the green line now has a slope of 5%. As a result, the rating of STATCOM can be decreased to one third and grid codes can be still fulfilled.

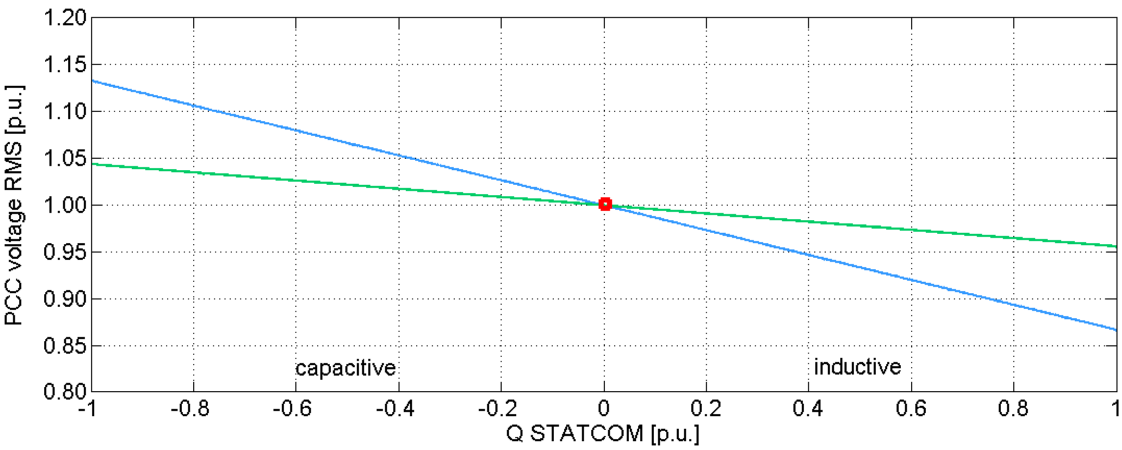


Figure 5.46: Q-U Characteristic.

Finally the next three figures show the waveforms and relations for currents and voltages for the STATCOM when is generating / absorbing reactive power.

In Figure 5.47 maximum reactive power is generated by STATCOM, thus the phase one current has amplitude of 1.0 pu. and is lagging the STATCOM voltage by 90 degrees. Assuming lossless operation STATCOM is producing a voltage in phase with the voltage at PCC. It can be observed as well that in this case the STATCOM voltage has higher amplitude than PCC voltage, which implies that capacitive VARs are flowing from STATCOM to PCC.

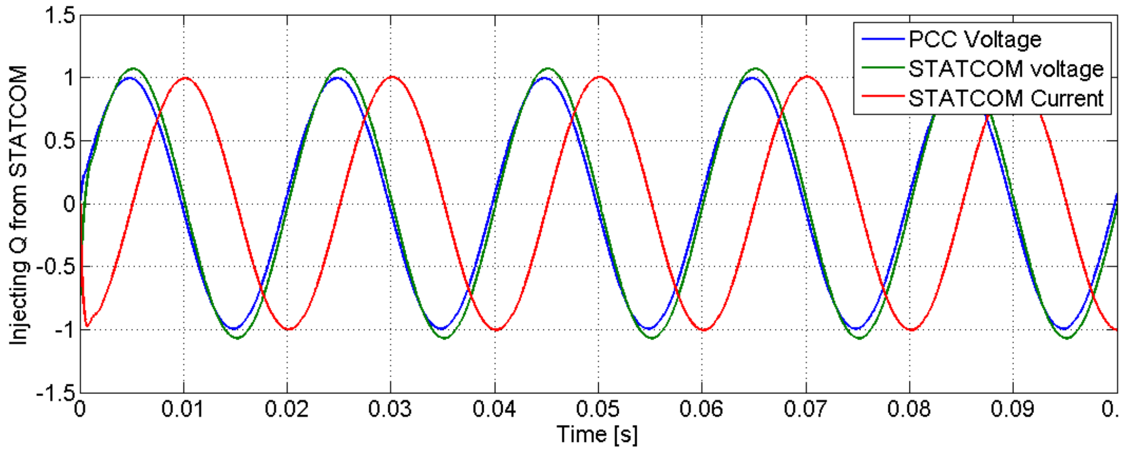


Figure 5.47: Phase one voltages and currents at PCC and STATCOM.

The results shown in the next figure, indicate that when the two voltages at the PCC and STATCOM have same amplitude, no reactive power generation / absorption takes place.

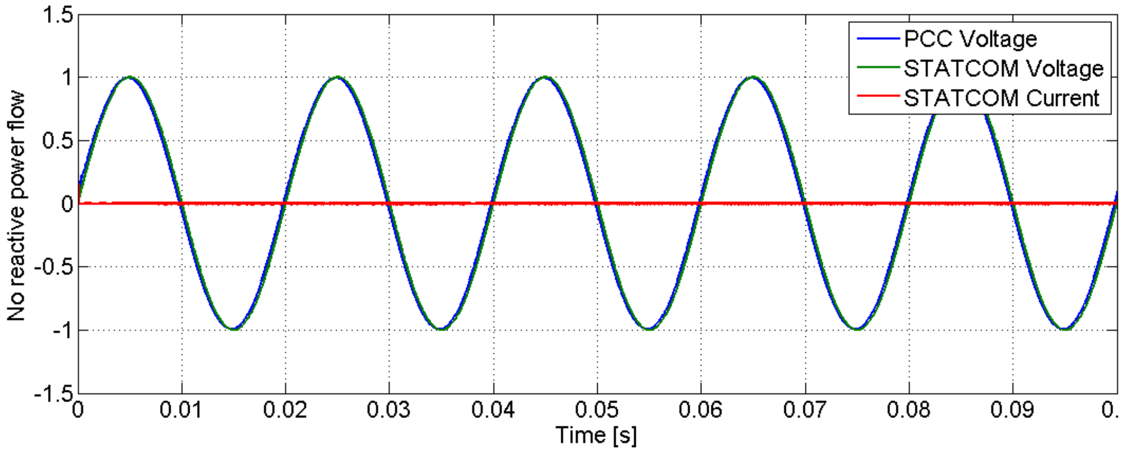


Figure 5.48: Phase one voltages and current at PCC and STATCOM.

In analogy with Figure 5.47, the results in Figure 5.49 show that maximum reactive power is absorbed by STATCOM, thus the phase one current has amplitude of 1.0 pu., it changes direction and now is leading the STATCOM voltage by 90 degrees. In this case the PCC voltage has higher amplitude than STATCOM voltage, which implies that reactive power flows from PCC to STATCOM.

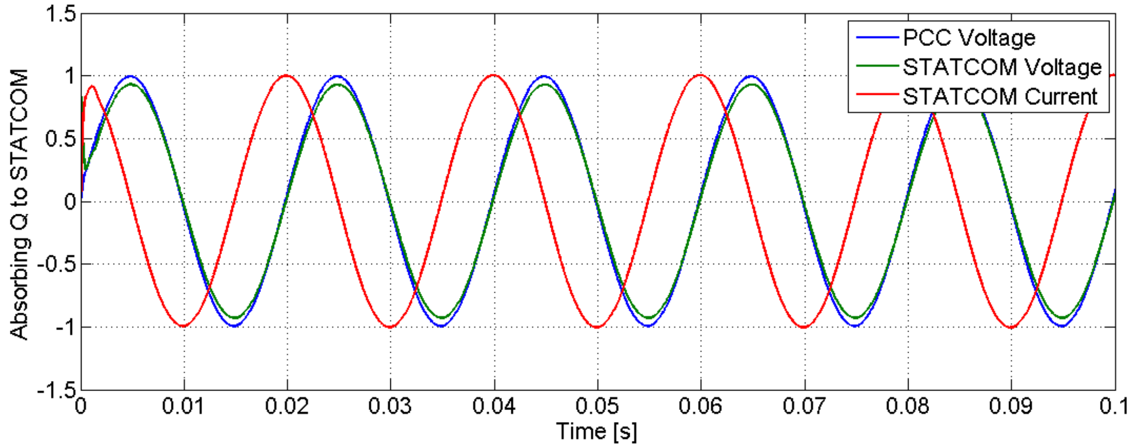


Figure 5.49: Phase one voltages and current at PCC and STATCOM.

## 5.4 Summary

The performance of STATCOM with regards to grid codes is investigated. The analysis is carried out by treating the small scale system model, as a starting point for doing a comprehensive analysis for large scale system model. The study is divided into several test cases. First the investigation of developed reactive power distribution algorithm is realized. In all of the cases the algorithm is showing satisfactory performance. The next test case looks into the impact of having a line between a WPP and PCC. In both cases for small scale system model the line influence is observed. It introduces a difference between the requested reactive power and actual delivered reactive power. For compensating the losses at PCC STATCOM is used. The third test case is a study of STATCOM control strategy, which is focusing on injecting/absorbing reactive power by STATCOM with a desired slope.For small scale system model the results almost identical. The same slope of 0.7% is reached. For the large scale system model two different STATCOM power ratings are compared. In the first case, where STATCOM is rated at same level as WPP slope of 13% is achieved. For the second case, where STATCOM is rated as one third of the power of WPP, slope of 4% is achieved.

For large scale system model additional test cases are carried out. The performance of the WPP for different TSO demands is analyzed. This includes zero reactive power demand, rated active power production with reactive power injection and absorption. Fast controller responses allow the whole system to comply with the grid codes requirements. It should be mentioned that this model is based on mathematical formulas which describe each element of the system. It is simulated in continuous time domain. The drawback of the model is that it does not map the real system behavior deeply enough. For example see the assumptions made in aggregating in Appendix A.9.

Performed simulations and experiments proved that STATCOM is a reliable, fast external reactive power compensator device. It can be used for enhancing the existing systems in respect to fulfilling the demanding grid codes. Furthermore it has the potential of ensuring the compliance of the WPP with the grid codes during faults, which will be investigated in the future.

Chapter 6

# Conclusions and Future Work

This project has been an attempt to address the importance of the reactive power compensation for WPP. The role and the impact of having an external devices for reactive power compensation is analyzed with regards to chosen grid codes. The VSC based STATCOM is chosen as modern, fancy and reliable solution for WP application.

Most of the objectives stated in the initial phase of the project were fulfilled. The investigation of ancillary service requested from WPP in terms of reactive power generation/absorption was performed. For us, master students it was a new research topic. In addition to the review of SOA of FACTS it is shown that grid codes from different TSO are becoming more and more demanding in term of grid voltage support. Modeling and laboratory implementation of the proposed system was completed successfully.

The extension of the conducted research was building the large scale model by means of simulation. However this successful analysis has some drawbacks, which were stated as limitations. Having an aggregated model of WPP is a simplification, which leaves a gap in research process that could be further investigated. This refers to including in the future work the examination of the cable connection in WPP and taking into consideration the interaction between the individual turbines.

The implemented control methods for both grid side converter emulating WPP and STATCOM are tuned according to the design requirements, what is shown in the appropriate section.

The study of the impact of WPP connection line confirmed the initial assumptions that the reactive power losses in line have a significant meaning for Q delivery from WPP. Nevertheless, having an auxiliary service as for example STATCOM can solve this problem.

The verification of the obtained results showed that the system with a STATCOM as a support device can meet the grid code requirements. Unfortunately, the results acquired in QU-slope strategy in the small scale system are not satisfactory. As it is explained before, several factors determined this outcome. Namely, the DC supply limitation and having a strong, stiff grid.

As future work, a number of points can be paid attention to, in order to further demonstrate the benefits of STATCOM devices in WPP applications:

- Different inputs to the inverter, taking in consideration power fluctuations caused by wind speed variations, tower shadowing, etc.
- Adding long transmission cables for the large scale model and investigate communication delay problems occurring between WPP / STATCOM and TSO.
- Moving from an aggregated WPP model to a real design of WPP with many turbines, experiencing different wind speed profiles, thus each WT working at a different set-point.
- Different control strategies can be implemented for STATCOM and a comparison between them to show which one offers higher performances.
- Investigate through simulations, the impact of changing the Short Circuit Ratio (SCR) of the grid, and STATCOM sizing depending on grid stiffness.

- Investigate various grid disturbances, and observe how STATCOM can assist the WPP with regards to voltage ride through requirements stated in the grid codes.
- Include an energy storage system on the DC side of STATCOM. This will allow compensation of power fluctuations and improve the active power control with respect to grid codes.
- Perform experiments using a PMSG machine and full scale back-to-back power converter for investigating the power flow from the rotor up till the grid.

# Bibliography

[1] The European Wind Energy Association (EWEA), "Pure Power", Report 2009

[2] The European Wind Energy Association (EWEA), "The Economics of Wind Energy", Report 2009

[3] The European Wind Energy Association (EWEA), "Wind Facts", Report 2007

[4] European Commission "20 20 by 2020 Europe's climate change opportunity", 2008, Brussels

[5] "World Market Update BTM Projects 1,000 GW of Wind Power by 2019", BTM Consult Aps, March 2010

[6] "World Market Update 2008. Forecast 2009-2013", BTM Consult Aps, March 2009

[7] J. Machowski, J. Bialek, J.R. Bumby "Power Systems Dynamics - Stability and Control", ISBN 978-0-479-72558-0, John Wiley & Sons, 2008

[8] X.P. Zhang, C. Rehtanz, B. Pal "Flexible AC Transmission Systems: Modeling and Control", ISBN-13 978-3-540-30606-1, Springer-Verlag Berlin Heidelberg 2006

[9] F. Iov and F. Blaabjerg, "Power electronics and control for wind power systems," PEMWA 2009. IEEE, pp. 116, 24-26 June 2009.

[10] "Wind Turbines Connected to Grids with Voltages above 100 kV - Technical regulation for the properties and the regulation of wind turbines" , Elkraft, Eltra, November 2004

[11] "Wind Power in Power Systems" T. Ackermann, 2005, ISBN 0-470-85508-8

[12] "Wind Turbine Blockset in Matlab/Simulink General Overview and Description of the Models" ,Florin Iov, Anca Daniela Hansen, Poul Sørensen, Frede Blaabjerg; AAU, March 2004

[13] "A New Single-Phase PLL Structure Based on Second Order Generalized Integrator" Ciobotaru, M.; Teodorescu, R.; Blaabjerg, F.; Power Electronics Specialists Conference, 2006. PESC '06. 37th IEEE 18-22 June 2006 Page(s):1 - 6

[14] "Proportional-Resonant Controllers and Filters for Grid-Connected Voltage-Source Converters" Teodorescu, R.; Blaabjerg, F.; Liserre, M.; Loh, P.C.; Electric Power Applications, IEE Proceedings

[15] "Synchronization Methods for Three Phase Distributed Power Generation Systems. An Overview and Evaluation"Timbus, A.; Teodorescu, R.; Blaabjerg, F.; Liserre, M.; Power Electronics Specialists Conference, 2005. PESC '05. IEEE 36th 16-16 June 2005 Page(s):2474 - 2481

[16] "PLL Algorithm for Power Generation Systems Robust to Grid Voltage Faults" Timbus, A.V.; Teodorescu, R.; Blaabjerg, F.; Liserre, M.; Rodriguez, P.; Power Electronics Specialists Conference, 2006. PESC '06. 37th IEEE 18-22 June 2006 Page(s):1 - 7

[17] "New Positive-sequence Voltage Detector for Grid Synchronization of Power Converters under Faulty Grid Conditions" Rodriguez, P.; Teodorescu, R.; Candela, I.; Timbus, A.V.; Liserre, M.; Blaabjerg, F.; Power Electronics Specialists Conference, 2006. PESC '06. 37th IEEE 18-22 June 2006 Page(s):1 - 7

[18] "Stationary-Frame Generalized Integrators for Current Control of Active Power Filters with Zero Steady-State Error for Current Harmonics of Concern Under Unbalanced and Distorted Operating Conditions" Xiaoming Yuan; Merk, W.; Stemmler, H.; Allmeling, J.; Industry Applications, IEEE Transactions on Volume 38, Issue 2, March-April 2002 Page(s):523 - 532

[19] "A New Control Structure for Grid-Connected PV Inverters with Zero Steady-State Error and Selective Harmonic Compensation" Teodorescu, R.; Blaabjerg, F.; Borup, U.; Liserre, M.; Applied Power Electronics Conference and Exposition, 2004. APEC '04. Nineteenth Annual IEEE Volume 1, 2004 Page(s):580 - 586 Vol.1

[20] "Power Electronics for ModernWind Turbines", Frede Blaabjerg, Zhe Chen,Copyright © 2006 by Morgan and Claypool Publishers

[21] "Wind Turbine Operation in Electric Power System", Z. Lubosny, Springer 2003

[22] German Transmission Code 2007 - Network and System Rules of the German Transmission System Operators.

[23] "Control in Power Electronics - Selected Problems" Academic Press Series in Engineering): Ramu Krishnan, JD Irwin, Marian P. Kazmierkowski, Frede Blaabjerg; ISBN: 0124027725

[24] "Grid Impedance Estimation via Excitation of LCL-Filter Resonance" Liserre, M.; Blaabjerg, F.; Teodorescu, R.; Industry Applications, IEEE Transactions on Volume 43, Issue 5, Sept.-oct. 2007 Page(s):1401 - 1407

[25] Liserre, M., Dell'Aquila, A., Blaabjerg, F., "Design and control of a three-phase active rectifier under non-ideal operating conditions" 2002

[26] P. Rodriguez, Student Member, IEEE, R. Pindado, Member, IEEE, and J . Pou, Member, IEEE, "Energy Control of Three-phase Four-wire Shunt Active Power Filter", Industrial Electronics Society, 2003. IECON '03. The 29th Annual Conference of the IEEE, 2003, Page(s): 1061 - 1066 Vol.2

[27] Industrial/Ph.D. Course in "Power Electronics for Renewable Energy Systems – in theory and practice", AAU Department of Energy Technology Aalborg, Denmark, October 12- 15, 2009

[28] "The theory of instantaneous power in three-phase four-wire systems: a comprehensive approach" Akagi, H.; Ogasawara, S.; Hyosung Kim; Industry Applications Conference, 1999. Thirty-Fourth IAS Annual Meeting. Conference Record of the 1999 IEEE Volume: 1

[29] "Wind Farms as Reactive Power Ancillary Service Providers—Technical and Economic Issues", N.R. Ullah, K. Bhattacharya, T. Thiringer, IEEE TRANSACTIONS ON ENERGY CONVERSION, VOL. 24, NO. 3, SEPTEMBER 2009

[30] M. Chinchilla, S. Arnaltes, and J. C. Burgos, "Control of permanent magnet generators applied to variable-speed wind-energy systems connected to the grid," IEEE Trans. Energy Convers., vol. 21, no. 1, pp. 130– 135, Mar. 2006.

[31] "CONTROL OF PERMANENT MAGNET SYNCHRONOUS GENERATOR FOR LARGE WIND TURBINES" C. Busca,A.I. Stan, T. M. Stanciu, D. I. Stroe, Autumn Semester, 2009

[32] "Power Electronic Control in Electrical Systems", E. Acha, V. G. Agelidis, O. Anaya-Lara, T. J. E. Miller, ISBN 0750651261, 2002

[33] "THE GRID CODE", National Grid Electricity Transmission plc, March 2010

[34] "Reactive Power Compensation Technologies, State of the Art Review", J. Dixon, L. Morán,J. Rodríguez, R. Domke,

# Appendices

# Modeling

## A.1 WPP and STATCOM in small scale system.

The diagram showing three-phase two-level inverter incorporated for WPP and STATCOM model is presented below.

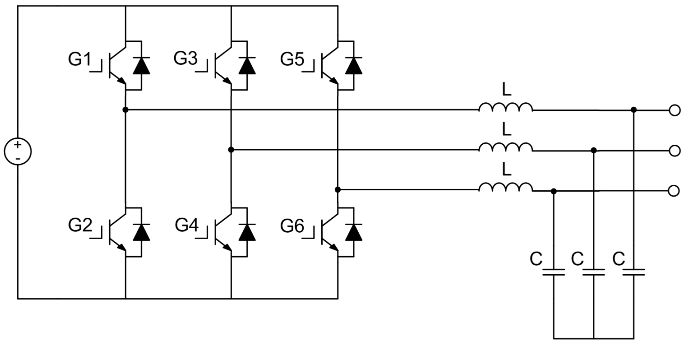


Figure A.1: Two-level three phase inverter.

The mathematical model behind this structure is widely explained in Appendix A.8.

## A.2 Transformer and cable in small scale system.

For making the simplification regarding control design of emulated WPP system in laboratory, transformer was modeled as inductance connected in series with a resistance. The transformer ratio is 1:1. The connection line was modeled as a variable inductor. The figure showing transformer and line model is presented below:


Figure A.2: Modeled transformer (a) and connection line (b).

## A.3 Grid model in small scale system.

Grid was defined as a controllable three-phase voltage source. The phase voltages defined as:

$$V_a = E_m \cdot cos(\omega \cdot t) \tag{A.1}$$

$$V_b = E_m \cdot cos\left(\omega \cdot t - \frac{2\pi}{3}\right) \tag{A.2}$$

$$V_c = E_m \cdot cos\left(\omega \cdot t - \frac{4\pi}{3}\right) \tag{A.3}$$

In the above equations $\omega$ represents the angular frequency and $E_m$ represents the phase voltage amplitude.

## A.4 Wind model

Simulations concepts concerning wind modeling that the wind speed is characterized by the sum of the four following components [11]:

- the average value;
- a ramp component, which describes a steady increase in wind speed;
- a gust component, representing a sudden wind gust;
- a turbulence component;

The equation below describes the whole concept:

$$v_w(t) = v_{wa} + v_{wr}(t) + v_{wg}(t) + v_{wt}(t) \tag{A.4}$$

where $v_w(t)$ is the wind speed at time t, $v_{wa}$ is the average wind speed, $v_{wr}(t)$ is the ramp component, $v_{wg}(t)$is the gust component and $v_{wt}(t)$ is the turbulence. All the wind speed components are in "meters per second" and time t is "in seconds". The model does not include the tower shadowing effect.

#### Average wind speed

The average speed of the wind is based on wind classes stated in IEC 61400 which are presented in the table below:

| WTG class | I | II | III | IV |
|---|---|---|---|---|
| $V_{ave}$ average wind speed at hub-height (m/s) | 10 | 8.5 | 7.5 | 6 |
| $I_{15}$ characteristic turbulence Class A | | 18% | | |
| $I_{15}$ characteristic turbulence Class B | | 15% | | |

Table A.1: IEC classification of wind turbines.

Except class specification of the average wind speed user has an opportunity to use his own average speed and turbulence inputs.

#### Turbulence component

The turbulence component is obtained by the means of using a normally distributed white noise generator. The model uses a new normally distributed white noise generator which has been implemented using a 'C' S-Function based on the Ziggurat Algorithm shown in [12].

#### Ramp component

To characterize the wind speed ramp one needs to define three parameters - the amplitude of the wind speed ramp, $\hat{A_r}$ (in m/s), the starting time of the wind speed ramp $T_{sr}$ (in seconds), and the end time of the wind speed ramp, $T_{er}$ (in seconds). The equation (A.5) describes the relation for the ramp component:

$$
\left.\begin{array}{lll}
t < T_{sr} & for & v_{wr} = 0 \\
T_{sr} \leq t \leq T_{er} & for & v_{wr} = \hat{A}_r \dfrac{(t - T_{sr})}{(T_{er} - T_{sr})} \\
T_{er} < t & for & v_{wr} = \hat{A}_r
\end{array}\right\} \tag{A.5}
$$

The model includes the possibility of using n-ramps with predefined offset time between them.

### Gust component

For modeling the wind speed gust one needs to define three parameters - the amplitude of the wind speed gust, $\hat{A}_g$ (in m/s), the starting time of the wind speed gust $T_{sg}$ (in seconds), and the end time of the wind speed gust, $T_{eg}$ (in seconds). The gust component is modeled using equation (A.6):

$$
\left.\begin{array}{lll}
t < T_{sg} & for & v_{wg} = 0 \\
T_{sg} \leq t \leq T_{eg} & for & v_{wg} = \hat{A}_g \left\{1 - cos\left[2\pi\left(\dfrac{(t - T_{sg})}{(T_{eg} - T_{sg})}\right)\right]\right\} \\
T_{eg} < t & for & v_{wg} = 0
\end{array}\right\} \tag{A.6}
$$

The model includes the possibility of using n-gusts with predefined offset time between them.

For the turbulence, gust and ramp components 'C' S-Functions were used. For specifying all the input parameters the mathematical model was implemented in Simulink using a masked subsystem. It can be seen in Figure A.3.

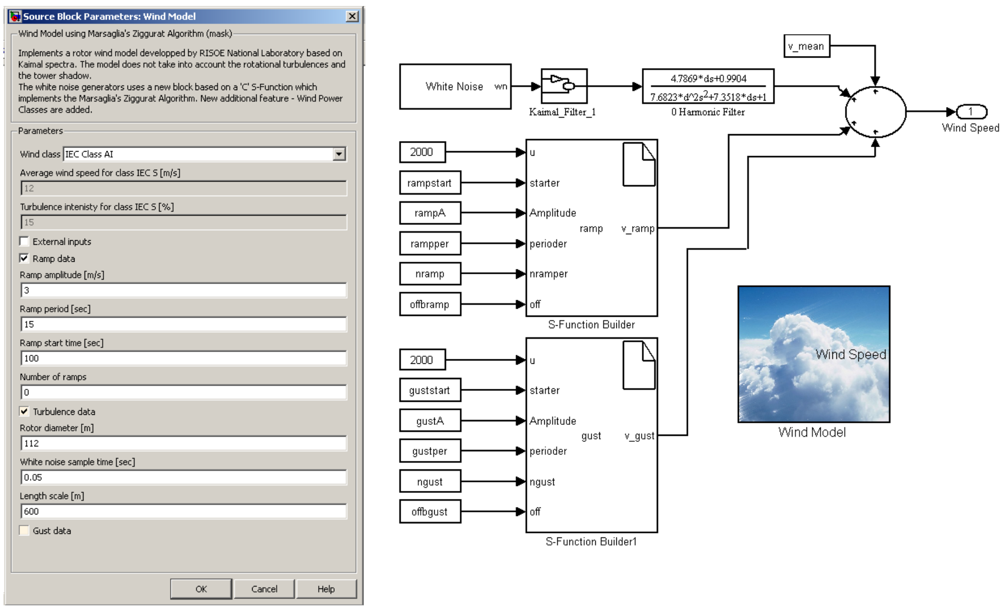


Figure A.3: Implemented wind mathematical model.

To present the performance of the implemented model a simulation was carried out. The results can be seen in Figure A.4.

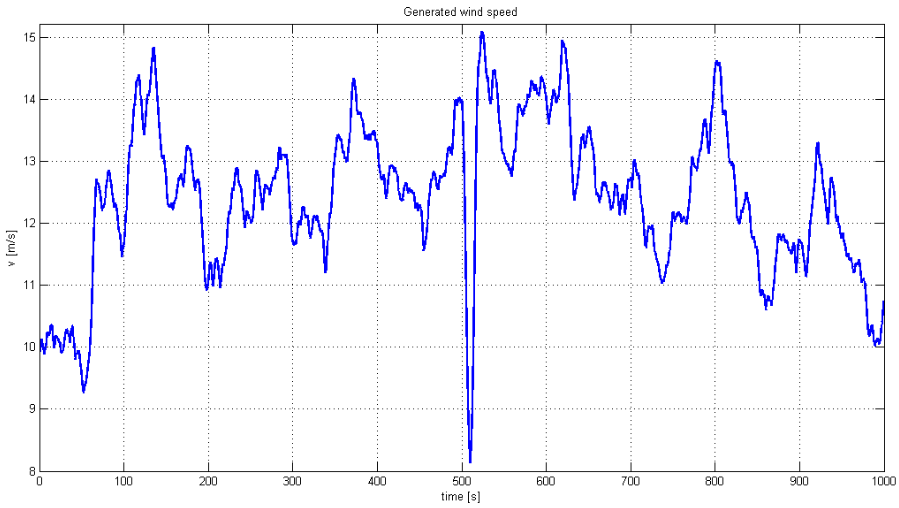


Figure A.4: Example of a simulated wind speed sequence, with the following input values: average wind speed, $v_{wa}$, 10 m/s (IEC class AI); start time of wind speed ramp, $T_{sr}$, 80 s; end time of wind speed ramp, $T_{er}$, 400 s; amplitude of wind speed ramp, $\hat{A_r}$, 3 m/s; start time of wind speed gust, $T_{sg}$, 500 s; end time of wind speed gust, $T_{eg}$, 520 s; amplitude of wind speed gust, $\hat{A_g}$ -6 m/s.

## A.5 Rotor model

The model of the mechanical rotor of wind turbine is based on concepts presented by [11]. The mechanical power extracted from the wind from the wind as a function of wind speed is given by the equation:

$$P_{wt} = \frac{\rho}{2} A_{wt} c_p(\lambda, \theta) v_w^3 \tag{A.7}$$

where $P_{wt}$ is the power coming from wind in watts, $\rho$ is the air density ($kg/m^3$), $c_p$ is the power coefficient , $\lambda$ is the tip speed ratio $v_t/v_w$ - between the blade tip speed and wind speed, $\theta$ is the pitch angle and $A_{wt}$ is the area covered by the wind turbine rotor. As stated in [11] most of the individual wind turbines have very similar power curves. Therefore an individual approximation of a power curve for each wind turbine is not necessary. Instead a general approximation of $c_p(\lambda, \theta)$ will be used. The general equation describing the fixed speed and variable speed win turbines is presented below.

$$c_p(\lambda, \theta) = c_1 \left( \frac{c_2}{\lambda_i} - c_3\theta - c_4\theta^{c_5} - c_6 \right) exp\left( \frac{-c_7}{\lambda_i} \right) \tag{A.8}$$

where

$$\lambda_i = \left[ \left( \frac{1}{\lambda + c_8\theta} \right) - \left( \frac{c_9}{\theta^3 + 1} \right) \right]^{-1} \tag{A.9}$$

The constant coefficients from $c_1$ to $c_9$ are presented in table .

| | $c_1$ | $c_2$ | $c_3$ | $c_4$ | $c_5$ | $c_6$ | $c_7$ | $c_8$ | $c_9$ |
|---|---|---|---|---|---|---|---|---|---|
| Heier (1998) | 0.5 | 116 | 0.4 | 0 | - | 5 | 21 | 0.08 | 0.035 |
| Fixed-speed wind turbines | 0.44 | 125 | 0 | 0 | 0 | 6.94 | 16.5 | 0 | -0.002 |
| Variable-speed wind turbines | 0.73 | 151 | 0.58 | 0.002 | 2.14 | 13.2 | 18.4 | -0.02 | -0.003 |

Table A.2: Approximation of power curves.

Above model was implemented in MATLAB Simulink software and it is presented in Figure A.5.

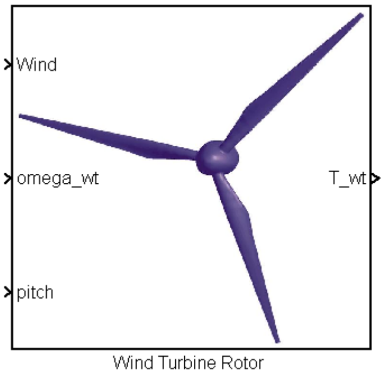


Figure A.5: Implemented rotor model.

## A.6 Drive train model

The simulated wind turbine uses a drive train with a single stage gearbox. To analyze the behavior of the wind rotor during transients, a mechanical model for the wind turbine drive train was used.

The drive train behavior can be analyzed by the simplified two-mass model, if the following assumptions are made [12]:

- the moments of inertia for the low speed shaft, high speed shaft, and gearbox wheels are neglected, being small quantities when compared to wind wheel and generator inertias (around 2 – 4 % of total inertia [21]);
- the shaft torsional stiffness and the damping coefficient of the low-speed shaft and high-speed shaft are combined together and moved on either side of the gearbox.

In the presented model, the system equivalent stiffness and damping factor are put on the low speed shaft, to illustrate that in a real wind turbine, the stiffness of the low speed shaft is about 100 times less than the generator shaft [21], here considered as stiff. The component diagram for the drive train with its parameters is shown in Figure A.6.

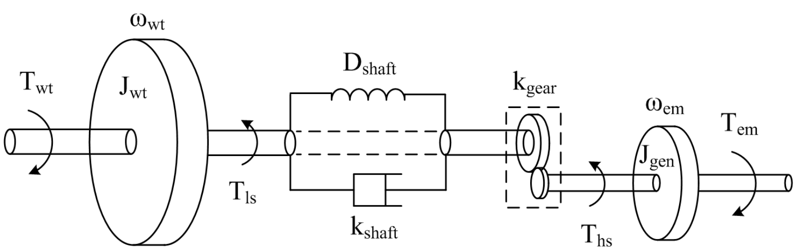


Figure A.6: The drive train component diagram

The following equations are forming the two-mass model of the drive train:

$$J_{wt}\frac{d\omega_{wt}}{dt} = T_{wt} - T_{ls} \tag{A.10}$$

$$T_{ls} = k_{shaft}\left(\theta_{wt} - \theta_{ls}\right) + D_{shaft}\left(\omega_{wt} - \omega_{ls}\right) \tag{A.11}$$

$$J_{gen}\frac{d\omega_m}{dt} = T_{hs} - T_{em} \tag{A.12}$$

$$\frac{d\theta_{wt}}{dt} = \omega_{wt} \tag{A.13}$$

$$\frac{d\theta_m}{dt} = \omega_m \tag{A.14}$$

$$k_{gear} = \frac{T_{ls}}{T_{hs}} = \frac{\omega_{hs}}{\omega_{ls}} \tag{A.15}$$

By using equation (A.15), all the equations can be transferred to one side of the gearbox. In this case (A.12) will be transferred to the rotor side.

Having written the differential equations for the two mass model, the Matlab/Simulink block of the drive train can be built. Above model was implemented in MATLAB Simulink software and it is presented in Figure A.7. The detailed model, showing the implemented differential equations, is presented in Appendix D, and it is based on [12].

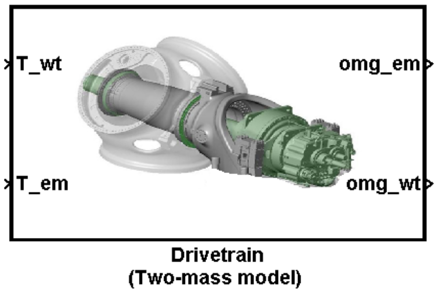


Figure A.7: Implemented drive train model.

The values for parameters of the drive train model are given in Appendix . The presented drive train model is a simplified but a sufficient approach to inspect the behavior of the mechanical part in a wind turbine.

## A.7 Wind turbine generator model

The Wind Turbine Generator (WTG) is the most important component in a wind energy conversion system. It converts the mechanical energy from the rotor shaft into electrical energy, with the use of electromagnetic induction principle. The Permanent Magnet Synchronous Generator (PMSG) is a synchronous generator which has permanent magnets (PM's) mounted on the rotor.

The dynamic model of PMSG is made simpler by transforming the three phase 'abc' reference frame in the two phase 'dq' synchronous reference frame, in which the quadrature $q$-axis is $90^o$ ahead of the direct $d$-axis, referring to the rotation direction.

The electrical equations describing the PMSG model in 'dq'-reference frame are given in (A.16).

$$\begin{cases} \dfrac{di_d}{dt} = -\dfrac{R_s}{L_d}i_d + \omega_e\dfrac{L_q}{L_d}i_q + \dfrac{1}{L_d}u_d \\ \dfrac{di_q}{dt} = -\dfrac{R_s}{L_q}i_q - \omega_e\left(\dfrac{L_d}{L_q}i_d + \dfrac{1}{L_q}\Psi_{PM}\right) + \dfrac{1}{L_q}u_q \end{cases} \tag{A.16}$$

where:

- $u_d$,$u_q$ and $i_d$,$i_q$ - represent the $d$- and $q$-axis stator voltages and currents respectively
- $\omega_e$ - represents the electrical rotor speed obtained from equation:

$$\omega_m = \frac{\omega_e}{n_{pp}} \tag{A.17}$$

- $n_{pp}$ - represents the number of pole pairs
- $\omega_m$ - represents the mechanical speed
- $\Psi_{PM}$ - represents the PM flux linkage

The equation for the electromagnetic torque $T_{em}$ is shown in (A.18).

$$T_{em} = \frac{3}{2} n_{pp} \left[ \Psi_{PM} i_q + (L_d - Lq)\, i_d i_q \right] \tag{A.18}$$

Assuming that the PMSG generator has Surface-mounted magnets on the rotor (SMPSG), resulting in equal values for direct and quadrature axis inductances ($L_d = L_q = L$). Thus the generator electric model is simplified resulting in the following set of equations:

$$\begin{cases} \dfrac{di_d}{dt} = -\dfrac{R_s}{L} i_d + \omega_e i_q + \dfrac{1}{L} u_d \\ \dfrac{di_q}{dt} = -\dfrac{R_s}{L} i_q - \omega_e \left( i_d + \dfrac{1}{L} \Psi_{PM} \right) + \dfrac{1}{L} u_q \end{cases} \tag{A.19}$$

The equivalent circuit for one phase of the PMSG in dq-reference frame is presented in Figure A.8.

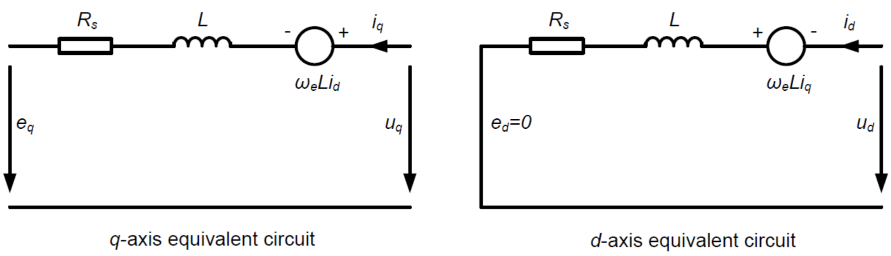


Figure A.8: PMSG electrical circuit in synchronous reference frame

The electromagnetic torque equation (A.18) can also be rewritten as:

$$T_{em} = \frac{3}{2} n_{pp} \left( \Psi_{PM} i_q \right) \tag{A.20}$$

The last equation which completes the PMSG model is the mechanical equation given in (A.21).

$$\begin{cases} T_L - T_{em} = J \dfrac{d\omega_m}{dt} \\ \dfrac{d\theta_m}{dt} = \omega_m \end{cases} \tag{A.21}$$

where:

- $T_L$ - represents the driving torque

- $J$ - represents the rotor and generator equivalent moment of inertia
- $\theta_m$ - represents the rotor angular position

The input/output signals of the generator modeled in Simulink are shown in Figure A.9. The values for the generator parameters are presented in Appendix.

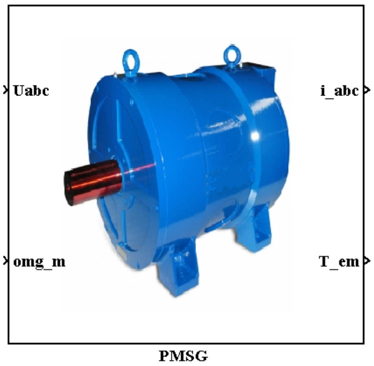


Figure A.9: PMSG block diagram

## A.8 Full scale converter model

Modeled converter is presented in Figure A.10.

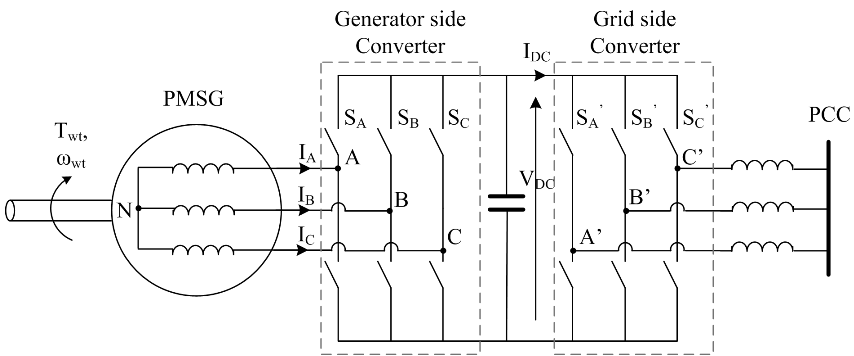


Figure A.10: Full scale converter scheme.

The ability to operate in rectifier and inverter mode allows to achieve bidirectional power flow. This project assumes that the WPP will deliver power to the grid, so the machine side converter works as a rectifier, controlling the torque and the speed and the grid side converter works as an inverter keeping the DC-link voltage constant and it can control the grid side voltage.

Three phase VSC consists usually of six IGBT-s, two on each leg. To implement a mathematical model of a VSC into Simulink three switching variables $S_a$, $S_b$ and $S_c$ are introduced. These variables can only have two values, either 1 or 0 and each of them is associated with one leg of the converter (either its machine side converter or grid side converter).

In order to define the three phase voltages of the converter the switching variables $S_a$, $S_b$ and $S_c$ and the DC-link voltage must be known. The voltages can be found from formula:

$$\begin{bmatrix} v_{an} \\ v_{bn} \\ v_{cn} \end{bmatrix} = \frac{V_{DC}}{3} \begin{bmatrix} 2 & -1 & -1 \\ -1 & 2 & -1 \\ -1 & -1 & 2 \end{bmatrix} \begin{bmatrix} S_a \\ S_b \\ S_c \end{bmatrix} \tag{A.22}$$

To express DC-link current one can use an expression:

$$I_{DC} = \begin{bmatrix} S_a & S_b & S_c \end{bmatrix} \begin{bmatrix} i_a \\ i_b \\ i_c \end{bmatrix} \tag{A.23}$$

Above model was implemented in MATLAB Simulink software and it is presented in Figure A.11.

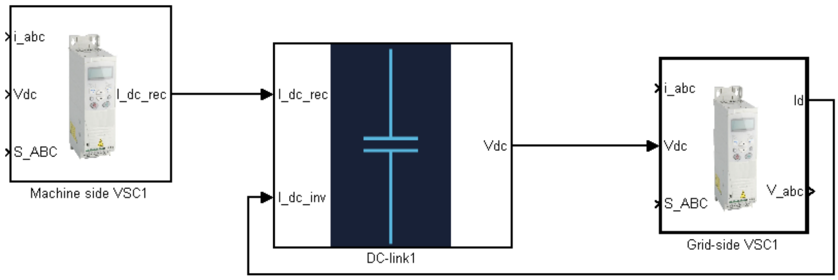


Figure A.11: Implemented full scale converter model.

## A.9 Aggregated WPP model

According to [11] one can express the simulated behavior of many wind turbines by a single equivalent model. The reason allowing to make such assumption is that the WT's in large WPP show a coherent response when they are exposed to transient incidences in the power system. Since this project focuses on modeling large WPP consisting of many VSWT with PMG one can make following assumption: If control system for all converters are tuned properly it is likely that there is no risk of mutual interaction between them [11].

In conclusion in this case, a large WPP expressed as single machine model can be used in terms of analysis of voltage stability. This means that a single WT represents a large WPP and the following additional assumption has to be taken into consideration :

- The sum of the power capacities of all of the WT's in the WPP corresponds to the power capacity of the single machine equivalent [11]
- The sum of the power all of the WT's in the WPP corresponds to the power supplied by the single machine equivalent [11]
- The impact of connection cables in WPP is neglected (no different cable reactances between specific WT and collectro bus)
- reactance values for transformers are chosen to be equal and calculation of an equilvalent reactance is shown in Figure 4.8
- Only one connection line is considered between WPP and PCC
- There are no delays in communication between WPP and STATCOM

Taken assumption allow to analyze the behavior of WPP using a single equivalent model.

## A.10 Grid model

Grid was defined as a controllable three-phase voltage source. The phase voltages defined as:

$$V_a = E_m \cdot cos\,(\omega \cdot t) \tag{A.24}$$

$$V_b = E_m \cdot cos\left(\omega \cdot t - \frac{2\pi}{3}\right) \tag{A.25}$$

$$V_c = E_m \cdot cos\left(\omega \cdot t - \frac{4\pi}{3}\right) \tag{A.26}$$

In the above equations $\omega$ represents the angular frequency and $E_m$ represents the phase voltage amplitude.

The three-phase voltage source line-to-line voltages are defined as:

$$V_{ab} = V_a - V_b \tag{A.27}$$

$$V_{bc} = V_b - V_c \tag{A.28}$$

$$V_{ca} = V_c - V_a \tag{A.29}$$

Figure A.12 presents the vector representation of the grid voltage and current.

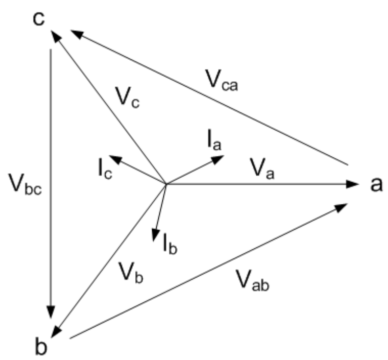


Figure A.12: The vector representation of the symetrical three-phase grid

Above model was implemented in MATLAB Simulink software and it is presented in Figure A.5.

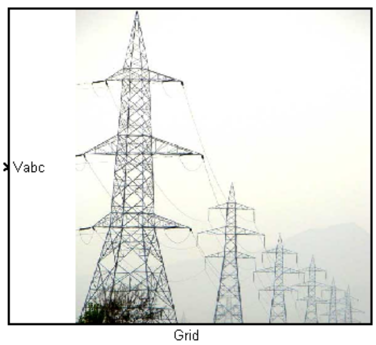


Figure A.13: Implemented grid model.

# Wind Turbine Performance

This section presents the results obtained by simulating the whole WT plant (from the wind model to the VSC). The test was performed by applying steps in the wind speed and the outcome was to observe the generator shaft speed response and the DC-link current at the output of the rectifier.

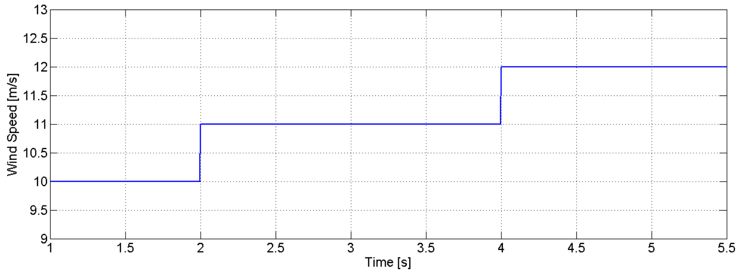


Figure B.1: Wind speed steps.

As an be seen, the shaft speed rises slow as a ramp, limited by the rotor and generator inertia, after oscillations occurring due to the effect of the two mass drive train. The steady state is reached after 0.7s, and very small overshoot is occurring.

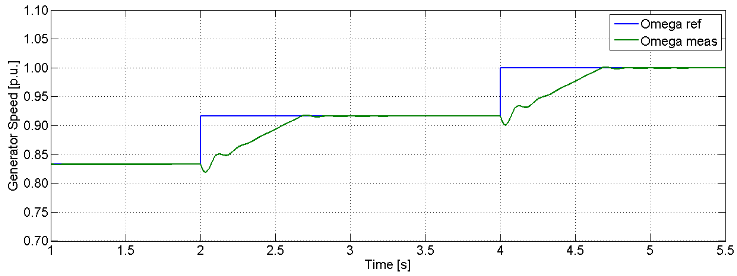


Figure B.2: Generator speed.

The last Figure shows the measured DC-link current, which has a waveform similar with the generator speed. The value of the current changes with the same rate as the speed.

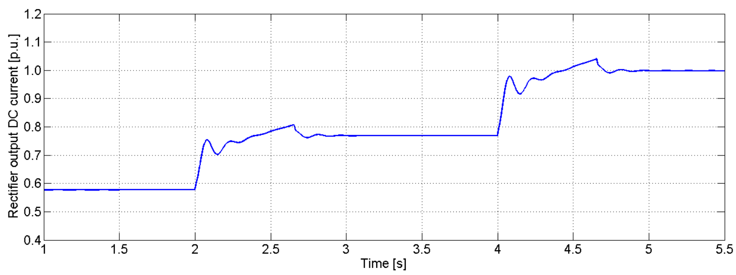


Figure B.3: DC link current measured after the rectifier.

Appendix C

# Control design

## C.1 Grid converter controller

An easy and effective engineering way for tuning the PI controller parameters is called "trying-adjusting" method, which gains the robustness to any parametric uncertainties and having no complicated calculation and analysis for parameter estimations.

Thanks to the independent operating areas of $k_p$ and $k_i$, separately tuning them is made possible. The basic principle of designing a PI controller is from high frequency domain to low frequency domain and from inner loop to outer loop. $K_p$ and $k_i$ are more or less independent in determining a PI controller's performance, where $k_p$ is dominant in determining the high frequency domain response (dynamic response) and $k_i$ is dominant in low frequency zone. Furthermore $k_p$ directly contributes to the whole control gain of the system. So, based on the basic rule of tuning PI controller $k_p$ should be tuned ahead of $k_i$. By increasing $k_p$, the dynamic response of system is improved but phase margin is decreased, resulting in reduced reliability. On the other side, $k_i$ dominates low frequency response, like steady state error and overshoot. In general, high $k_p$ provides better ability to reject high-frequency disturbances, while high $k_i$ helps the control system reject lower-frequency disturbances, like eliminating the steady-state error.

The basic steps of tuning the PI controller parameters using the "trying-adjusting? method are:

- Keeping $k_p$ initially to zero. Now phase margin is 90 degrees and the system is stable. Trying to increase $k_p$ to a small value and continue in small steps until further increasing kp will result in response oscillation.

- Keeping $k_p$ fixed to the found value, start increasing ki until no steady-state error showed up and desired maximum overshoot is reached. Increasing in $k_i$ value will cause a little affect on the higher frequency zone, which is determined by $k_p$, therefore it is no need to tune $k_p$ again.

For multiple loops design, like in the case of VOC, the inner loop is always designed first and overshoot should be not over 5%. Then the outer loop controller is design with the same basic steps.

## C.2 STATCOM control

The DC link controller for STATCOM was based on [26]. It takes into consideration the variation of the DC link energy. The reason for using an energy controller is simple - the relation between DC link energy variation and power of STATCOM is linear. That means that used controller can only have a proportional term. In [26] the DC-link voltage controller was developed for Shunt Active Power Filter (SAPF). For this SAPF the relation between energy variations at DC-link of SAPF and power of the filter was described as:

$$\Delta w_{dc} = w_{dc} - w_{dc}(0) = -\int_0^t (p_{F3\phi} + p_{L_F})dt \tag{C.1}$$

Where $p_{F3\phi}$ is the instantaneous active power developed by the filter, and $p_{L_F}$ is the instantaneous power associated to the link inductances of the legs. As STATCOM can be treated as a SAPF ([27]) the relation expressing the DC link energy variation can go as follows:

$$\Delta W_{dc} = -\frac{U_{dc,ref}^2 - U_{dc,meas}^2}{2 \cdot C_{dc}} \tag{C.2}$$

Using simple proportional controller will allow to keep the dc voltage at the desired value. The constant gain value for the proportional controller (P on figure 4.6) was taken from [27]. Figure C.1 shows the used controller.

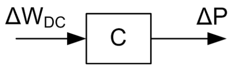


Figure C.1: Proportional controller for DC link.

Having the reference active power from the energy controller and the reactive power from one of the control strategies described in section 4.4.1 one can calculate the reference currents for PR controllers. The reference current calculation was based on Instantaneous active-reactive control startegy [27], [28]. The active currents components were calculated according to the formulas:

$$I_{abcp} = \frac{P}{\sqrt{V_a^2 + V_b^2 + V_c^2}} \tag{C.3}$$

And the reactive components:

$$\begin{aligned} I_{aq} &= \frac{Q}{\sqrt{V_a^2 + V_b^2 + V_c^2}} \cdot \frac{V_c - V_b}{\sqrt{3}} \\ I_{bq} &= \frac{Q}{\sqrt{V_a^2 + V_b^2 + V_c^2}} \cdot \frac{V_a - V_c}{\sqrt{3}} \\ I_{cq} &= \frac{Q}{\sqrt{V_a^2 + V_b^2 + V_c^2}} \cdot \frac{V_b - V_a}{\sqrt{3}} \end{aligned} \tag{C.4}$$

The reference current are calculated as follows:

$$I_{abc} = I_{abcp} + I_{abcq} \tag{C.5}$$

And then for the purpose of using them in PR controllers they are transformed to stationary reference frame ($abc \rightarrow \alpha\beta$). The adjustment of the current controllers was done using Control and Estimation Tools Manager (CETM) feature of MATLAB Simulink. From the control point of view the plant of the system for the STATCOM inverter is represented by the LCL filter transfer function, which was obtained using also CETM. The parameters of the filter are shown in table D. The transfer function used for adjusting the gains is presented in equation (C.8). The obtained controller is shown by the next equation:

$$G_{PR} = 14.807 + \frac{(58 \cdot s^2)}{s^2 + \omega^2} \tag{C.6}$$

From which the proportional and integral gain are:

$$K_p = 14.807, \quad K_i = 58 \tag{C.7}$$

In the process of adjusting $K_p$ and $K_i$ some requirements regarding the stability of the system should be fulfilled. Namely, the damping factor should be 0.707, the phase margin of the Open

Loop Bode Diagram should be larger than $45^o$ [23] [24] [25]. The above gains were obtained using the Root Locus and Open Loop Bode Diagram of the system. The next figure presents both plots. The position of the dominant poles was chosen in a way to fulfill the damping criteria. In the Open Bode Loop diagram the gain margin is 6.19 dB and the phase margin is $64.5^o$, according to the demands.

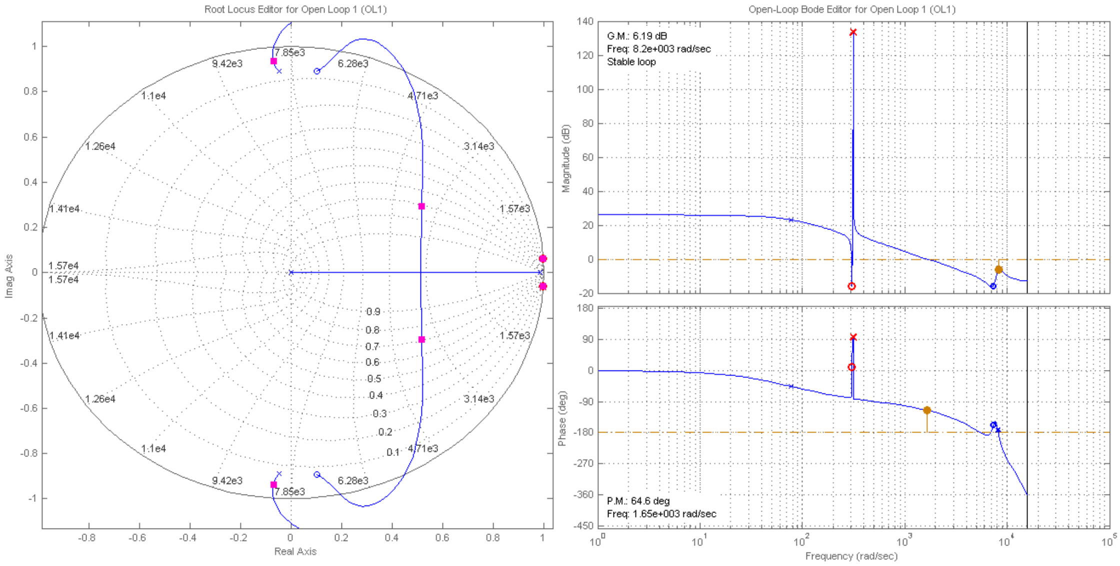


Figure C.2: Root Locus and Open Loop Bode Diagram of the system.

## C.3 Emulated system

For the synchronizing the output voltage of the two inverters with the grid voltage a Phase Locked Loop (PLL) was used. The adjustment of the current controllers was done using CETM feature of MATLAB Simulink. From the control point of view the plant of the system for the WPP inverter is represented by the LCL filter transfer function, which was obtained using also CETM. The parameters of the filter are shown in table D. The obtained transfer function is presented in the next equation:

$$G(s) = \frac{i_G}{V_i} = \frac{144.9 \cdot s^2 + 1.449 \cdot e^5 s + 7.342 \cdot e^9}{s^3 + 1232 \cdot s^2 + 6.615 \cdot e^7 s + 5.139 \cdot e^9} \tag{C.8}$$

The obtained controller is shown by the next equation:

$$G_{PI} = \frac{23.437(s + 212.8)}{s} \tag{C.9}$$

From which the proportional and integral gain are:

$$K_p = 23.437, \quad K_i = 4987 \tag{C.10}$$

In the process of adjusting $K_p$ and $K_i$ some requirements regarding the stability of the system should be fulfilled. Namely, the damping factor should be 0.707, the phase margin of the Open Loop Bode Diagram should be larger than $45^o$ and the bandwidth should be larger than 500Hz [23] [24] [25]. The above gains were obtained using the Root Locus and Open Loop Bode Diagram of the system. This can be seen in the next figure. On the Root Locus the position of the dominant poles is chosen in such a way to fulfill the damping criteria. In the Open Bode Loop diagram the gain margin is 4.84 dB and the phase margin is $60^o$, according to the demands.

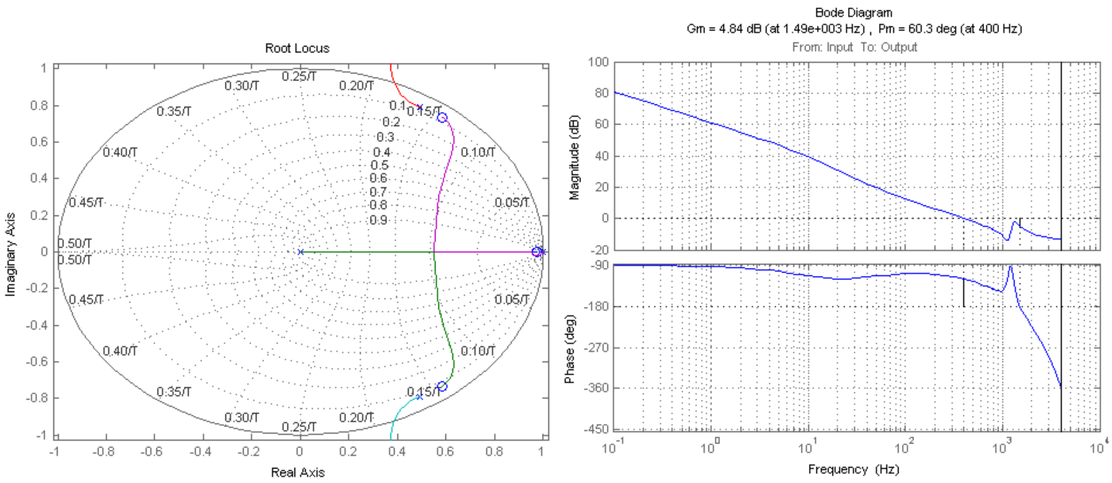


Figure C.3: Root Locus and Open Loop Bode Diagram of the system.

In the Closed Loop Bode Diagram in the Fig.C.4 the bandwidth of the control loop is approximately 700Hz, fulfilling the constraint.

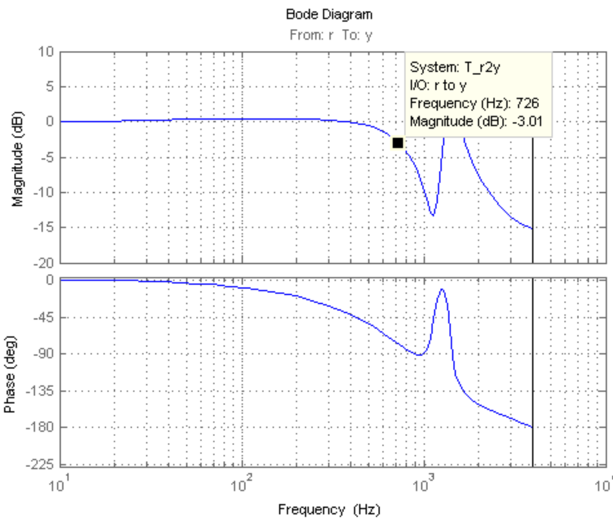


Figure C.4: Closed loop Bode Diagram for the system

Appendix D

# Parameters

## WT Parameters

| Parameter | Simbol | Value | Unit |
|---|---|---|---|
| Rotor blade radius | $R$ | 40 | $[m]$ |
| Air density | $\rho$ | 1.225 | $[kg/m_3]$ |
| Cut-in speed | $v_{cut-in}$ | 3 | $[m/s]$ |
| Cut-out speed | $v_{cut-out}$ | 20 | $[m/s]$ |
| Rated speed | $v_{rated}$ | 12 | $[m/s]$ |
| Rated rotor speed | $\omega_{rated}$ | 1.71 | $[rad/s]$ |
| Optimum TSR | $\lambda_{opt}$ | 5.7 | $[-]$ |

## Drive Train Parameters

| Parameter | Simbol | Value | Unit |
|---|---|---|---|
| Inertia of the wind turbine rotor | $J_{wt}$ | $9.0 \cdot 10^4$ | $[kg \cdot m^2]$ |
| Inertia of the generator | $J_{gen}$ | 70 | $[kg \cdot m^2]$ |
| Shaft stiffness | $k_{shaft}$ | $1.64 \cdot 10^8$ | $[Nm/rad]$ |
| Damping factor | $D_{shaft}$ | $7.4 \cdot 10^5$ | $[Nmsec/rad]$ |
| Gearbox ratio | $k_{gear}$ | 46 | $[-]$ |

## PMSG Parameters

| Parameter | Simbol | Value | Unit |
|---|---|---|---|
| Rated voltage | $V$ | 690 | $[V]$ |
| Rated power | $P$ | 2 | $[MW]$ |
| Stator resistance | $R_s$ | 2 | $[m\Omega]$ |
| d-axis stator inductance | $L_d$ | 0.11 | $[mH]$ |
| q-axis stator inductance | $L_q$ | 0.11 | $[mH]$ |
| No. of pole pairs | $n_{pp}$ | 4 | $[-]$ |
| Permanent magnet flux linkage | $\psi_m$ | 2.91 | $[mWb]$ |

## Grid Connection Parameters

| Parameter | Simbol | Value | Unit |
|---|---|---|---|
| DC-link Voltage | $V_{DC}$ | $690 \cdot \sqrt{3} \cdot \sqrt{2}$ | $[V]$ |
| DC-link Capacitor | $C_{DC}$ | 0.01 | $[F]$ |
| Grid Voltage (RMS) | $v_g$ | 690 | $[V]$ |

## Control Parameters

| Parameter | Simbol | Value |
|---|---|---|
| FOC | | |
| PI Current Control Proportional Gain | $k_{pi}$ | 0.5467 |
| PI Current Control Integrator Gain | $k_{ii}$ | 0.047 |
| PI Speed Control Proportional Gain | $k_{ps}$ | 700 |
| PI Speed Control Integrator Gain | $k_{is}$ | 0.6 |
| VOC | | |
| PI Current Control Proportional Gain | $K_{pi}$ | 0.7 |
| PI Current Control Integrator Gain | $K_{ii}$ | 50 |
| PI DC Voltage Control Proportional Gain | $K_{pv}$ | 0.04 |
| PI DC Voltage Control Inegrator Gain | $K_{iv}$ | 10 |

## LCL filter parameters

| | |
|---|---|
| Sampling frequency | $f_s = 5kHz$ |
| Filter inverter side inductance | $6.9mH$ |
| Filter grid side inductance | $2mH$ |
| Filter capacitance | $4.7\mu F$ |

## Laboratory system reactance

| | |
|---|---|
| $X_{system}$ (consists of L and C of LC filter of a inverter) | 0.23 |
| Maximum active Power from WPP inverter | $1pu.$ |

Appendix E

# Hardware

## Inverters

The characteristics of the used inverters is presented below:

- Rated power: 3.9 kVA
- Rated input voltage:3x360 $V_{rms}$-500 $V_{dc}$
- Rated input current:5.0/4.3 A
- Rated input frequency:50-60 Hz
- Rated output voltage:3x0-V-in
- Rated output current:5.6/4.8A
- Rated output frequency:0-1000Hz

## LC filters

LC filter for each inverter:

| | |
|---|---|
| Filter inductance | $6.9mH$ |
| Filter capacitance | $4.7\mu F$ |
| Rated filter power | $3kW$ |
| Maximum filter current | $8A$ |

## Transformer

Used 1x1 transformer data:

| | |
|---|---|
| Primary windings | $3x400$ |
| Secondary windings | $3x400+N$ |
| Rated Transformer Power | $5kVA$ |
| Maximum Transformer current | $7.2A$ |
| Output frequency | $50/60Hz$ |
| Windings connection | $Dyn11$ |

## DC source

For having a DC supply for the inverters 2 x Delta Elektronika DC power supplies connected in series are used:

- Type: SM300 D10

- Rated power: 3kW
- Rated voltage: 300V
- Rated current: 10A

## Lem boxes

The measuring system consists of:

- 2 x LEM box for measurement of $U_{dc}$ (1 x voltage transducer LV25-800, LEM)
- 3 x LEM box for measurement of WPP, STATCOM and grid currents and voltages (3 x current/voltage transducer LA55-P, LEM)

## Line inductors

Used line inductors for emulating a line between WPP and PCC:

| Number of inductors connected in series | Inductance | Line length |
|---|---|---|
| 1 | $1.8mH$ | $1.4km$ |
| 2 | $3.6mH$ | $2.8km$ |
| 3 | $5.4mH$ | $4.2km$ |
| 4 | $7.2mH$ | $5.6km$ |